UC Berkeley

Title

Nonlinear Analysis of Reinforced Concrete Hyperbolic Paraboloid Shells

Permalink

https://escholarship.org/uc/item/5js4z0kd

Author

Muller, Gunter

Publication Date

1977-10-01

Structures and Materials Research
Department of Civil Engineering
Division of Structural Engineering
and
Structural Mechanics

NONLINEAR ANALYSIS OF REINFORCED CONCRETE HYPERBOLIC PARABOLOID SHELLS

by

Guenter Mueller
Visiting Scholar

Faculty Investigator: A. C. Scordelis

College of Engineering
Office of Research Services
University of California
Berkeley, California

October 1977

BIBLIOGRAPHIC DATA SHEET	1. Report No.		2.	3. Recipient's Accession No.
4. Title and Subtitle Nonlinear Analysis of Reinforced Concrete Hyperbolic Paraboloid Shells				5. Report Date October 1977
				6.
7. Author(s) Guenter Mueller				8. Performing Organization Rept. No. UC-SESM 77-6
9. Performing Organization Name and Address Department of Civil Engineering University of California Berkeley, CA 94720				10. Project/Task/Work Unit No.
				11. Contract/Grant No. ENG 77-00146
12. Sponsoring Organization Name and Address National Science Foundation Washington, D.C. 20550				13. Type of Report & Period Covered Final Report
				14.

15. Supplementary Notes

16. Abstracts

A nonlinear analysis based on the finite element method is used to trace the quasi-static responses of reinforced concrete shells under instantaneous loading and also under sustainted loading including the time dependent effects of creep and shrinkage. Three common types of HP shells - saddle, gable and inverted umbrella - with fixed proportions are investigated in detail. The behavior through the elastic, cracking, inelastic and ultimate ranges is studied. Comparisons are made between this behavior under instantaneous loading and underlying time loading.

17. Key Words and Document Analysis.   17a. Descriptors

Structural engineering; reinforced concrete; hyperbolic paraboloid shells; nonlinear analysis; finite elements; material nonlinearities; cracking; creep; shrinkage, load history; ultimate strength.

17b. Identifiers/Open-Ended Terms

17c. COSATI Field Group

18. Availability Statement	19. Security Class (This Report)	21. No. of Pages 107

Structures and Materials Research
Department of Civil Engineering
Division of Structural Engineering
and
Structural Mechanics

NONLINEAR ANALYSIS OF REINFORCED CONCRETE HYPERBOLIC PARABOLOID SHELLS

by

Guenter Mueller
Visiting Scholar

Faculty Investigator: A. C. Scordelis

College of Engineering
Office of Research Services
University of California
Berkeley, California

October 1977

ACKNOWLEDGEMENTS

TABLE OF CONTENTS

iv

NOTATIONS

x, y, z ... coordinate system

u, v, w ... deflections in x, y, z-directions

CST-element ... constant strain triangle (membrane) element with 6 DOF

LCCT9-element ... linearly constrained curvature triangle (bending) element with 15 DOF

DOF ... degree of freedom

Concrete Properties

E_o ... uniaxial initial tangent modulus

f'_c ... uniaxial compressive strength

f'_t ... uniaxial tensile strength

ε_c ... strain corresponding to f'_c

ε_{cu} ... ultimate strain in compression

ε_{tu} ... ultimate strain in tension

ν ... Poisson's ratio

β ... cracked shear constant ($0.0 \leqslant \beta \leqslant 1.0$)

Steel Properties

E_s ... initial tangent modulus

E_{sh} ... strain-hardening modulus

f_y ... yield stress

σ_c ... stress in concrete

σ_s ... stress in steel

A_c ... area of concrete cross-section

A_s ... area of steel cross-section

$\rho = \dfrac{A_s}{A_c}$ ... reinforcement ratio

1. INTRODUCTION

Shells have many of the qualities of an ideal structure. Their construction requires relatively little material. They permit spans over large areas without intermediate supports, and they offer many possible esthetic forms. Applications of shell roofs cover a broad scope. They have been used for sport arenas, auditoriums, churches, supermarkets, airplane hangars, theaters, and exhibition halls.

Among the most common shell types are the hyperbolic paraboloid shells. The hyperbolic paraboloid (HP) shells are translational shells generated either by parabolas or by straight lines (Fig. 1.1a).

HP shells are favored for several reasons. From an architectural point of view, they offer the advantage that by using different arrangements of the basic shape, a great variety of distinct forms can be developed (Fig. 1.1b). From an engineering point of view, mainly two advantages are important. First, the doubly curved surface is advantageous since a great part of the load is transmitted to the support by membrane forces. Hence, stresses are small and require only a thin cross-section. The thickness of a shell is determined mainly by the necessary concrete cover of the steel reinforcement and not by the stresses. (Recently, in Stuttgart [1] a shell, 31 m in diameter and made of fiber reinforced concrete, was erected with a thickness of only 1 to 1.2 cm!)

The second major advantage is that their forming is simple, even though the doubly curved surface has the appearance of posing a complicated forming problem. Because the surface is defined by two intersecting systems of straight lines, the usual plywood framework requires only

straight wood joist supports.

A large number of these shells have been built during the past 20 years. Designs have been mostly based on membrane theory with some thought given to secondary effects. A Portland Cement Association Bulletin [2] has been used as a design guide in many applications in the United States. Several investigators [3, 4] have presented formulas for special loading cases and different geometric configurations. Moreover, Scordelis, et. al. [5, 6, 7] have developed computer programs which permit the membrane analysis of any HP shell.

Today, the finite element method is often used to take into account both membrane and bending stresses. However, for the purpose of preliminary design, the membrane theory is still an excellent means to estimate the required dimensions with little effort and to give an insight into the behavior. The analysis is usually based on the assumption that the materials are uncracked, homogeneous, isotropic and linearly elastic. Time-dependent environmental effects such as creep, shrinkage and temperature fluctuations are also usually not considered, or, if so, only in an approximate manner. However, there is a great interest to get more information on the influence of these parameters. For many structures, long time behavior may prove to be more critical to the serviceability requirements than short time loading effects. The failure of an HP gable shell roof in Virginia [8] and the large vertical deflections at the crown observed in two similar roofs in the same area underline the importance of the application of realistic models.

Until now, the nonlinear behavior of such concrete shells was investigated experimentally on small-scale reinforced microconcrete models

STRAIGHT LINES

PARABOLIC ARCHES

PARABOLIC CABLES

L_1 = CABLE SPAN

h_1SAG

h_2 = RISE

L_2 = ARCH SPAN

(a) GENERAL DESCRIPTION

GABLE

SADDLE

INVERTED UMBRELLA
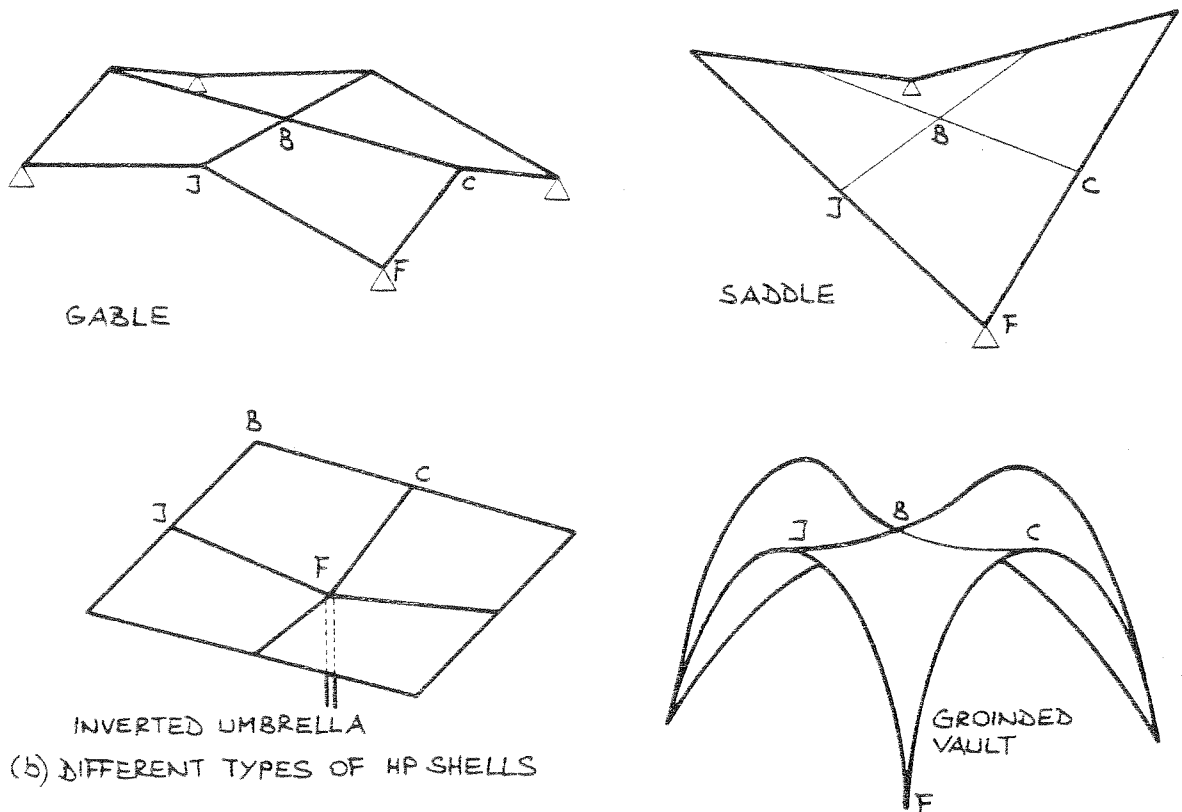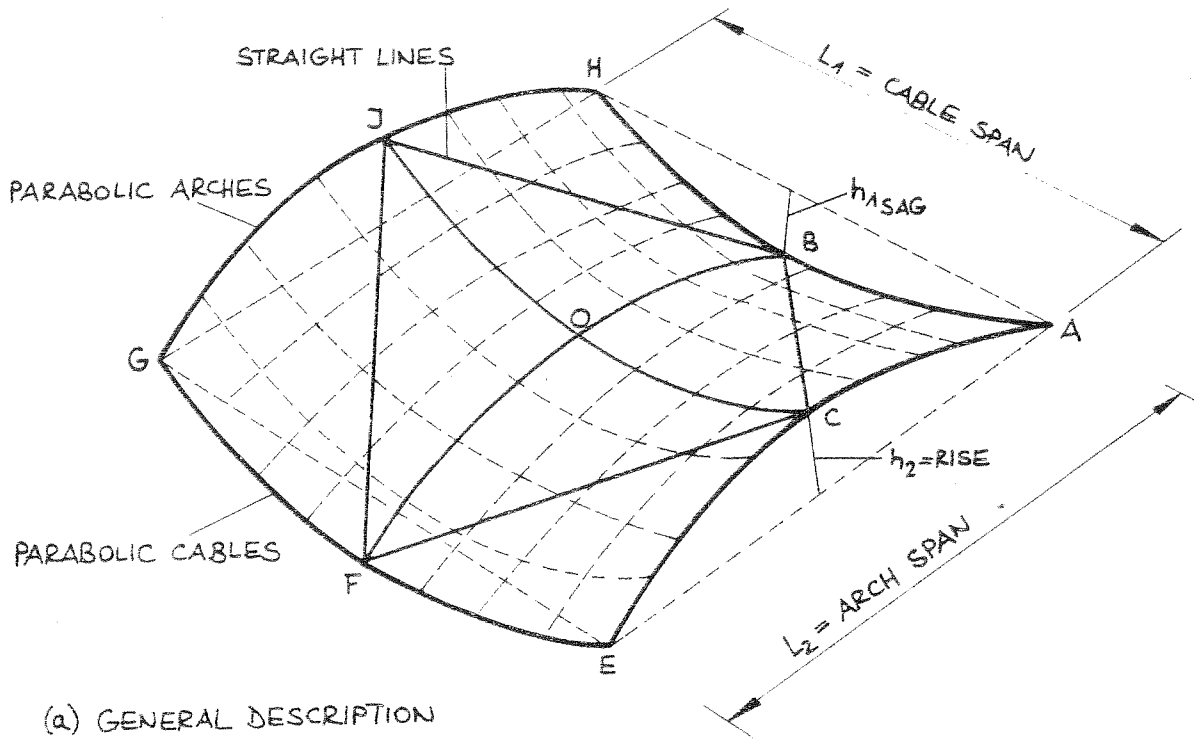
GROINDED VAULT

(b) DIFFERENT TYPES OF HP SHELLS

FIG. 1.1 HYPERBOLIC PARABOLIC SHELLS (HP SHELLS)

and on polyvinylchloride (PVC) models. A review of a number of experimental investigations is given by White [9].

It is recognized that experiments on models can furnish valuable insight into the behavior of prototypes, but, on the other hand, it is known that tests are very expensive and time-consuming. This is particularly true when parameter studies are to be performed and a large number of models needs to be tested. Therefore, it is essential to develop general methods of analysis to complement and to reduce the number of necessary physical experiments. Experiments can not be replaced totally, since the accuracy and reliability of the numerical analysis have to be confirmed by selected well controlled experiments.

A comprehensive state-of-the-art review of the finite element method for analyzing reinforced concrete structures was presented by Scordelis [10]. More recently, Schnobrich [11], Wegner [12] and Eibl/Ivanyi [13] have also surveyed the various applications of the finite element method to predict the behavior of reinforced concrete structures. From these surveys, the following conclusions can be drawn:

1. Numerical procedures to deal with all kinds of nonlinearities and time dependencies have been developed. Some more work has to be done to reduce the computer time and to improve the convergence of these solutions.

2. Before the finite element method can be expected to predict more accurately the actual response of reinforced concrete structures, additional basic experimental research must be conducted to obtain a more realistic material description of concrete. Better information on constitutive relations, failure criterias, creep and shrinkage,

tensile strength, tension stiffening, cracked shear modulus and bond are needed to improve the accuracy of future analyses.

3. Analyses have been performed mainly for beams, panels, slabs and axisymmetric solids under short time loading. Time dependent effects such as creep and shrinkage were usually neglected. Little work has been done in treating free form shell structures and general three-dimensional solids. Common types of shells such as HP shells have been analyzed only by Lin [14] and Kabir [15].

2. AIM OF THE PRESENT STUDY

This study was performed during a stay at the University of California, Berkeley. The author could spend only a relatively short time on this study during his stay. Much more time would be required to make a comprehensive investigation. Therefore, this report should be considered as a pilot study in which all of the parameters have not been completely studied.

For a study from which general conclusions could be drawn, many detailed analyses would be necessary in which all of the parameters would be varied to discover the most important ones. Linear analyses [15, 16] show (Fig. 6.1), for example, that the dimensions of the beams and even their arrangement can have considerable influence on the deflections and, thus, the behavior of the shells.

The present investigation will be performed using the following steps:

1. Dimensions of the shells and edge beams for a given shell geometry are determined on the basis of the membrane theory as is done in

a preliminary design in practice.

2. Linear finite element analyses incorporating membrane and bending effects are performed to check the validity of the mesh layout and to get some information on the shell behavior.

3. The structures are loaded incrementally up to the ultimate load to get the nonlinear load-deflection relation.

4. The same as that in 3 is done only including the time dependent effects of creep and shrinkage.

The objective is to identify some principal properties of the behavior of each type of shell and to get some knowledge of the influence of time-dependent behavior. Also, by virtue of the acquired experiences, it is expected that some recommendations for further studies may be given.

For the finite element analysis the computer program NOTACS is used. A brief description of the program is given in the subsequent section.

3. BRIEF DESCRIPTION OF THE COMPUTER PROGRAM NOTACS [15]

The method of analysis is based on a finite element tangent stiffness formulation coupled with a time step integration scheme. Within a time step, an incremental load procedure, with an iterative approach to solve the equilibrium equations for each load increment, is adopted to trace the nonlinear behavior. All load changes are considered to occur at the beginning of a time step and the resultant state of stress is assumed to prevail throughout the time step. The creep and shrinkage strains are taken as initial strains and are assumed to occur at the end of each time step. The unbalanced forces at the end of each iteration or load increment are treated as initial stresses in the following step.

Two types of finite elements are implemented in the program: the flat triangular shell element for reinforced concrete shells and the boundary element. The shell element (Fig. 3. 1) is combined of a constant strain triangular (CST) membrane element and a linearly constrained curvature triangular (LCCT9) plate bending element. Thus the element has only five degrees of freedom at each node. The in-plane rotation is not considered as a degree of freedom. By constraining the appropriate degrees of freedom the element may be also used for panel-type and slab-type structures.

The boundary element is used to limit nodal displacements or rotations to specified values, to compute support reactions, to provide linear-elastic supports to nodes and to overcome the problem of the missing sixth degree of freedom at coplanar shell nodes. The element is defined by a single directed axis through a specified nodal point and has an extensional and/or rotational stiffness. The element stiffnesses are added directly to the total structural stiffness matrix and hence have no effect on the size of the stiffness matrix.

The reinforced concrete composite is represented as a layered system (Fig. 3. 1) consisting of concrete and "equivalent smeared" steel layers. Variations of properties through the depth of the member are due to different materials or level of deformation. Kirchhoff's assumption of plane sections remaining plane is adopted to interrelate the displacements at various levels through the section depth and thus reduce each layer to a two-dimensional problem.

The material behavior of concrete is characterized by a nonlinear constitutive relationship for the biaxial state of stress. The biaxial state of stress is accounted for by a family of equivalent uniaxial
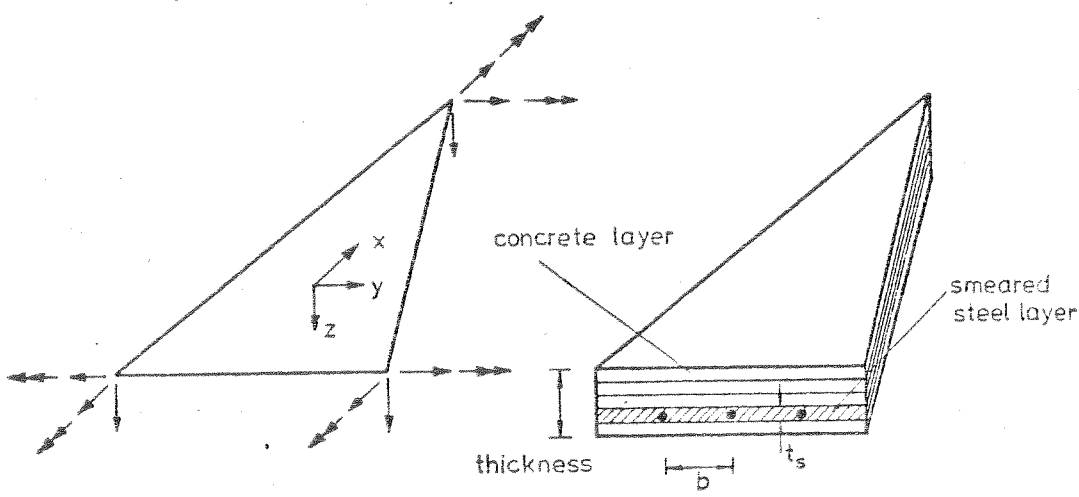
8

FIG. 3.1 COMBINED CST- AND LCCT3- ELEMENT

$$\sigma_i = \frac{E_0 \, \varepsilon_{iu}}{+ \left[\frac{E_0}{E_s} - 2\right]\left(\frac{\varepsilon_{iu}}{\varepsilon_{ic}}\right) + \left(\frac{\varepsilon_{iu}}{\varepsilon_{ic}}\right)^2}$$

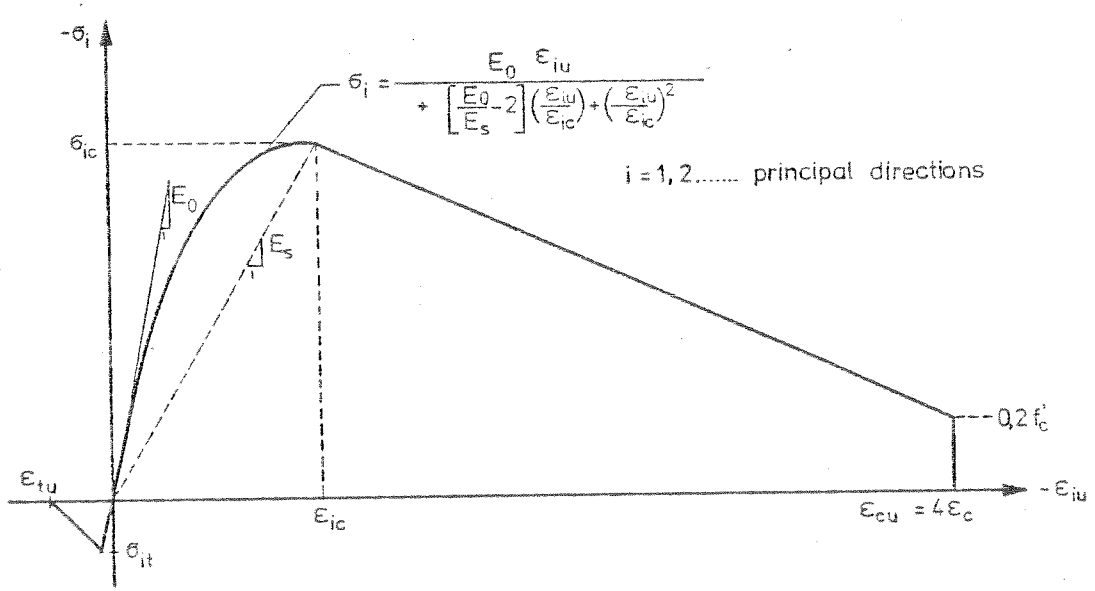$i = 1, 2 \ldots\ldots$ principal directions
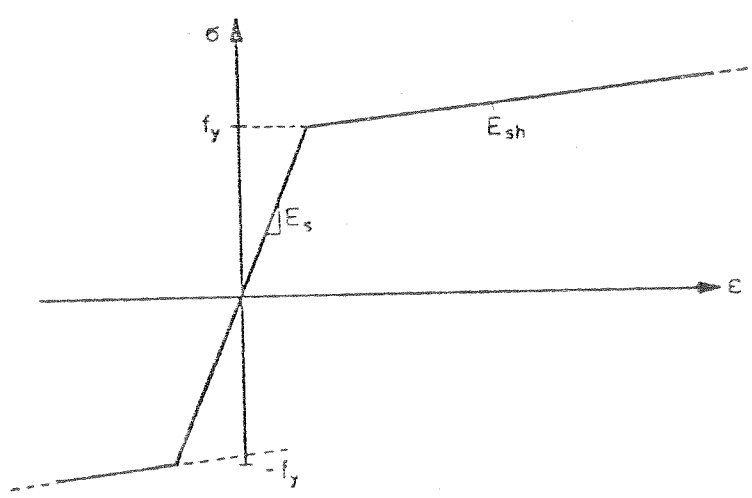
FIG. 3.2 EQUIVALENT UNIAXIAL STRESS-STRAIN MODEL FOR CONCRETE

FIG. 3.3 STRESS-STRAIN MODEL FOR STEEL

stress-strain curves (Fig. 3.2) depending on the biaxial stress ratio as suggested by Darwin and Pecknold (see reference in [15]).

Five material properties of concrete have to be prescribed for the construction of these curves: the uniaxial initial tangent modulus E_0, the uniaxial compressive strength f'_c, Poisson's ratio ν, the tensile strength f'_t, and the ultimate strain in tension ε_{tu}. These values can be taken either from uniaxial load tests or code recommendations. The maximum compressive stresses σ_{ic} and corresponding strains ε_{ic} in the principal directions $i = 1,2$ are obtained from the well known biaxial failure envelope of Kupfer and Gerstle and equations proposed by Darwin, Pecknold and Rajagopal (references in [15]).

One of the most significant properties of concrete is its low tensile strength. The tensile cracking reduces the stiffness of the concrete and is a major contributor to the nonlinear behavior of reinforced concrete structures. Herein a maximum stress criterion is used to determine concrete failure in tension. Whenever one of the principal stresses exceeds the uniaxial tensile strength of concrete a crack is assumed to form perpendicular to the direction of that stress and the corresponding tangent modulus is assumed to be zero. Once the concrete is cracked in one direction, the formation of a new crack is restricted to a direction orthogonal to the first crack. To account for the tension stiffening effect the unbalanced stresses are released gradually depending on the strain level as shown in Fig. 3.2. To estimate the effective shear modulus along the tensile cracks due to the effect of dowel action and aggregate interlock a cracked shear constant is introduced. β can be given the values from

0.0 to 1.0. Usually β is chosen to be 0.5.

The steel reinforcement is stressed only in one direction. The material is represented by a bilinear model which may either be elastic -perfectly plastic or strain- hardening with a Bauschinger-type effect as shown in Fig. 2.3.

For concrete, time-dependent effects such as creep and shrinkage are included. The effects of stress history are accounted for by the application of the linear superposition method in the calculation of creep strains. Variations of creep compliance due to slump of concrete mix, size of members, relative environmental humidity and high stress or temperature levels can be considered on the basis of available experimental data or code recommendations. Creep under biaxial state of stress is represented by the introduction of the creep Poisson's ratio observed in a uniaxial sustained load test. The incorporated computational procedure involving the stress state of only the last time step is very efficient in the sense that it reduces the computation time and storage considerably. Shrinkage strains are assumed to be uniform in each element. The values at each time step can either be read in from experimental curves available or can be predicted by code recommendations.

4. THE STRUCTURES AND THEIR DESIGN ON THE BASIS OF MEMBRANE THEORY

4.1 Geometry of the Shells:

The shell geometries (Fig. 4.1a) are mainly described by the half-span $L/2$, the ratio of half-span to rise $(L/2)/h$ and the ratio of half-span to thickness $(L/2)/t$. Following the examples of Lin [14] and Kabir [15] the values were chosen as:

gable shell   saddle shell   inverted umbrella shell
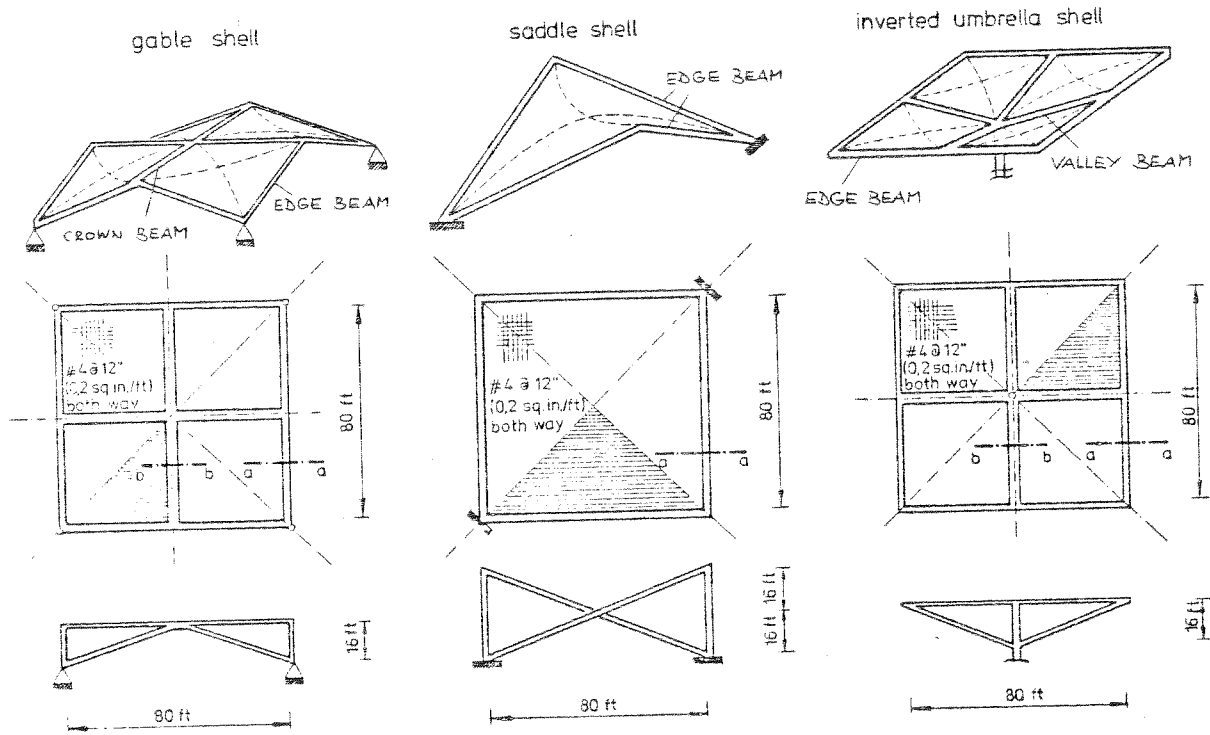
(a) GENERAL VIEWS, PLANS, ELEVATIONS AND SHELL REINFORCEMENT

sections a-a

sections b-b

| # 4 ə 12" ≙ 0,2 sq.in./ft |
| # 4 ≙ 0,2 sq.in. |
| # 10 ≙ 1,27 sq.in. |
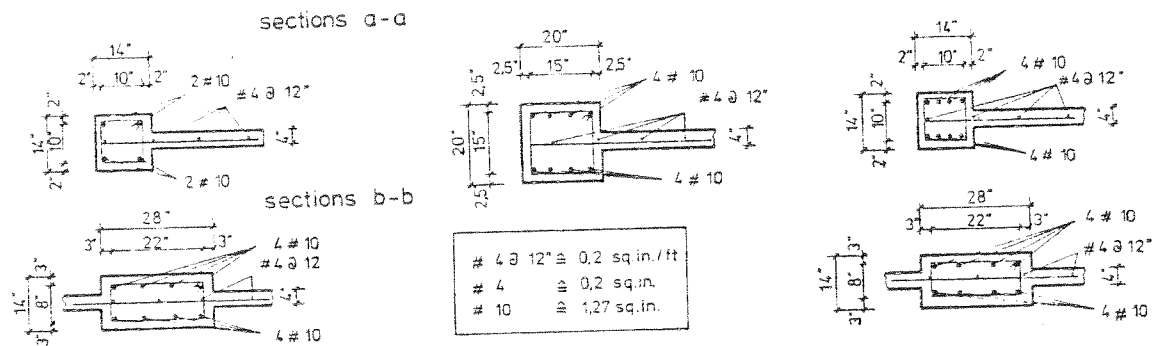
FIG. 4.1 DIMENSIONS OF THE STRUCTURES

$$L = 80 \text{ ft } (24 \text{ m})$$
$$h = 16 \text{ ft } (4.8 \text{ m})$$
$$t = 4 \text{ in. } (10 \text{ cm})$$

$$(L/2)/h = 2.5$$
$$(L/2)/t = 120$$

L and h have medium values whereas the thickness seems to be a little bit large. As mentioned before, the thickness is usually not determined by the compressive forces but by the required cover for the reinforcing steel and thus is also dependent on the environmental conditions.

The dimensions of the beams and the amount of reinforcing steel for both the shells and the beams are determined by membrane theory.

4.2 Membrane Theory

The derivation of the differential equation for the membrane theory of HP shells was given by Pucher [17] as early as 1934. For a rectangular shell segment as shown in Fig. 4.2a having three corners on the same level and loaded with a uniformly distributed load q the problem reduces to the very simple equation for the shear force

$$n_{xy} = \frac{qab}{2h} \qquad (4.1)$$

where a and b are the projected lengths of the segment on the xy plane and h is the rise.

For this particular loading, the shell is in a state of pure shear parallel to the straight line generators. This causes equal principal tensile and compressive stresses in the diagonal directions. Along the edges of each shell segment, these stresses accumulate and are picked up by the edge beams which transfer the load to the supports. In case of the saddle shell with no beams in the interior all forces flow to the edge beam and from there to the supports. The edge beam is loaded by a constant
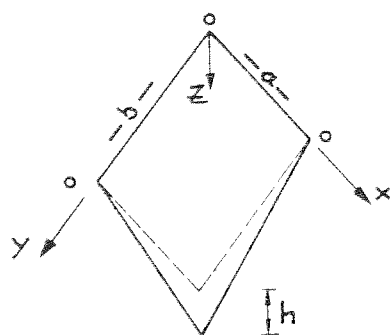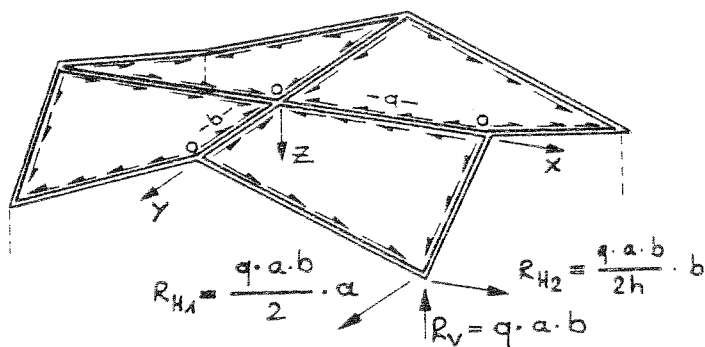
o ... POINTS ON THE SAME LEVEL

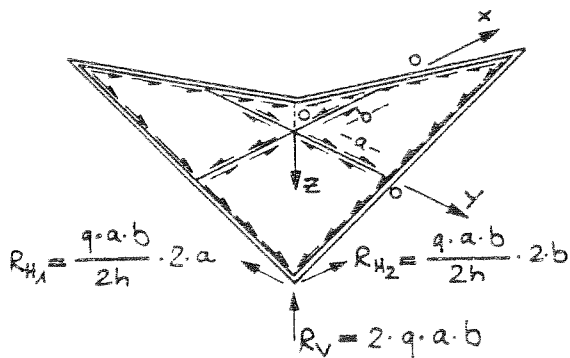GEOMETRY: $z = \dfrac{h}{a \cdot b} \cdot x \cdot y$

SHEAR FORCE: $n_{xy} = \pm \dfrac{q \cdot a \cdot b}{2h}$
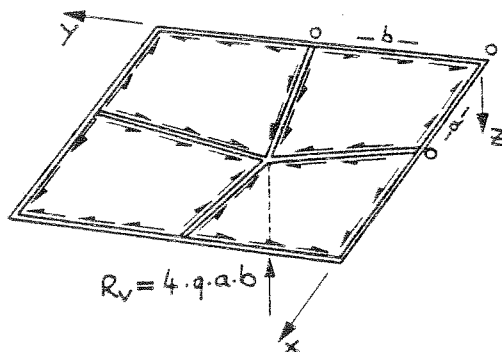
q ... UNIFORMLY DISTRIBUTED LOAD IN z- DIRECTION

(α) SHELL SEGMENT

$R_{H1} = \dfrac{q \cdot a \cdot b}{2} \cdot a$ $R_{H2} = \dfrac{q \cdot a \cdot b}{2h} \cdot b$

$R_V = q \cdot a \cdot b$

(b) GABLE

$R_{H1} = \dfrac{q \cdot a \cdot b}{2h} \cdot 2 \cdot a$ $R_{H2} = \dfrac{q \cdot a \cdot b}{2h} \cdot 2 \cdot b$

$R_V = 2 \cdot q \cdot a \cdot b$

(c) SADDLE

$R_V = 4 \cdot q \cdot a \cdot b$

(d) INVERTED UMBRELLA

FORCES ACTING ON EDGE MEMBERS !

FIG. 4.2 FORCES ON EDGE MEMBERS ACCORDING TO MEMBRANE THEORY

excentrically acting normal force. Bending stresses, not accounted for by membrane stresses, can be expected particularly in the vicinity of the free corner where the curvature of the shell is still small. The gable shell has edge beams as well as (inner) crown beams. The normal forces in these beams have only half the value of those of the saddle shell. The inverted umbrella shell differs from the other two shell types in as much as the exterior edge beams are in tension. The inner valley beams are in compression and transfer the load to the only support in the center. Three problems are obvious: the tensile stresses in the edge beams, the flat corners and the concentrated force at the support (punching shear).

The membrane analysis is presented in Fig. 4.3 to determine the cross sections. Recommended formulas in the PCA Bulletin [2] were used. According to these, the required cross section for the compression beams is calculated as:

$$A = \frac{N}{0.8(\sigma_c + \rho\sigma_s)} \qquad (4.2)$$

where $\sigma_c = 0.225\, f'_C$

$\sigma_s = 0.333\, f_y$

N . . . normal force

ρ . . . reinforcement ratio

With $f'_c = 3$ ksi (20.7 N/mm^2), $f_y = 60$ ksi (414 N/mm^2) and $\rho = 2.7\%$ an average stress of 940 psi (6.5 N/mm^2) acts on the cross section which is close to the often used value of about 1000 psi (6.9 N/mm^2). The ultimate normal compressive force is calculated by

$$N_u = 0.85\,(f'_c \cdot A_c + f_y \cdot A_s) \qquad (4.3)$$

For tensile forces the allowable stress in the steel is set to

15

	GABLE	SADDLE	INVERTED UMBRELLA
DEAD LOAD SHELL	50 psf	50 psf	50 psf
INCREASE DUE TO EDGE MEMBERS	15 psf	15 psf	15 psf
LIVE LOAD	20 psf	20 psf	20 psf
TOTAL LOAD	85 psf	85 psf	85 psf
SHEAR FORCE IN SHELL	4500 lb/ft	4500 lb/ft	4500 lb/ft
COMPRESSION FORCE IN SHELL	94 psi	94 psi	94 psi
MAXIMAL FORCE N IN			
EDGE BEAM	195 kips	390 kips	180 kips (TENSION!)
CROWN BEAM/VALLEY BEAM	360 kips	0 kips	330 kips

GIVEN:

$L = 80$ ft $(= 24$ m$)$

$h = 16$ ft $(= 4.8$ m$)$

$t = 4$ in $(= 10$ cm$)$

FIG. 4.3   MEMBRANE ANALYSIS

	GABLE	SADDLE	INVERTED UMBRELLA
SHELL REINFORCEMENT	#4 @ 12 in = 0.2 sq.in/ft	#4 @ 12 in = 0.2 sq.in/ft	#4 @ 12 in = 0.2 sq.in/ft
REINFORCEMENT RATIO ρ	0.4 %	0.4 %	0.4 %
EDGE BEAM :			
CROSS SECTION A	196 sq.in. $\triangleq$ 14×14 in.	400 sq.in. $\triangleq$ 20×20 in.	196 sq.in. $\triangleq$ 14×14 in.
REINFORCEMENT A_s	4 #10 $\triangleq$ 5.1 sq.in.	8 #10 $\triangleq$ 10.1 sq.in.	8 #10 $\triangleq$ 10.1 sq.in.
REINFORCEMENT RATIO ρ	2.6 %	2.5 %	5.2 %
ULTIMATE NORMAL FORCE N_u	750 kips	1520 kips	607 kips
RELATION N_u/N	4.0	3.9	3.4
CROWN BEAM/VALLEY BEAM			
CROSS SECTION A	392 sq.in. $\triangleq$ 28×14 in.		392 sq.in. $\triangleq$ 28×14 in.
REINFORCEMENT A_s	8 #10 $\triangleq$ 10.1 sq.in.		8 #10 $\triangleq$ 10.1 sq.in.
REINFORCEMENT RATIO ρ	2.6 %		2.6 %
ULTIMATE NORMAL FORCE N_u	1500 kips		1500 kips
RELATION N_u/N	4.2		3.8

FIG. 4.3 CONTINUATION

σ_s = 0.333 f_y (= 20 ksi = 138 N/mm^2). Concrete is assumed not to contribute in tension. Dimensions determined on the basis of these assumptions are illustrated in Fig. 4.1.

5. IDEALIZATIONS FOR THE FINITE ELEMENT ANALYSIS

5.1 Mesh Layout

Fig. 5.1 to Fig. 5.4 show the finite element idealizations. Due to symmetry the analysis can be performed on 1/4 th or 1/8 th of the shells. For all three types approximately the same mesh is chosen. Triangular shell elements (CST + LCCT9) represent both the shells and beams and are concentrated in the vicinity of the beams. The beam elements are concentric with the shell elements. The cross sections are idealized by 10 concrete layers and two steel layers (Fig. 5.6).

The supports are simulated by the use of boundary elements with a large extensional and/or rotational stiffness. The saddle shell and the inverted umbrella shell are assumed to be completely fixed into the abutments whereas the gable shell is simply supported at the four corners. Boundary elements are also fixed at nodes along the symmetry lines to account for the boundary conditions. A last group of boundary elements having no extensional stiffness but a large rotational one is used to overcome the problem of the missing sixth degree of freedom. These boundary elements are fixed at all shell nodes and are directed perpendicular to the shell surface. However, analyses with and without this group of boundary elements compared well, i.e., the boundary elements at the shell nodes are not mandatory for this special problem.

Idealizations for other solutions which will be used for control of

105 (CST + LCCT 9) ELEMENTS

58 BOUNDARY ELEMENTS
(6 AT SUPPORTS, 52 AT SHELL NODES)

77 NODES

373 DEGREES OF FREEDOM

$u = \theta_Y = \theta_Z = 0$

$v = \theta_X = 0$

$n \ldots$ NORMAL TO SHELL SURFACE

$v = \theta_X = \theta_Z = 0$

$\theta_n = 0$

$w = \theta_Z = 0$

$u = \theta_Y = 0$
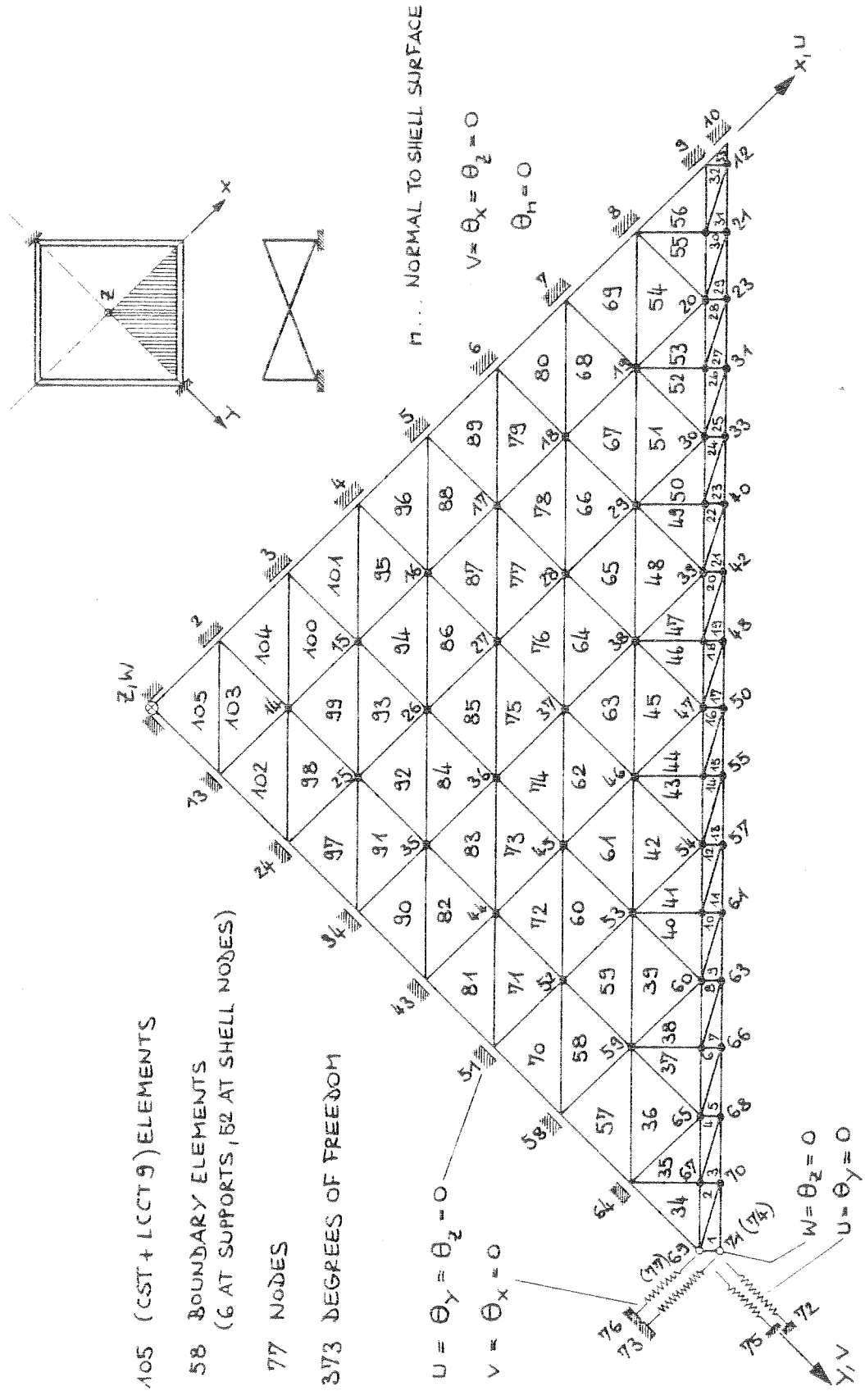
FIG. 5.1 SADDLE SHELL – FINITE ELEMENT MESH LAYOUT
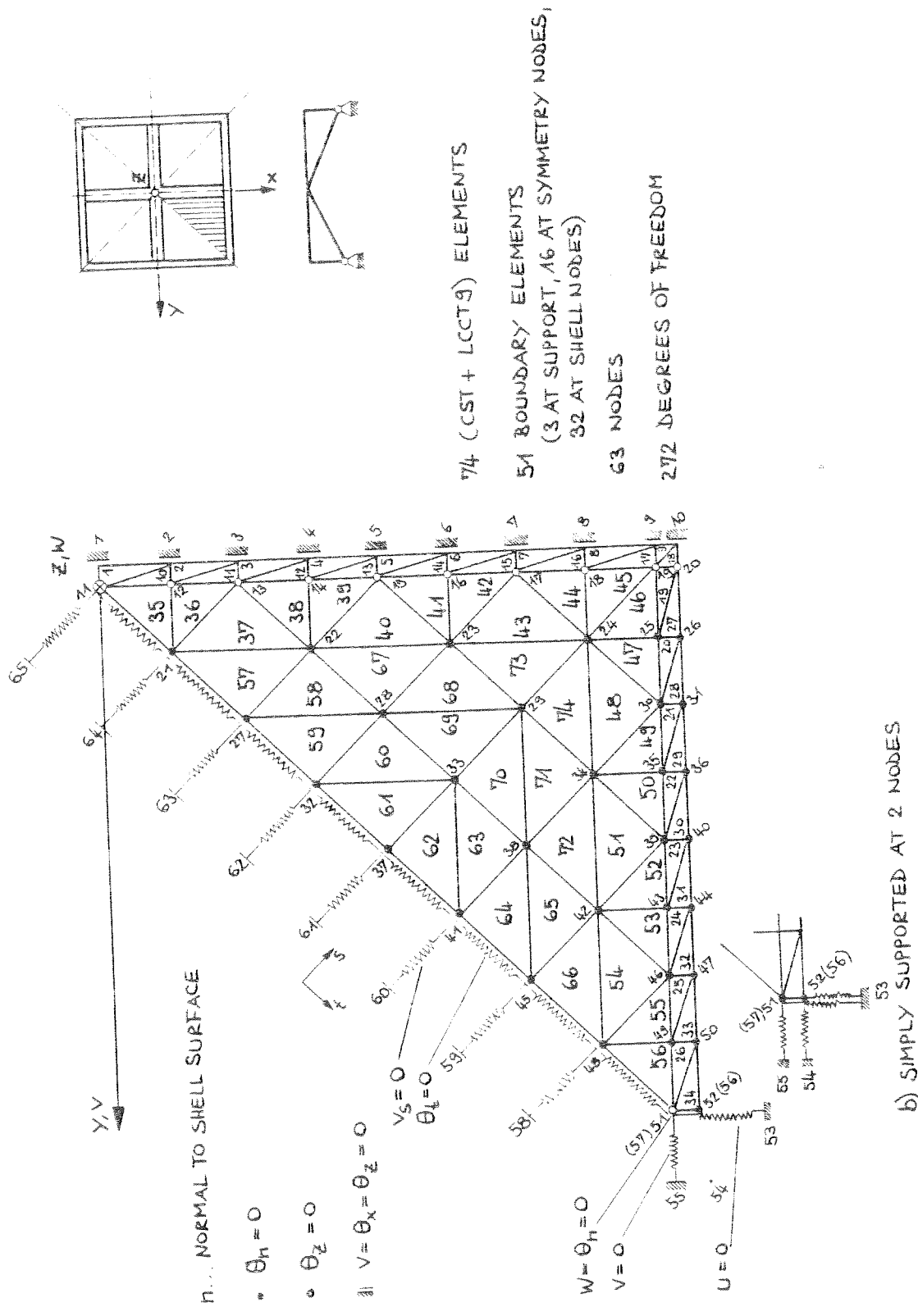
FIG. 5.2   GABLE SHELL — FINITE ELEMENT MESH LAYOUT

b) SIMPLY SUPPORTED AT 2 NODES

74 (CST + LCCT9) ELEMENTS

51 BOUNDARY ELEMENTS
(3 AT SUPPORT, 16 AT SYMMETRY NODES,
32 AT SHELL NODES)

63 NODES

272 DEGREES OF FREEDOM

n... NORMAL TO SHELL SURFACE

• $\theta_n = 0$

◦ $\theta_z = 0$

‖ $v = \theta_x = \theta_z = 0$

$v_s = 0$
$\theta_t = 0$

$w = \theta_n = 0$

$v = 0$

$u = 0$

FIG. 5.3 INVERTED UMBRELLA SHELL - FINITE ELEMENT MESH LAYOUT
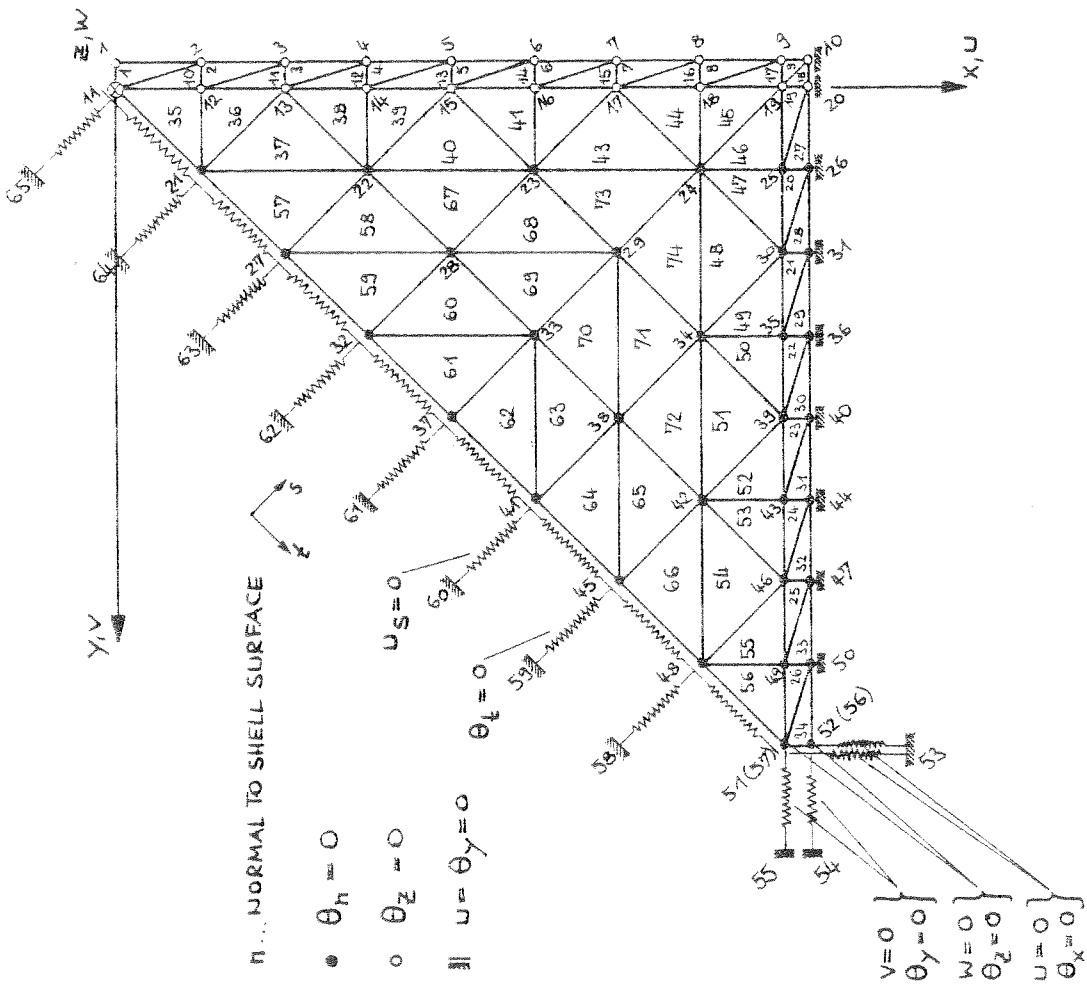
74 (CST + LCCT 9) ELEMENTS

52 BOUNDARY ELEMENTS
(6 AT SUPPORT, 16 AT SYMMETRY NODES,
30 AT SHELL NODES)

65 NODES

274 DEGREES OF FREEDOM

n... NORMAL TO SHELL SURFACE

● $\theta_n = 0$

○ $\theta_z = 0$

☰ $u = \theta_y = 0$

$U_s = 0$

$\theta_t = 0$

$v = 0$, $\theta_y = 0$

$w = 0$, $\theta_z = 0$

$u = 0$, $\theta_x = 0$
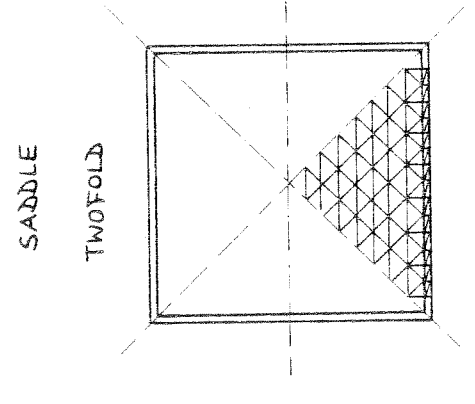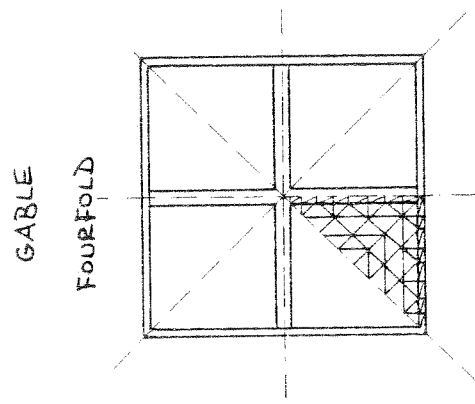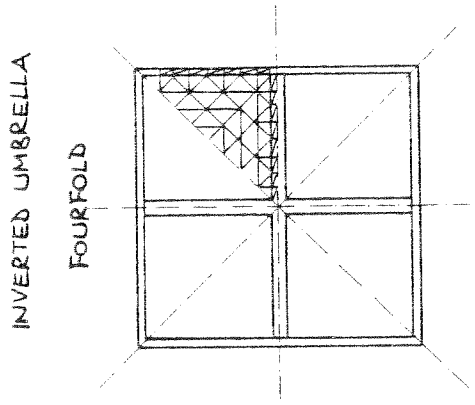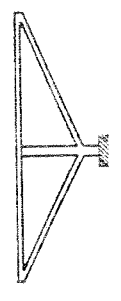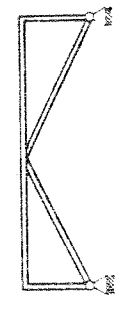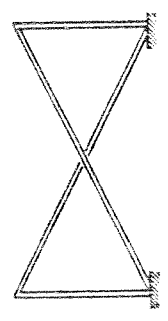
SYMMETRY:	SADDLE TWOFOLD	GABLE FOURFOLD	INVERTED UMBRELLA FOURFOLD
PLAN:			
ELEVATION:			
(CST + LCCT 9) ELEMENTS:	105	74	74
BOUNDARY ELEMENTS:	58	51	52
NODES:	77	63	65
DEGREES OF FREEDOM:	373	272	274

FIG. 5.4 FINITE ELEMENT IDEALISATIONS - COMPARISON
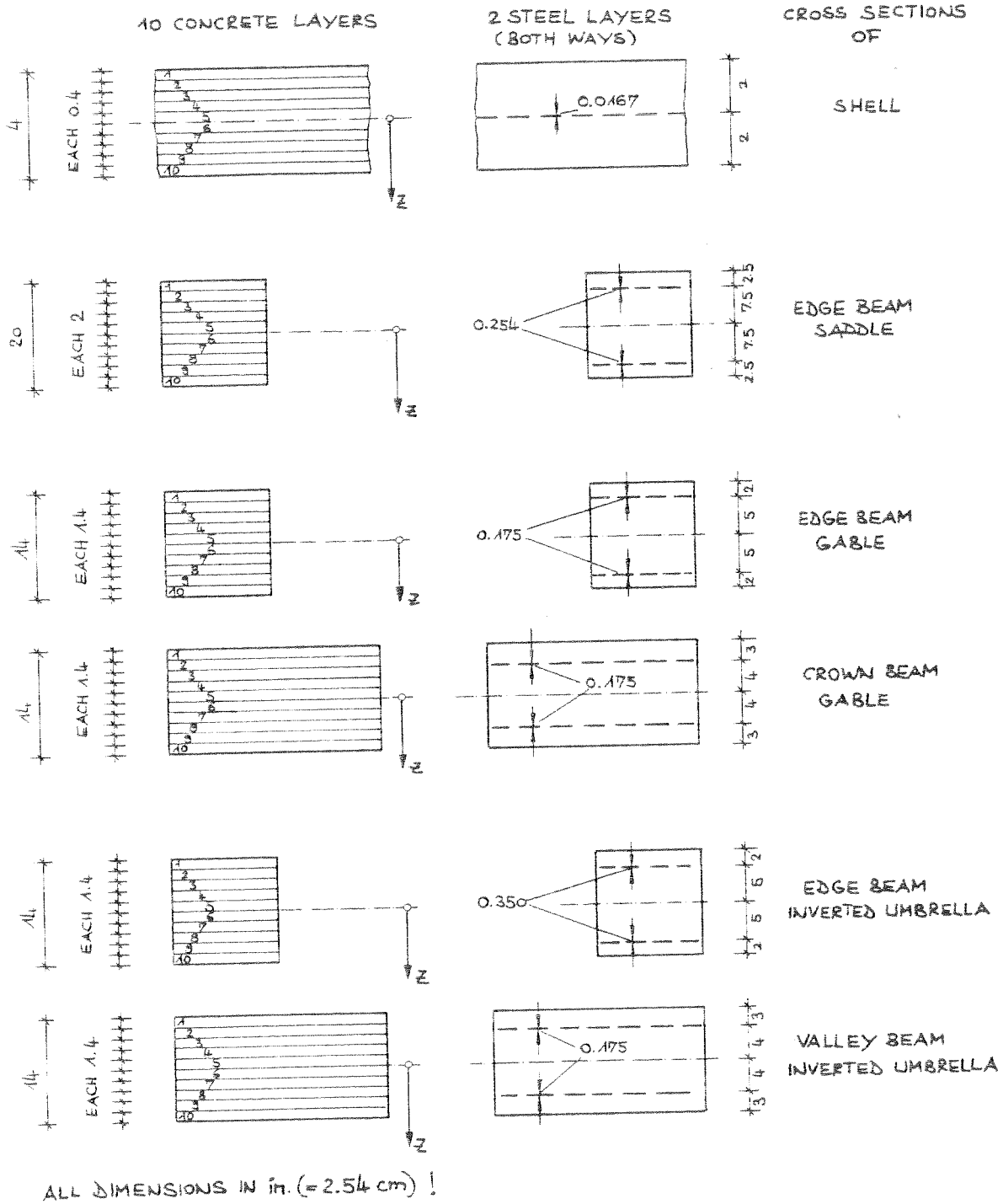
FIG. 5.5   LAYER SYSTEMS

the results are presented in Fig. 5.6 and Fig. 5.7.

5.2 Material Properties

The material properties are chosen as follows (Fig. 5.8)

Concrete:

unit weight	:	150 pcf (2400 kg/m^3)
uniaxial initial tangent modulus:		E_0 = 3330 ksi (23.0 KN/mm^2)
uniaxial compressive strength	:	f'_c = 3.0 ksi (20.7 N/mm^2)
strain at compressive strength	:	ε_c = 0.0018
uniaxial tensile strength	:	f'_t = 471 psi (3.25 N/mm^2)
ultimate strain in tension	:	ε_{tu} = 0.0005
Poisson's ratio	:	ν = 0.15
cracked shear constant	:	β = 0.5

ε_{tu} being 0.0005 a slight tension stiffening effect is taken into account.

Steel: (elastic-perfectly plastic)

modulus of elasticity before yielding: E_s = 29000 ksi (199.8.KN/mm^2)

modulus of elasticity after yielding : E_{sh} = 0

yield strength : f_y = 60 ksi   (411.6 N/mm^2)

5.3 Consideration of Creep and Shrinkage

It is assumed that the structures are subjected to a dead load DL from 28 to 180 days after casting. Then they are loaded by multiples of uniformly distributed live load LL. The time period is divided in 6 time steps: 28 - 32 - 40 - 60 - 100 - 140 - 180 days. Within the time steps the stresses are assumed to be constant. Standard values recommended by ACI Committee 209 [18] based on extensive studies by Branson and his

24

64 (Q-18)-ELEMENTS

32 BEAM ELEMENTS

55 BOUNDARY ELEMENTS
(6 AT SUPPORTS, 49 AT SHELL NODES)

87 NODES

486 DEGREES OF FREEDOM

$u = \theta_x = 0$
$v = \theta_y = 0$
$w = \theta_z = 0$

x, u

z, w

$\theta_n = 0$

y, v

$v = \theta_x = 0$
$w = \theta_z = 0$

$v = \theta_y = 0$

SAP IV [15]

n ... NORMAL TO THE SHELL SURFACE

48 (CST + LCCT9) - ELEMENTS

24 BOUNDARY ELEMENTS
(AT THE SHELL NODES)

34 NODES

166 DEGREES OF FREEDOM

$\begin{cases} u = v = w = 0 \\ \theta_x = \theta_y = \theta_z = 0 \end{cases}$

y, v

$u = \theta_x = \theta_z = 0$

z, w

$v = \theta_x = \theta_z = 0$

$\theta_n = 0$

x, u

NARCS [14]

FIG. 5.6   SADDLE SHELL - OTHER IDEALISATIONS
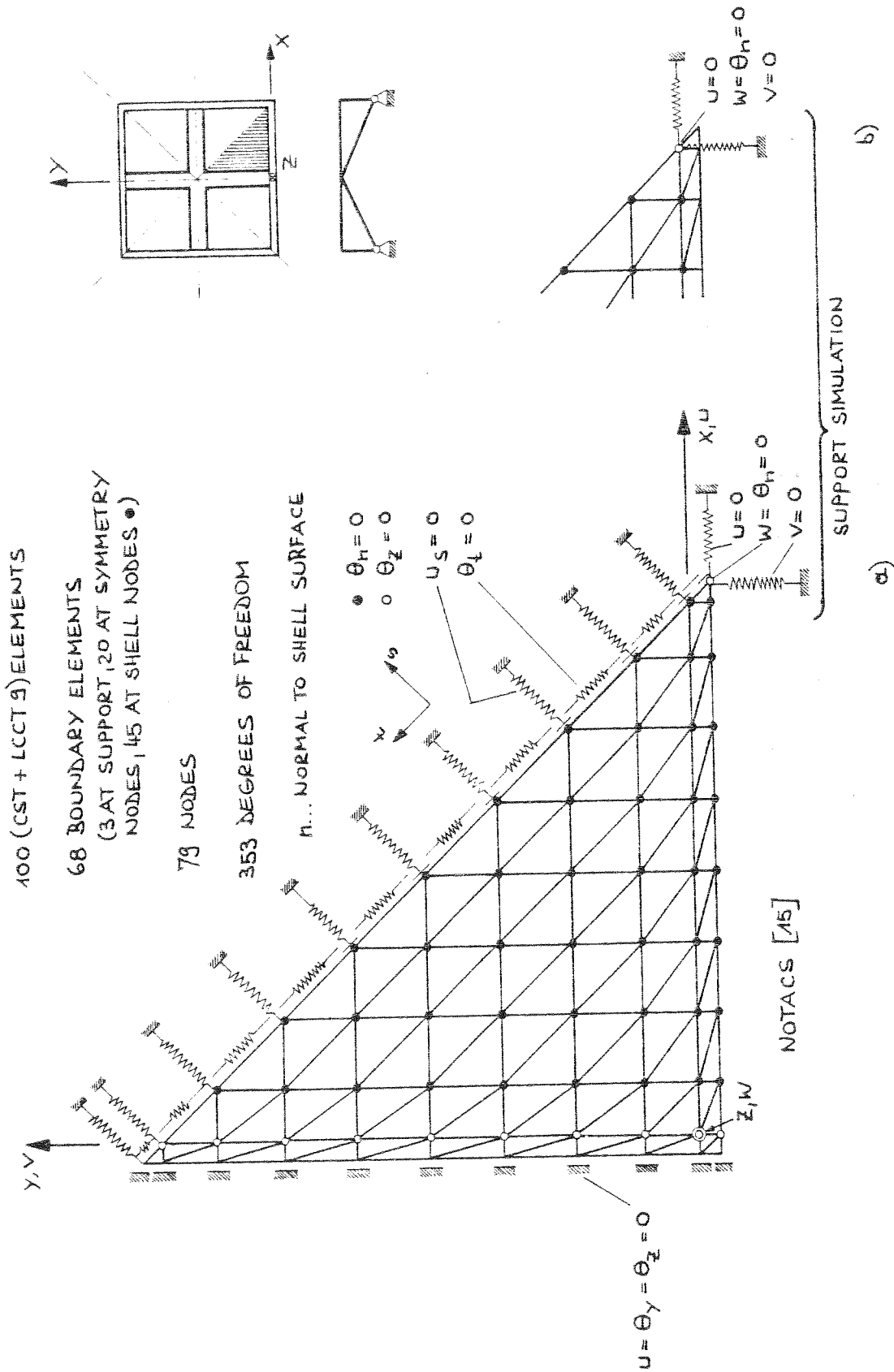
FIG. 5.7 GABLE SHELL – OTHER IDEALISATION

(a) UNAXIAL STRESS-STRAIN RELATION FOR CONCRETE

(b) STRESS-STRAIN RELATION FOR STEEL

$$ksi = 6.9 \ N/mm^2$$
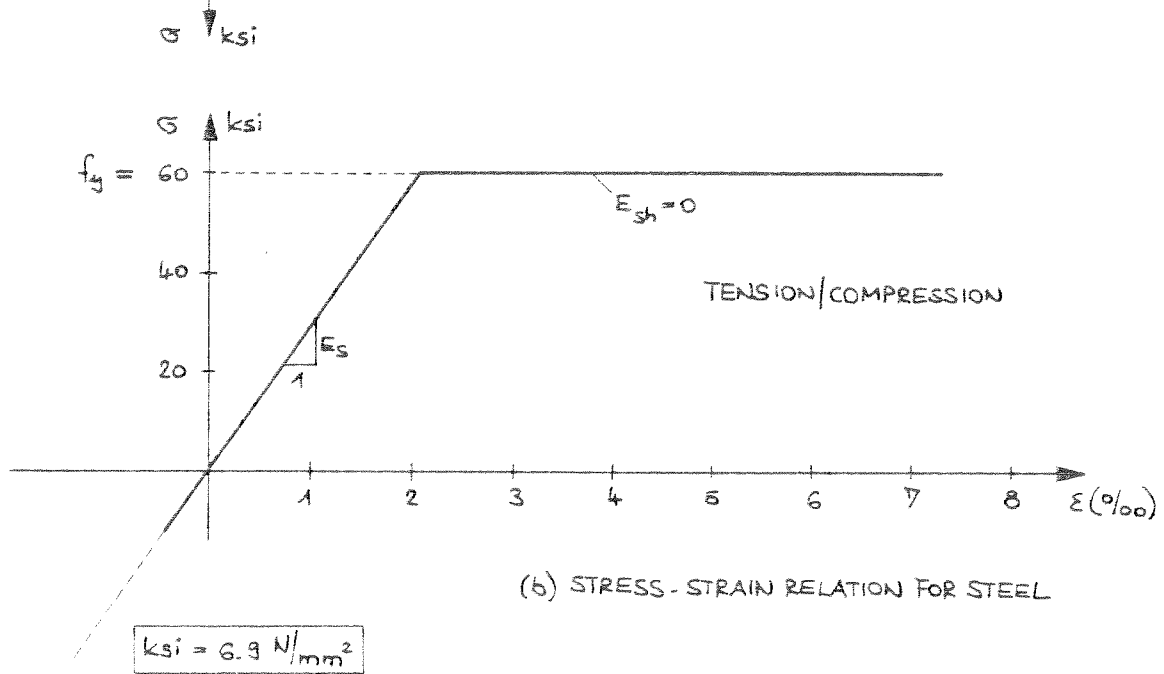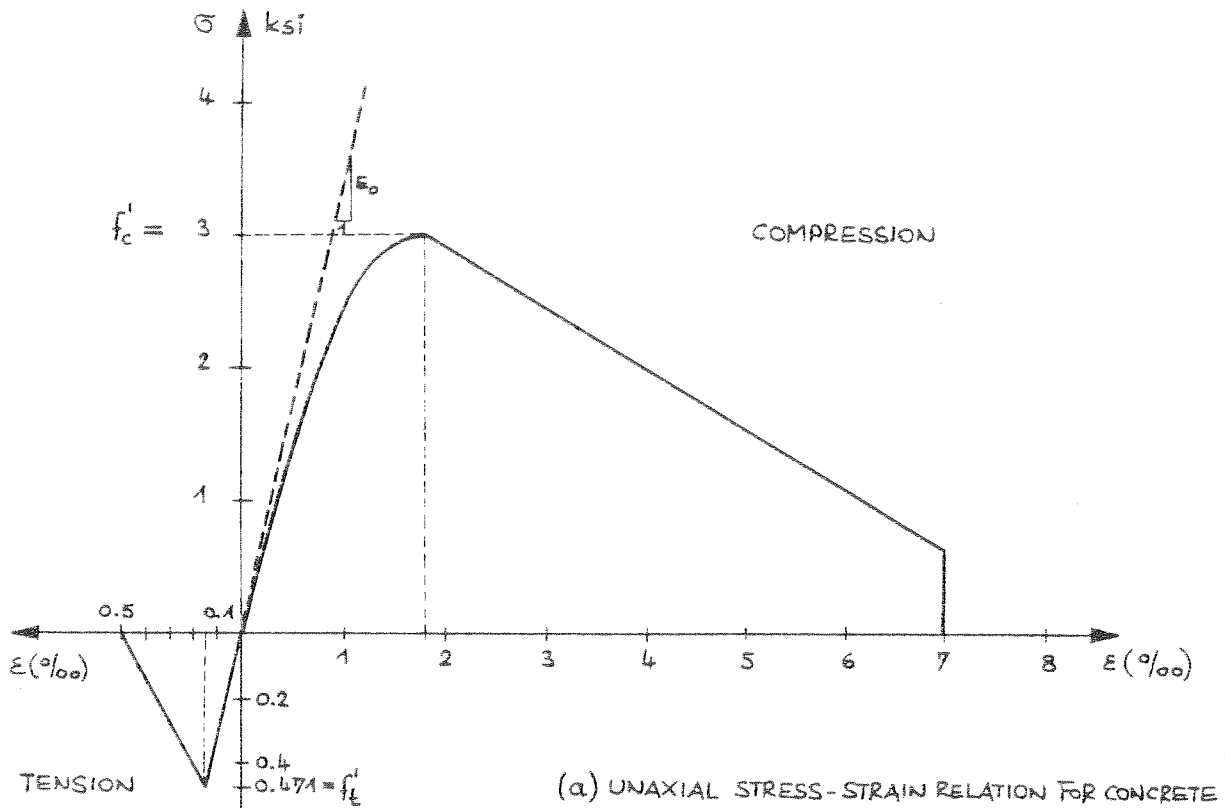
FIG. 5.8 MATERIAL PROPERTIES STRESS-STRAIN RELATIONS

colleagues [21] have been used to describe the time dependent behavior.

6.   SADDLE SHELL

6.1   Linear Analysis

Linear analyses are performed

a)   to check the reliability of the finite element model

b)   to study the behavior of the structures in the linear regime

The structures are loaded by dead load DL   150 = pcf(2400 kg/m^3) and live load LL = 20 psf (960 N/m^2).

In Fig. 6.1 some results obtained with NOTACS are compared with other solutions based on SAP and NARCS (see [14]). The finite element discretizations for these solutions are shown in Fig. 5.6. The NOTACS solution compares well with the SAP solution, which can be expected to be the best approach. Compared to the NARCS solution, which uses the same element, a considerable improvement is achieved.

Analyses were also carried out for nodal loads instead of distributed loads and without boundary elements fixed at the shell nodes. The differences in the results were less than 10%. The following analyses are all based on the original idealization.

The sketch in Fig. 6.2 serves as a rough check of the equilibrium. The agreement is considered to be satisfactory.

In Fig. 6.3 separate solutions for dead load of shell, dead load of beam and live load demonstrate the big influence of the edge beam weight. Undoubtedly the edge beam is carried by the shell structure. Without support of the shell the beam deflections due to its weight would be six times as large and the bending moments would be even larger, namely ten
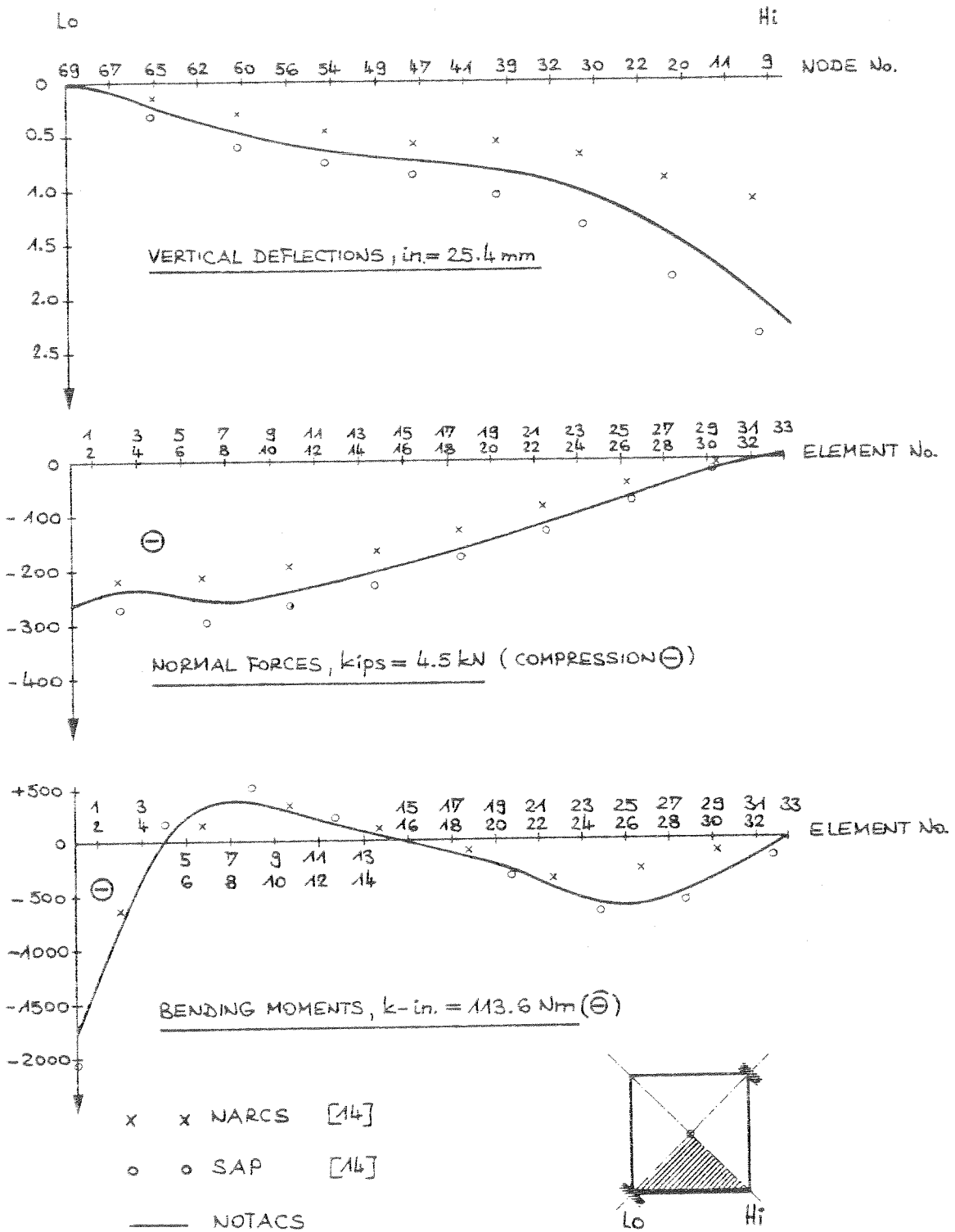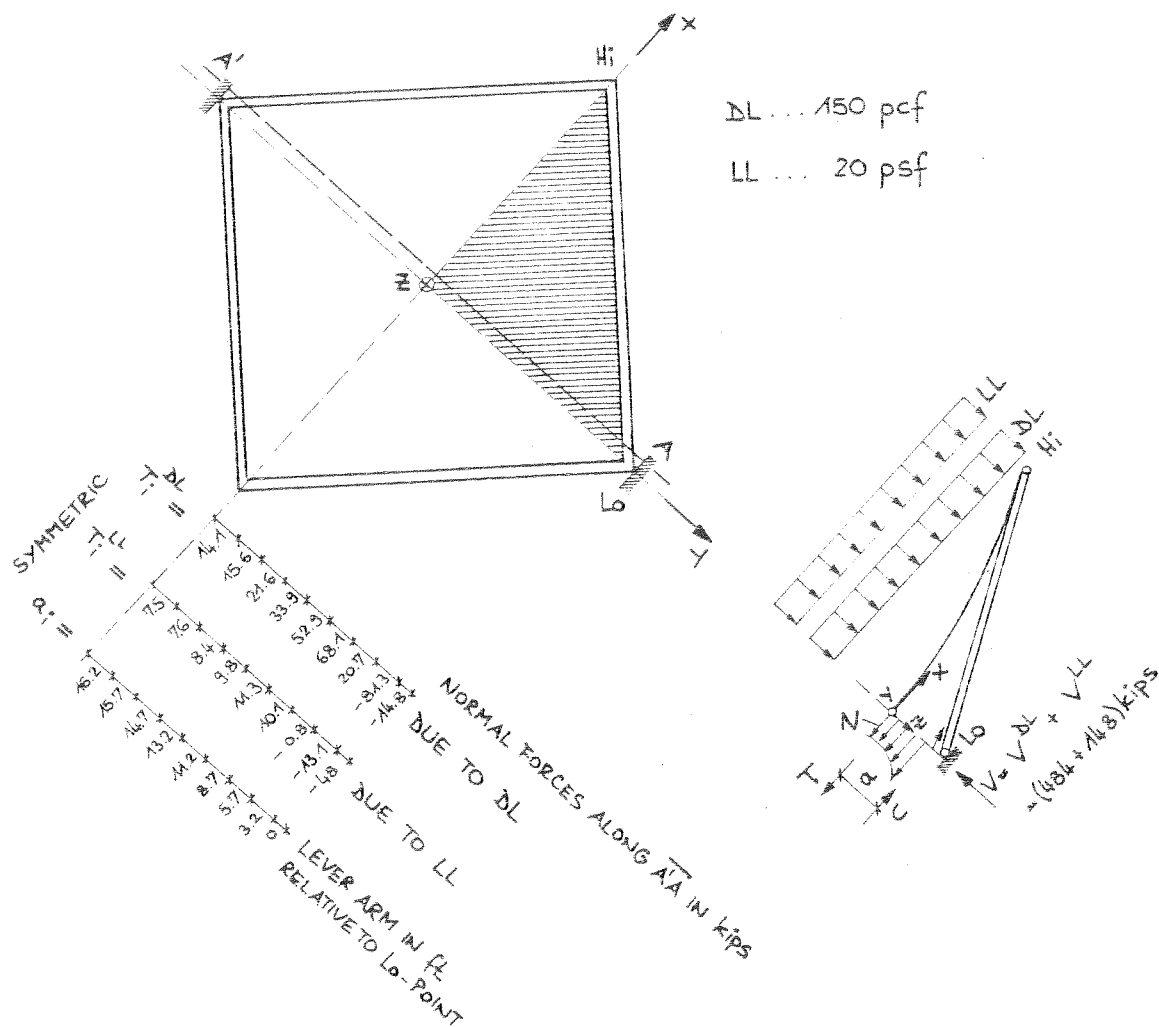
FIG. 6.1 SADDLE SHELL - EDGE BEAM , LINEAR ANALYSIS

DL ... 150 pcf

LL ... 20 psf

SYMMETRIC

$T_i^{DL} =$

$T_i^{LL} =$

$a_i =$

NORMAL FORCES ALONG $\overline{A'A}$ IN kips

DUE TO DL

DUE TO LL

LEVER ARM IN ft.
RELATIVE TO L_o-POINT

$V = V^{DL} + V^{LL}$
$= (484 + 148) kips$

(a) VERTICAL FORCES (1/4 TH OF THE SHELL)

DL $\triangleq$ 114 kips
LL $\triangleq$ 35 kips

REACTION

$V^{DL} = 121$ kips
$V^{LL} = 37$ kips

(b) MOMENTS ALONG A'A

DUE TO DL : 4800 k-ft
DUE TO LL : 1350 k-ft

$\sum_{i=1}^{9} a_i T_i^{DL} = 5022$ k-ft

$\sum_{i=1}^{9} a_i T_i^{LL} = 1366$ k-ft

(c) HORIZONTAL FORCES:

TENSION $T^{DL} = 454$ kips
TENSION $T^{LL} = 109$ kips

COMPRESSION $C^{DL} = 460$ kips
COMPRESSION $C^{LL} = 122$ kips

FIG. 6.2 SADDLE SHELL - ROUGH STATICAL CHECK

Lo
Hi

VERTICAL DEFLECTIONS, in. = 25.4 mm

NORMAL FORCES, kips = 4.5 kN (COMPRESSION ⊖)

MEMBRANE THEORY, DL + LL (= 85 psf)

BENDING MOMENTS, k-in. = 113.6 Nm (⊖)

1) ——— DL SHELL
2) — — — DL EDGE BEAM
3) LL
4) —·— 1) + 2) + 3)

Lo   Hi
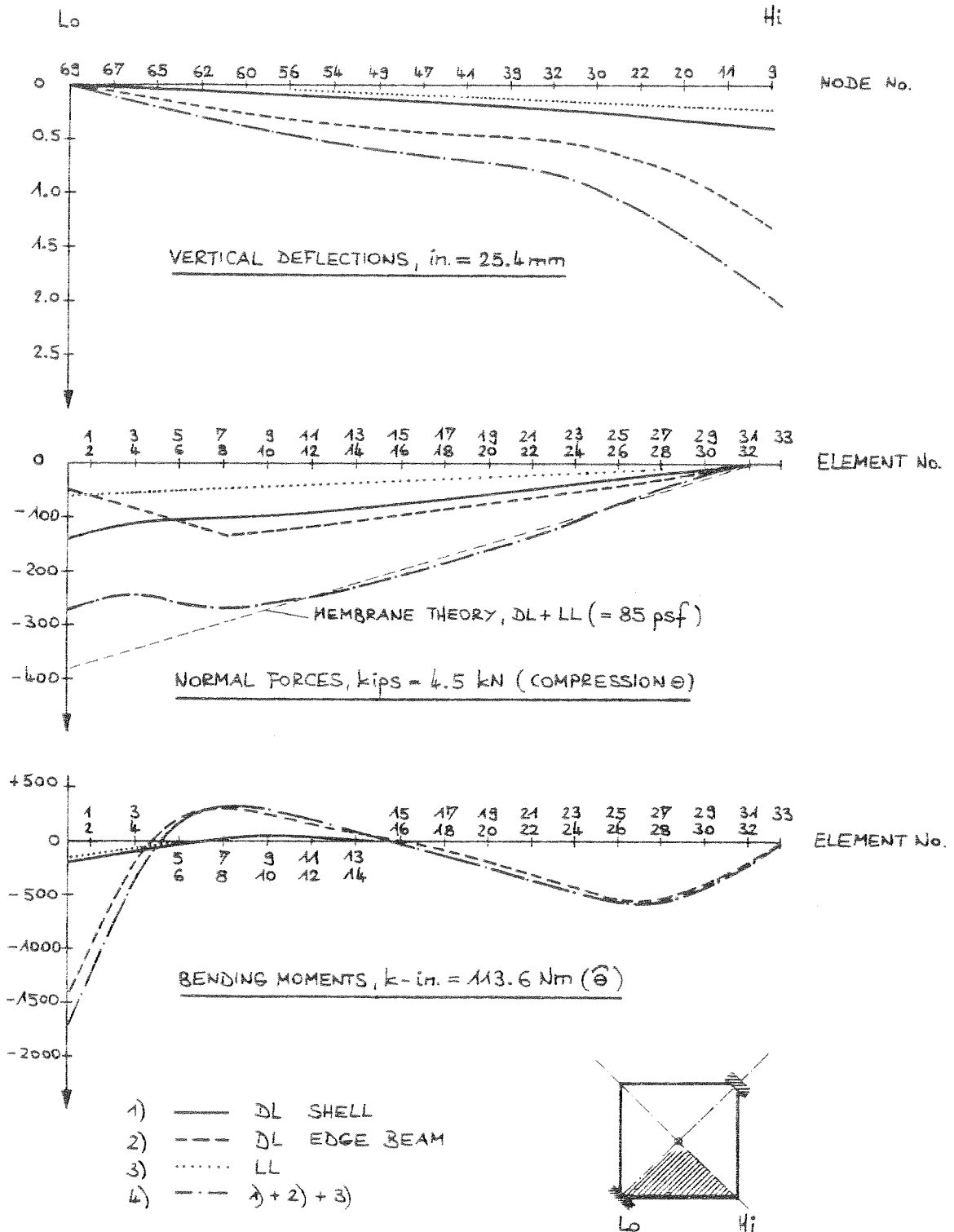
FIG. 6.3   SADDLE SHELL - EDGE BEAM, LINEAR ANALYSIS

times as large.

Membrane theory predicts normal forces quite well.

6.2 Nonlinear Analysis

According to the linear analyses the first cracks could be expected at a load of about DL + 4 LL. Additional nonlinear analyses starting from this load level with increments of 1.0 LL and 0.5 LL showed that the load deflection curve remains nearly linear up to DL + 7.5 LL. For this reason a final run was started at DL + 7.5 LL. Then, two increments of 0.25 LL followed by increments of half that size were added.

In Table 6.1 and Fig. 6.4 load-deflection relations for several points are presented numerically as well as graphically. Table 6.1 shows a fast convergence for loads smaller than DL + 8.0 LL. As a convergence criteria an increase of 10% of the value of the vertical deflection increment of the first iteration was used. Additionally the remaining unbalanced forces were checked. They turned out to be small compared to the total nodal forces. At the load level of DL + 8.125 LL even with 30 iterations, no convergence could be reached. The same is true for DL + 8.250 LL. Therefore the solution was stopped.

To prove that at DL + 8 LL the ultimate capacity is reached, additional indications have to be considered. First of all, from a practical point of view the ultimate state is reached because the permissible deflections are probably exceeded and it is questionable if a further calculation without taking into account geometric nonlinearities is admissible.

A first hint is given by the development of the deflection increments which is graphically displayed in Fig. 6.5. There it can be seen that the values oscillate with a tendency to increase.

TABLE 6.1 SADDLE SHELL LOAD-DEFLECTION RELATION, NODE 10

LOAD INCREMENT * DL+	TOTAL LOAD * DL+	NUMBER OF ITERATIONS	DEFLECTION NODE 10 (in. = 25.4mm)	DEFLECTION INCREMENT (in. = 25.4mm)
7.750 LL	7.750 LL	1	3.747	
		2	4.192	0.445
		3	4.261	0.069
0.125 LL	7.875 LL	1	4.307	0.046
		2	4.314	0.007
		3	4.316	0.002
0.125 LL	8.000 LL	1	4.364	0.048
		2	4.368	0.004
0.125 LL	8.125 LL	1	4.418	0.050
		2	4.425	0.007
		3	4.431	0.006
		4	4.437	0.006
		5	4.444	0.007
		6	4.455	0.011
		7	4.470	0.015
		8	4.496	0.026
		9	4.543	0.047
		10	4.674	0.131
		11	5.111	0.437
		12	5.755	0.644
		13	6.113	0.358
		14	6.356	0.243
		15	6.470	0.114
		16	6.590	0.120
		17	6.778	0.188
		18	7.097	0.319
		19	7.511	0.414
		20	7.974	0.463
		21	8.414	0.440
		22	8.746	0.332
		23	9.034	0.288
		24	9.371	0.337
		25	9.822	0.451
		26	10.422	0.600
		27	10.809	0.387
		28	11.146	0.237
		29	11.533	0.387
		30	11.889	0.356
0.125 LL	8.250 LL	1	12.340	0.351
		2	12.547	0.207
		3	12.663	0.116
		4	12.768	0.105
		5	12.881	0.113
		6	12.997	0.116
		7	13.096	0.099
	STOP	8	13.205	0.109

* ... MULTIPLES OF LIVE LOAD LL = 20psf (= 960 N/m²)
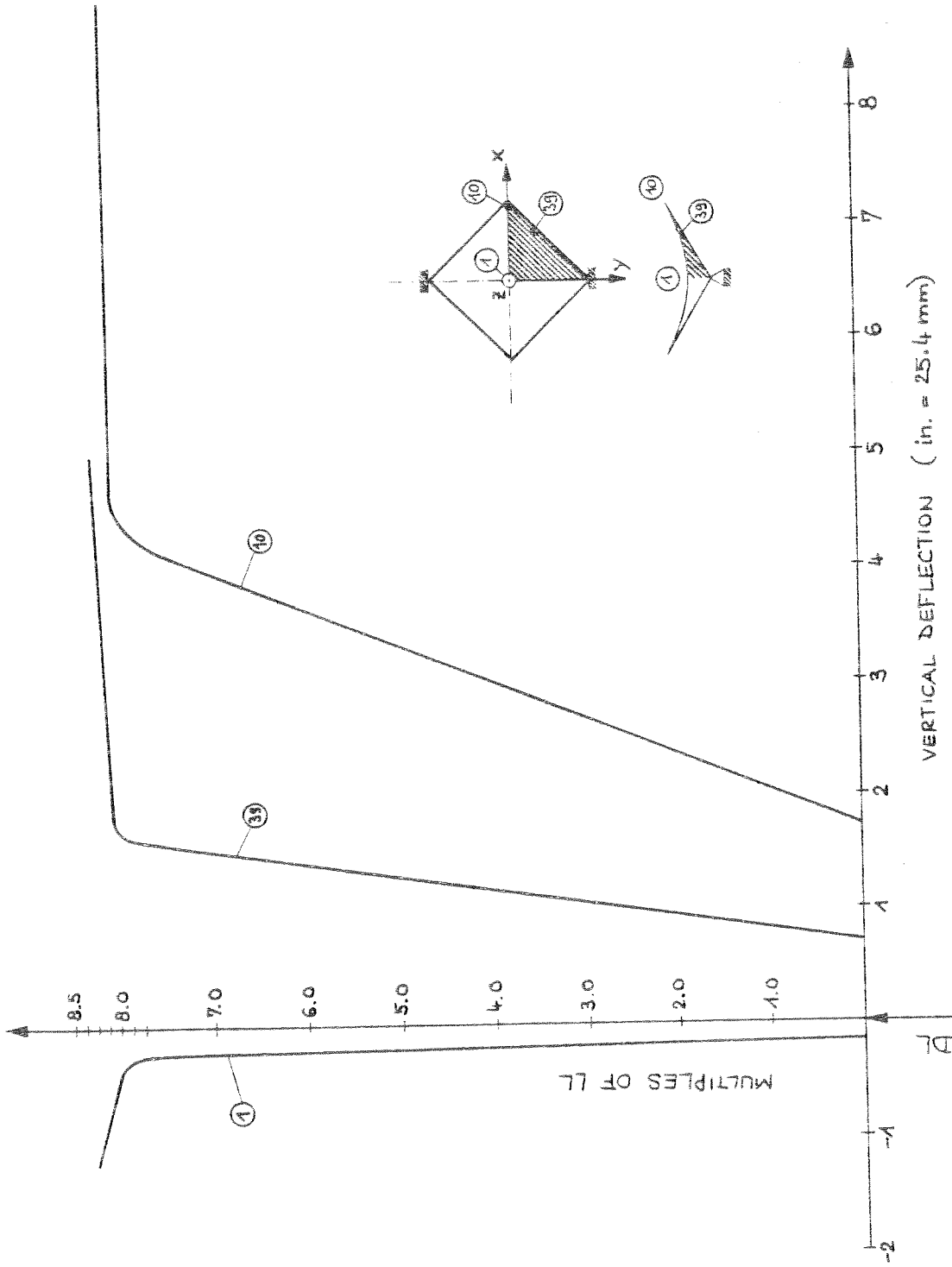
FIG. 6.4 SADDLE SHELL, LOAD-DEFLECTION-CURVES
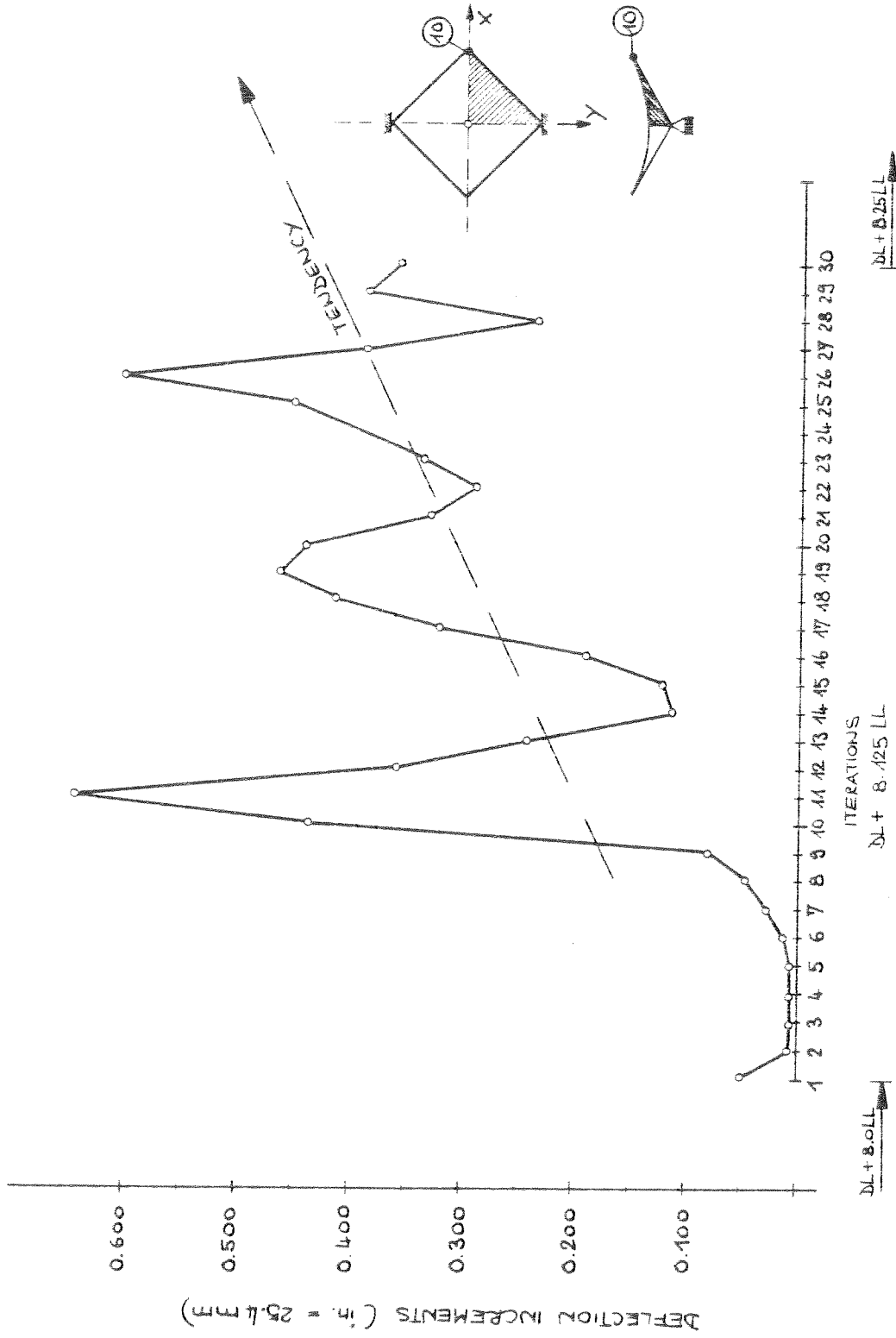
FIG. 6.5 SADDLE SHELL - DEFLECTION INCREMENTS

From Fig. 6.6 and Fig. 6.7 a sudden increase of the bending moments at the load level DL + 8.0 LL can be ascertained. This is to be seen in connection with Fig. 6.8. There one can recognize that the ultimate normal force (yield force) is reached in cross sections parallel to the center section between the two abutment supports (see also Fig. 6.9), i.e., additional load cannot be taken any more by shell membrane force and hence this load is shifted to the beams causing a sudden increase of the beam bending moments. The beams are not designed for this loading and lead to the total collapse of the structure. Assuming as an approximation, pure bending, the ultimate capacity would be approximately 4000 k-in. (454 KN-m) from which 75% is already needed. The rest of 1000 k-in. (113.6 KN-m) could be used to carry additional loading. As the shell does not contribute any more, the additional loading is only about 0.2 LL. Because the beams are also subjected to torsional moments and normal forces the additional capacity is probably less, if not negligible, i.e., the ultimate load is approximately DL + 8.0 LL.

In Fig. 6.10 to 6.13 crack patterns at various levels of loading are shown. It is interesting to note that the first cracks do not appear in the center section between the two abutment supports, but parallel to it in a region nearer to the tip region where the curvature of the shell is still small and therefore bending stresses prevail. With additional load increments the cracks spread and progress through the depth. However, these cracks have little influence on the overall behavior which remains almost linear up to DL + 8.0 LL. Then, immediately the cracks propagate throughout the depth and cause the steel reinforcement to yield.
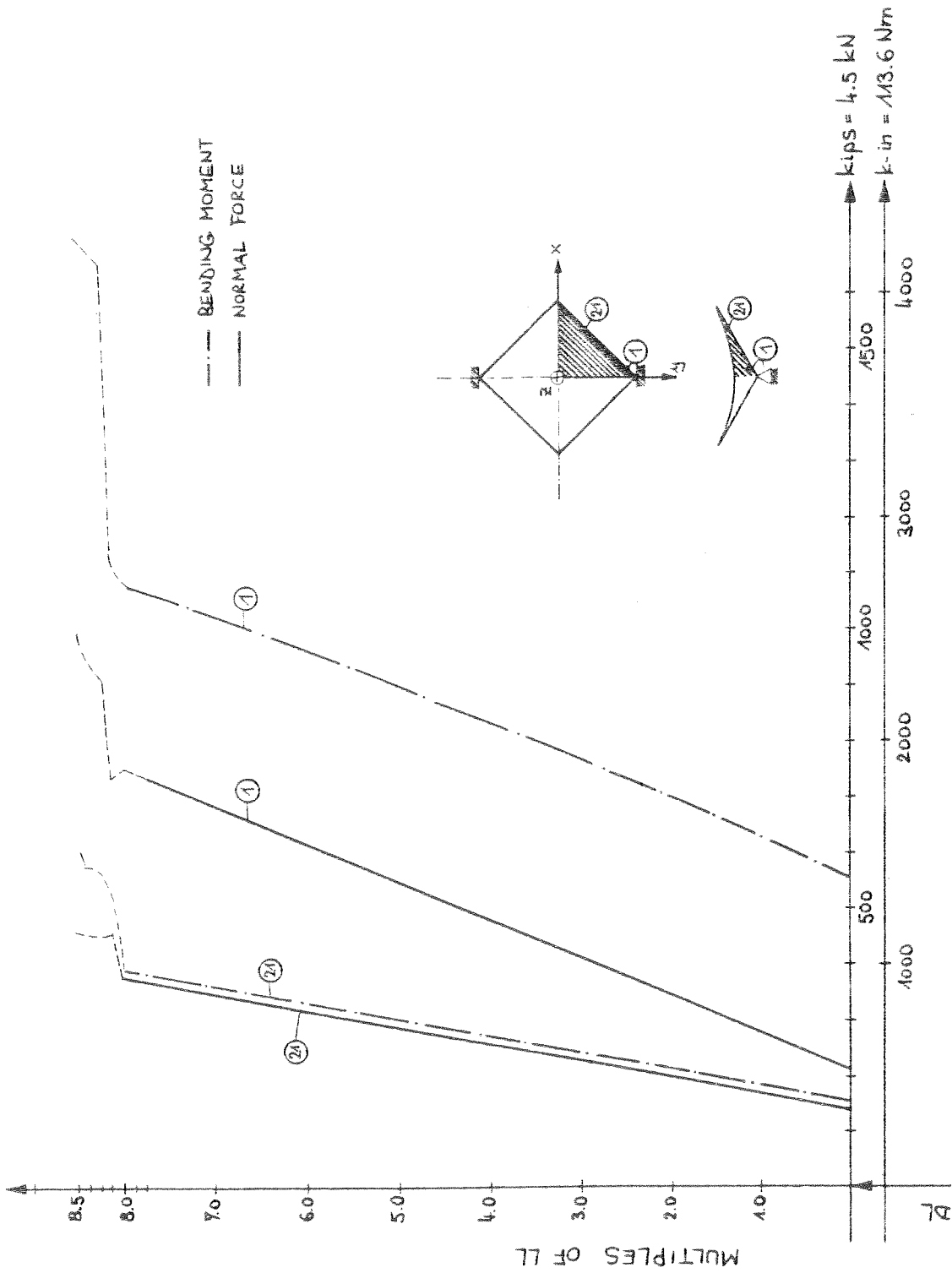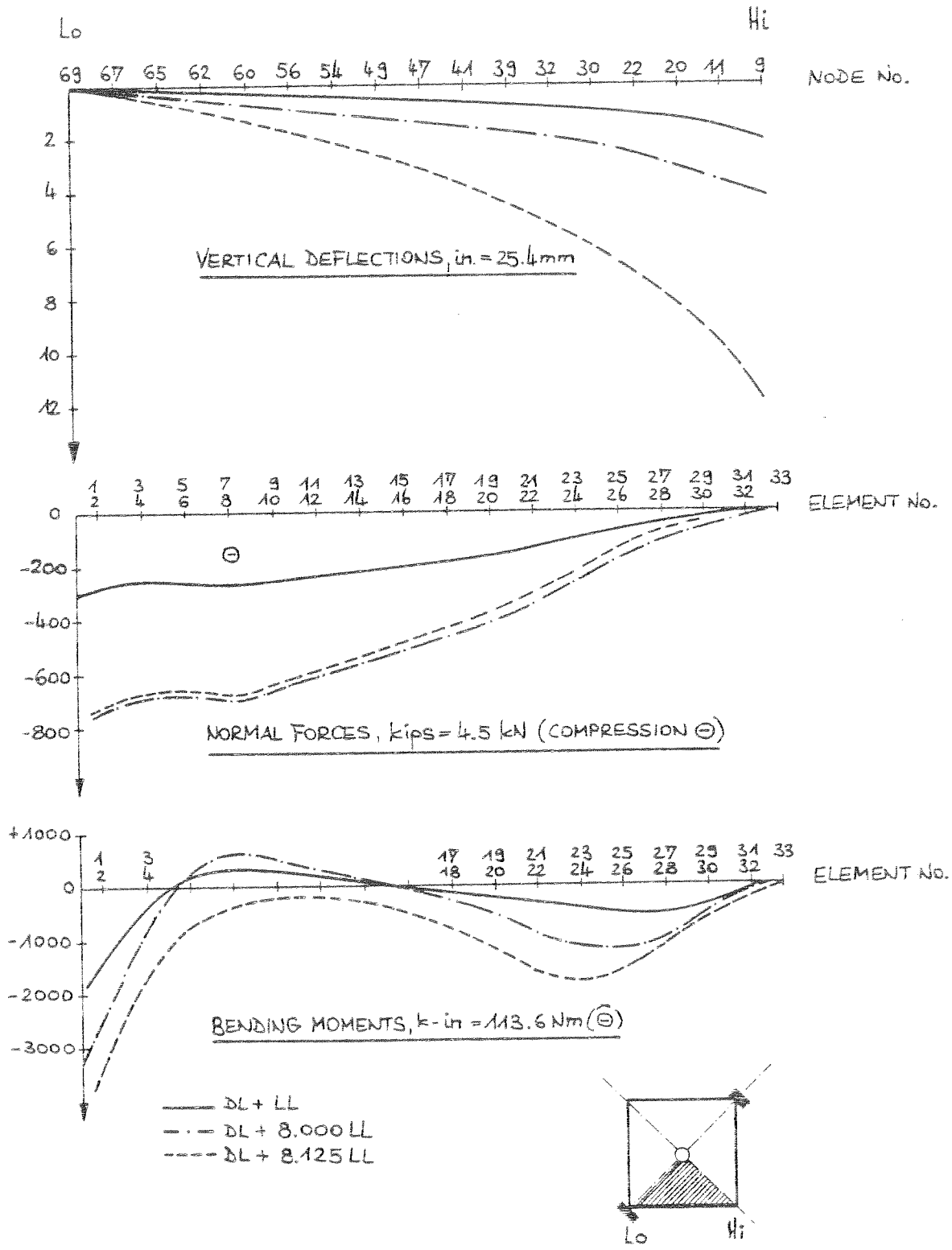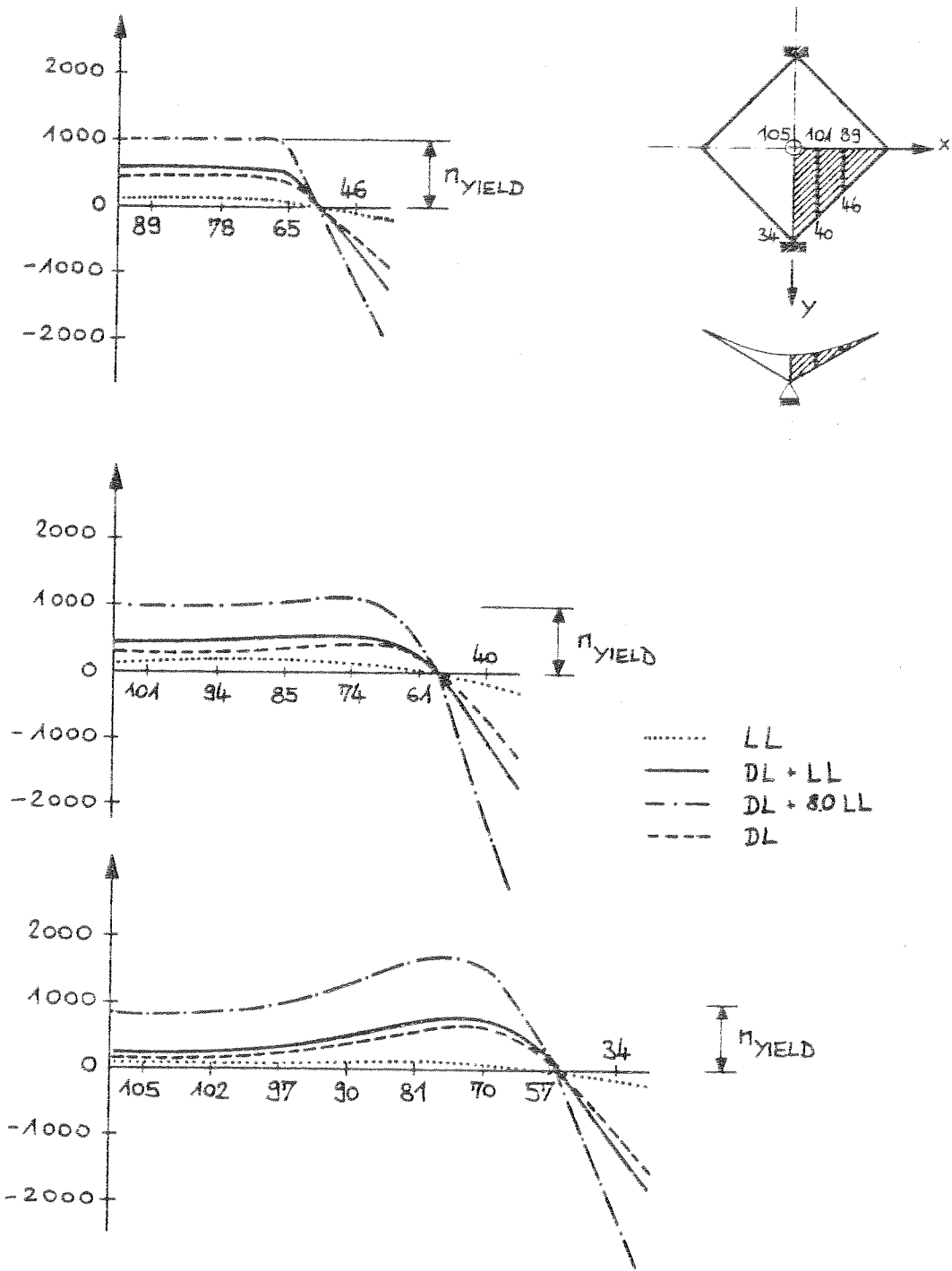
FIG. 6.6   SADDLE SHELL - LOAD-STRESS- RESULTANT CURVES

Lo   Hi

69 67 65 62 60 56 54 49 47 41 39 32 30 22 20 11 9   NODE No.

VERTICAL DEFLECTIONS, in. = 25.4mm

1   3   5   7   9   11 13 15 17 19 21 23 25 27 29 31 33
2   4   6   8   10 12 14 16 18 20 22 24 26 28 30 32   ELEMENT No.

NORMAL FORCES, kips = 4.5 kN (COMPRESSION ⊖)

17 19 21 23 25 27 29 31 33
1   3
2   4   18 20 22 24 26 28 30 32   ELEMENT No.

BENDING MOMENTS, k-in = 113.6 Nm (⊖)

———— DL + LL
—·—· DL + 8.000 LL
----- DL + 8.125 LL

Lo   Hi

FIG. 6.7 SADDLE SHELL - EDGE BEAM, NONLINEAR ANALYSIS

FIG. 6.8 SADDLE SHELL - NORMAL FORCES IN SHELL

DIMENSIONS IN Lbs/in. = 175 N/m

$n \uparrow (lbs/in = 175 \ N/m)$

CRACK NORMAL FORCE n_{CR}

2000

YIELD NORMAL FORCE n_y

1000

0.14 0.5 1 2 $\varepsilon (^o/_{oo})$

SHELL NORMAL FORCE - STRAIN RELATION

$\boxed{DL + 8.000 \ LL}$

$\boxed{DL + 8.000 LL + \Delta LL}$

ΔLL

$DL + 8.00 LL$

80

46

M_{BEAM}

STRAINS $\simeq (0.2 \div 0.25) \%$

STRAINS $\simeq 2 \ ^o/_{oo}$

ELEVATION

z x

n_y n_y

z x

TORSIONAL COMPONENT

M_{BEAM} FOR ΔLL

ULTIMATE STATE
$\rightarrow$ EQUILIBRIUM

y

ADDITIONAL LOADING ΔLL CAN
ONLY BE TAKEN BY BEAM BENDING
AND TORSIONAL MOMENTS, BUT, BEAM
IS NOT DESIGNED FOR THEM $\rightarrow$ FAILURE

y

PLAN

FIG. 6.9 SADDLE SHELL - ULTIMATE STATE

40

DL + 4.0 LL
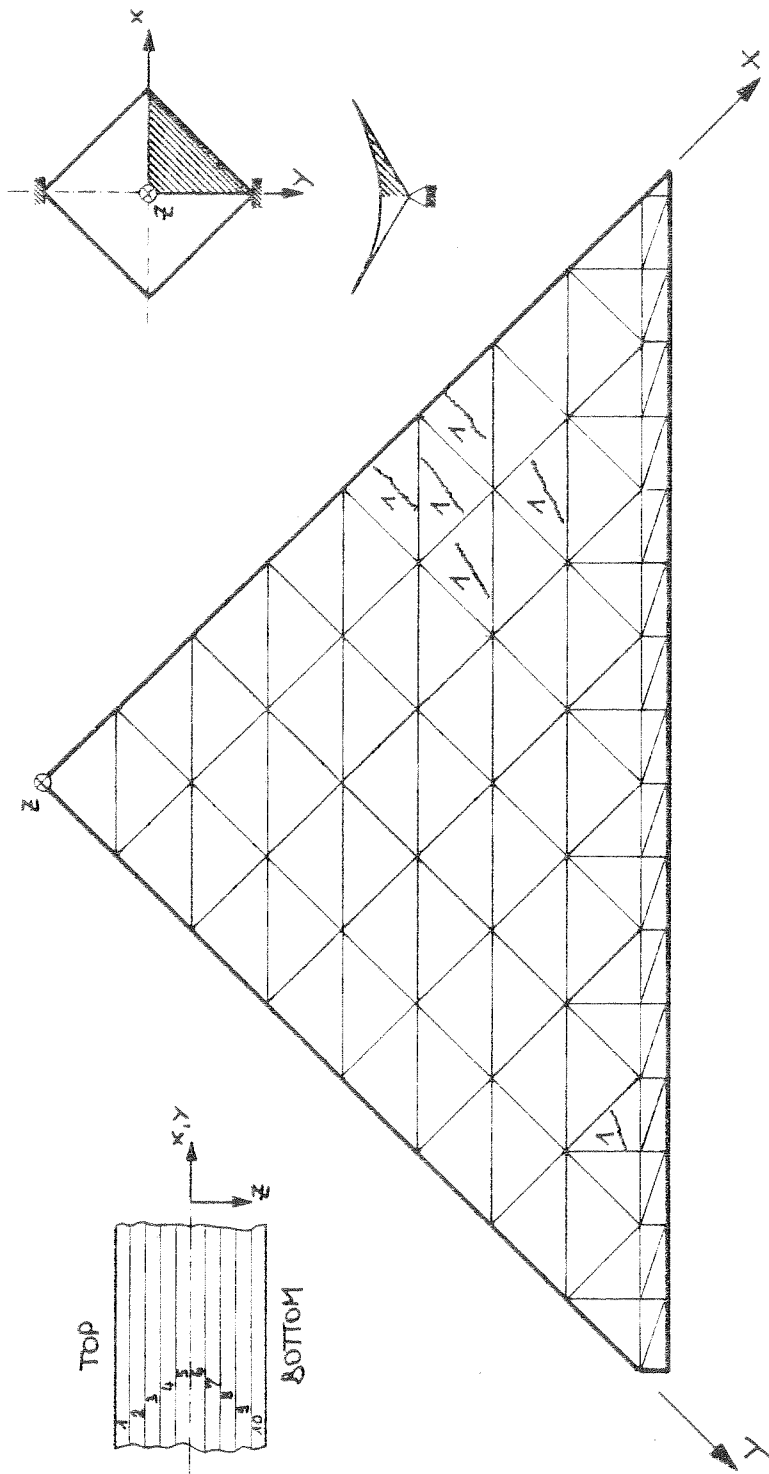
— CRACKS START AT THE TOP LAYER
  NUMBERS SHOW CRACKDEPTH

6.10 SADDLE SHELL - CRACK PROPAGATION, DEPTH AND AVERAGE DIRECTIONS

41

DL + 6.0 LL
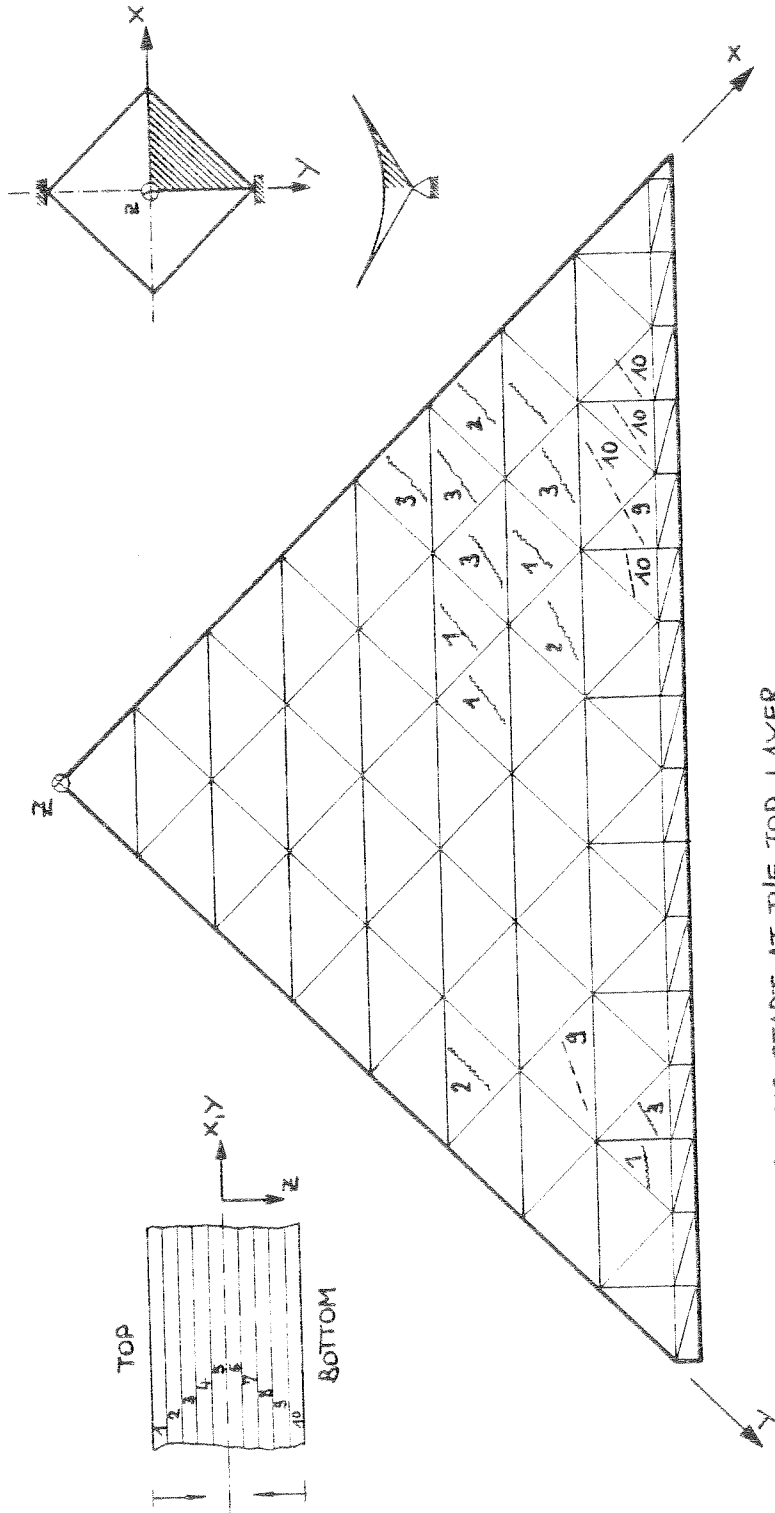
— CRACKS START AT THE TOP LAYER
— CRACKS START AT THE BOTTOM LAYER
----- NUMBERS SHOW CRACK DEPTH

6.11 SADDLE SHELL - CRACK PROPAGATION, DEPTH AND AVERAGE DIRECTIONS

DL + 8.0 LL
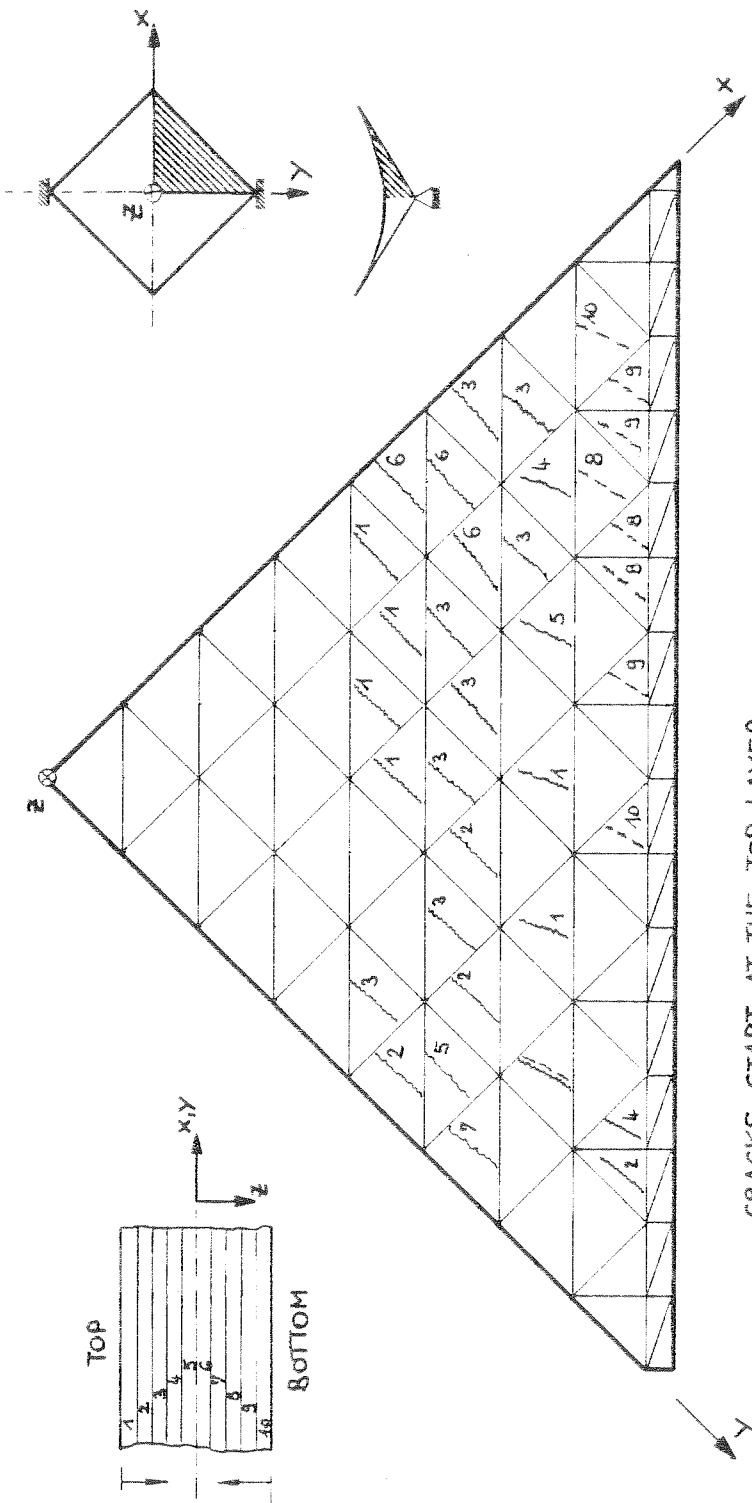
CRACKS START AT THE TOP LAYER

CRACKS START AT THE BOTTOM LAYER

COMPLETELY CRACKED BUT CONCRETE CONTRIBUTES STILL

NUMBERS SHOW CRACK DEPTH

6.12   SADDLE SHELL — CRACK PROPAGATION, DEPTH AND AVERAGE DIRECTIONS

DL + 8.125 LL

STEEL YIELDED

$\bar{x} \geq 27 f_t$

CONCRETE YIELDED

TOP

BOTTOM

—————— CRACKS START AT THE TOP LAYER

– – – – – CRACKS START AT THE BOTTOM LAYER

═══════ COMPLETELY CRACKED BUT CONCRETE CONTRIBUTES STILL

═══════ COMPLETELY CRACKED

NUMBERS SHOW CRACK DEPTH
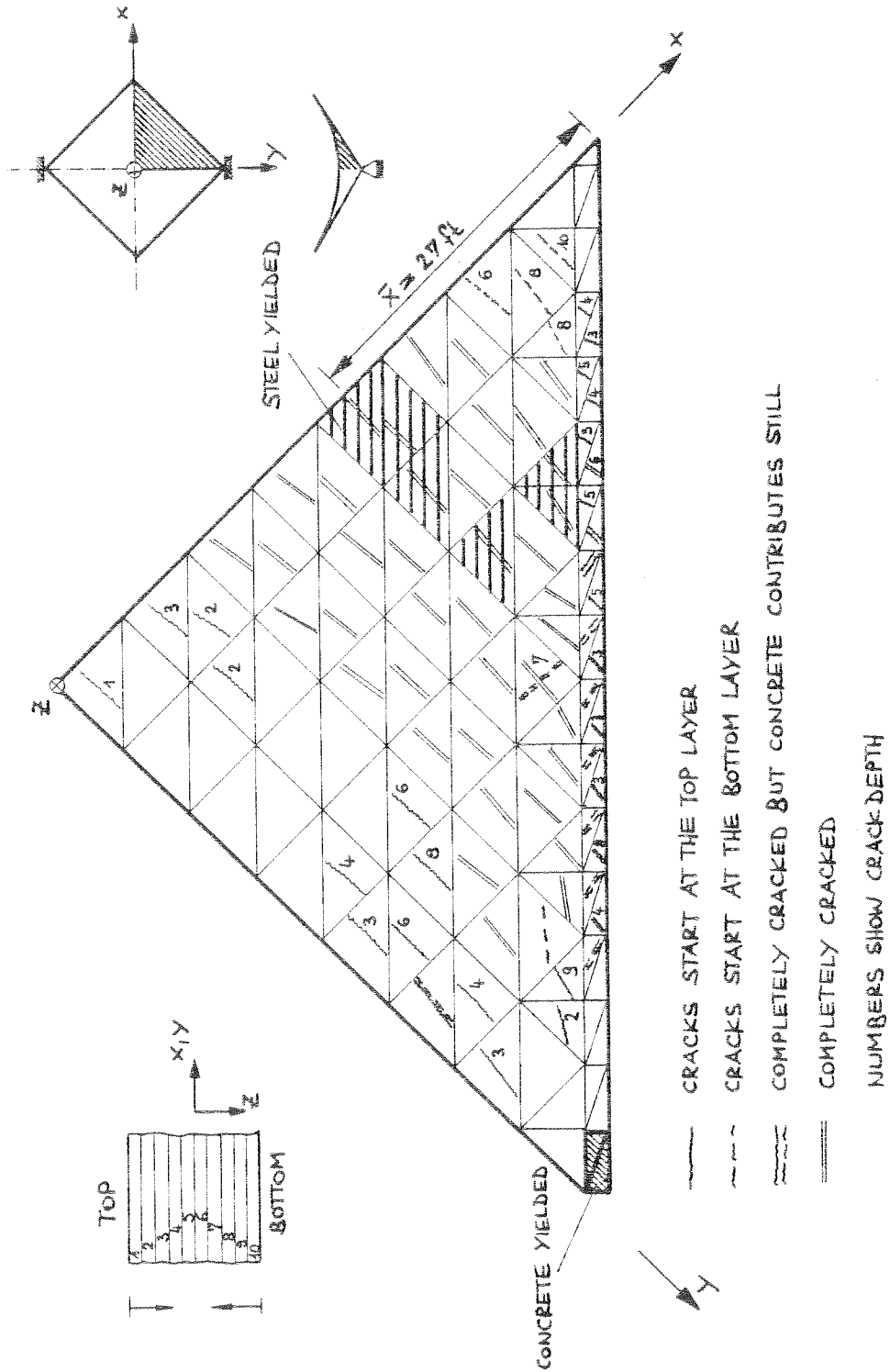
6.13 SADDLE SHELL CRACK PROPAGATION, DEPTH AND AVERAGE DIRECTIONS

A rough estimate on the basis of yield line theory is made in Fig. 6.14. Yield lines are assumed parallel to the center arc between the abutments. The internal moment is calculated by summing up the products of the ultimate normal force (yield force) and the appropriate lever arm. The external moment is determined as before in the statical check of the linear analysis. In the diagram the internal ultimate moment, the external moment and the ultimate bending moment capacity of the beams are compared. It can be seen that up to a distance of $\bar{x}$ = 16 ft (torsional moment not considered) from the tip the total load of DL + 8.0 LL can be carried by the beams. Then up to $\bar{x}$ = 30 ft the internal moment capacity due to the shell membrane forces is a little smaller than the external moment. For $\bar{x}$ > 30 ft the relation is reverse. That means, that according to yield line theory the ultimate load is of about DL + 8.0 LL and the yield lines can be expected to be in the region between 16 ft < $\bar{x}$ < 30 ft. This result is in good agreement with the result obtained by nonlinear analysis where yielding occurred at a distance of $\bar{x}$ = 27 ft from the tip (Fig. 6.13).

The previous comparisons have evoked no contradiction, hence it can be assumed that the ultimate load is DL + 8.0 LL.

6.3 Nonlinear Analysis Including Creep and Shrinkage

Creep and shrinkage is taken into account as described in Chapters 3 and 5.

In Fig. 6.15a the load deflection curve of the tip point is compared with the curve for instantaneous loading. The main difference is that the transition to the cracked state occurs at an earlier load level. As the reinforcing steel at that load level is not yet yielded an increase of the load up to DL + 8.0 LL is still possible.
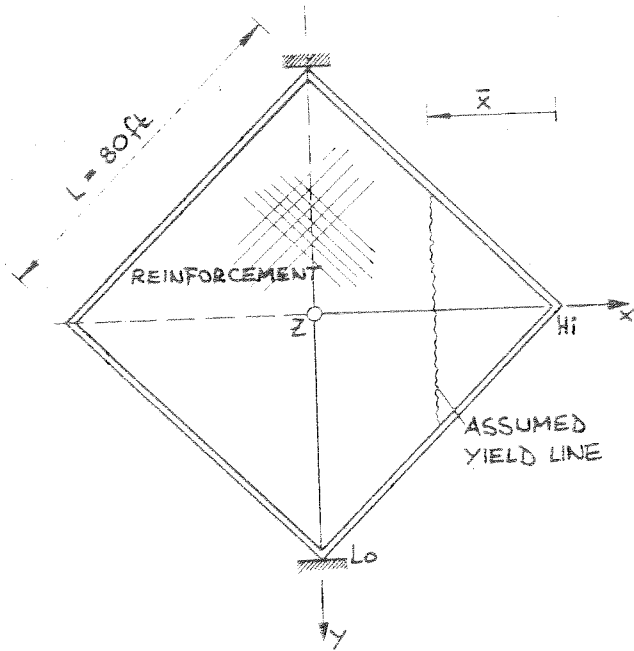
SECTION $\bar{x}$

$c\ a$
$+++$
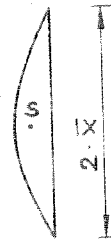
S... CENTER OF GRAVITY OF PARABOLA

LENGTH OF PARABOLA $\sim 2\bar{x}\cdot 1.05$

$$a = \frac{4}{6}\cdot\frac{\bar{x}^2}{200} = \frac{\bar{x}^2}{300}$$

$$c = \frac{1}{2}a = \frac{\bar{x}^2}{600}$$

(a) INTERNAL MOMENT M_i^{ULT} ALONG YIELD LINE

YIELD FORCE : $n_y = \frac{1}{2}(n_{y1} + n_{y2})$

$$n_y = \frac{1}{2}(60\,000\cdot 0.2 + 60\,000\cdot 0.2)$$

$$n_y = 12\ kips/ft$$
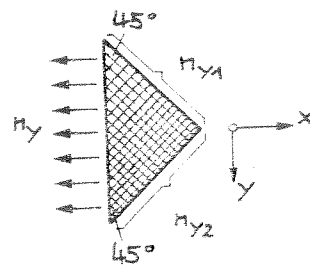
$$M_i^{ULT} = n_y\cdot 2\cdot\bar{x}\cdot 1.05\cdot a = \underline{0.084\ \bar{x}^3}\quad (k\text{-}ft)$$

FIG. 6.14   SADDLE SHELL , YIELD LINE THEORY

(b) EXTERNAL MOMENT M_a

DEAD LOAD   DL = 150 pcf
LIVE LOAD   LL = f·20 psf

$$M_a = \overbrace{(50 + f·20)\, \bar{x}^3/3000}^{\text{SHELL + LIVE LOAD}} + \overbrace{0.47\,\bar{x}^2}^{\text{BEAM}} \quad (k\text{-}ft)$$

(c) MOMENT CAPACITY OF THE BEAMS

$$\tfrac{1}{2}\, M_{BEND}^{ULT} \approx 365\ k\text{-}ft$$
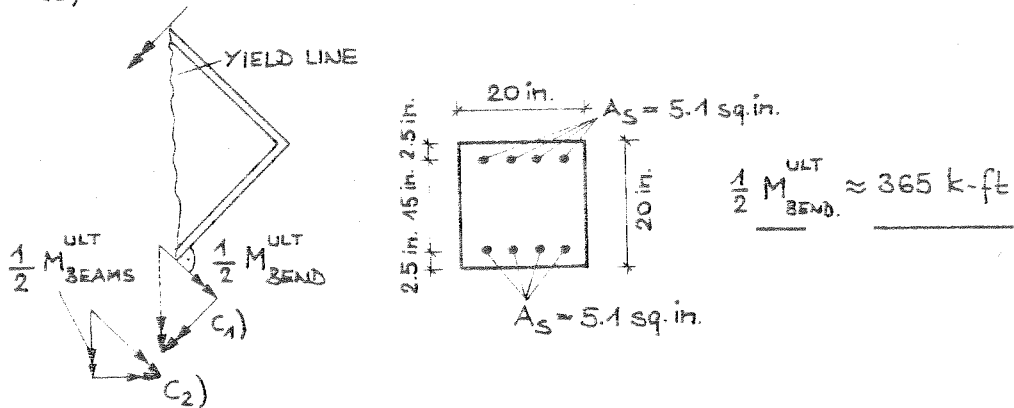
c_1) TORSIONAL MOMENTS CONSIDERED: $M_{BEAMS}^{ULT} = 2 \cdot \tfrac{1}{2} \cdot M_{BEND}^{ULT} \cdot \sqrt{2} = 1030\ k\text{-}ft$

c_2) TORSIONAL MOMENTS NOT CONSIDERED: $M_{BEAMS}^{ULT} = 2 \cdot \tfrac{1}{4} \cdot M_{BEND}^{ULT} \cdot \sqrt{2} = 515\ k\text{-}ft$
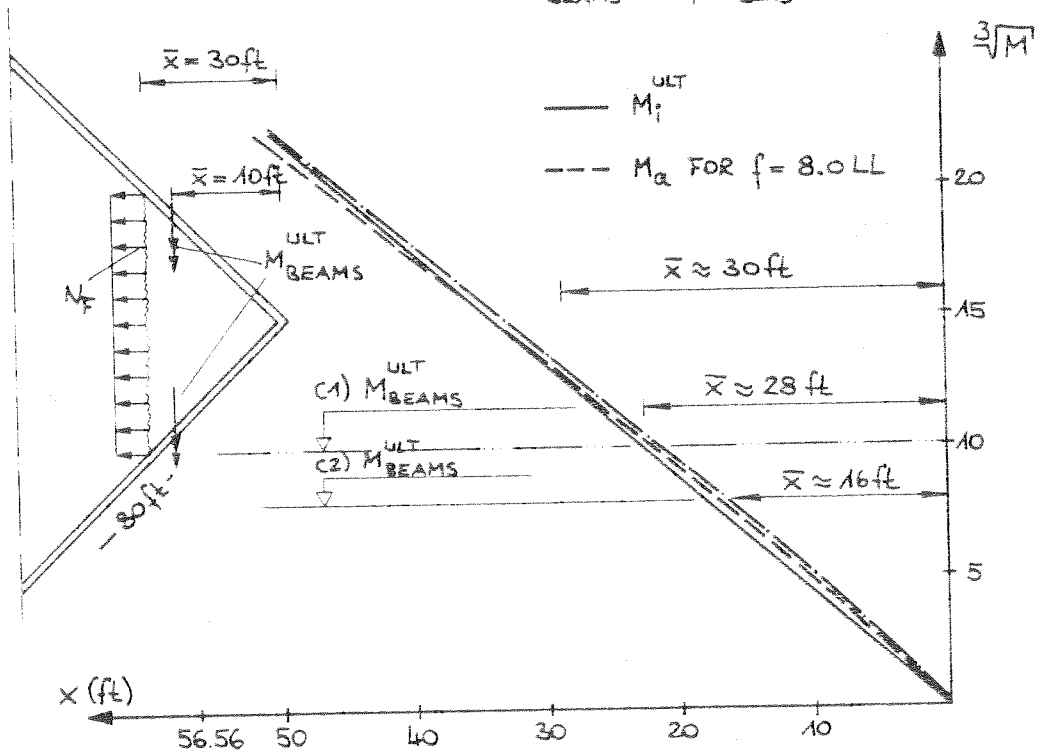
FIG. 6.14   CONTINUATION
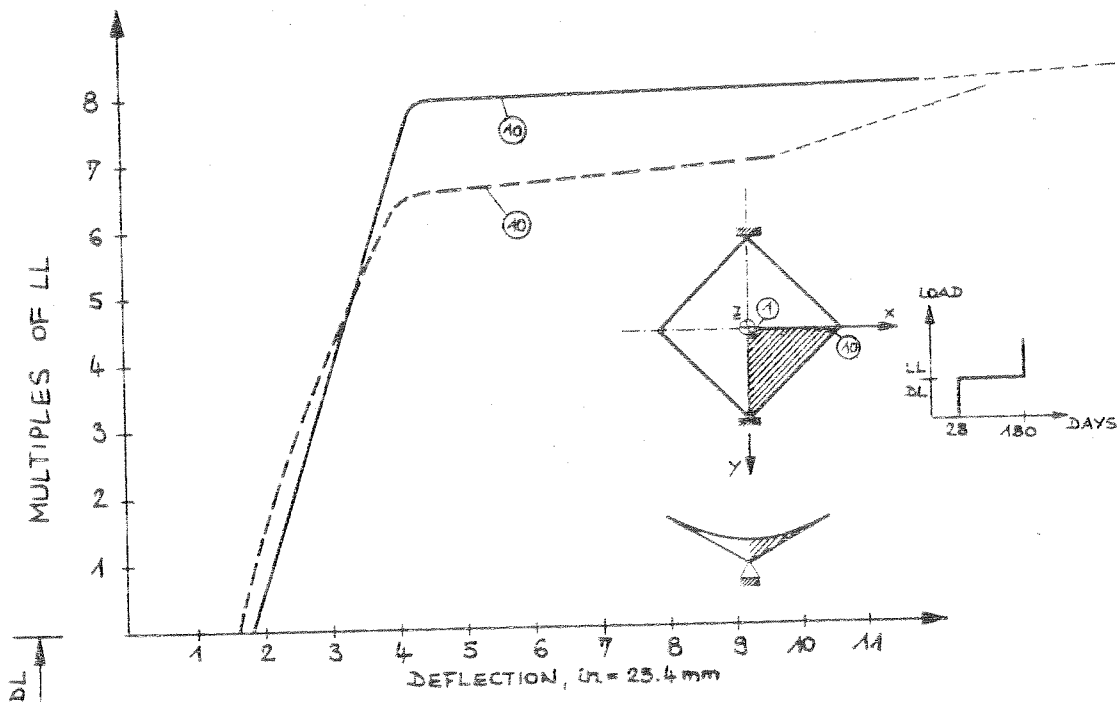
(a) LOAD - DEFLECTION CURVES
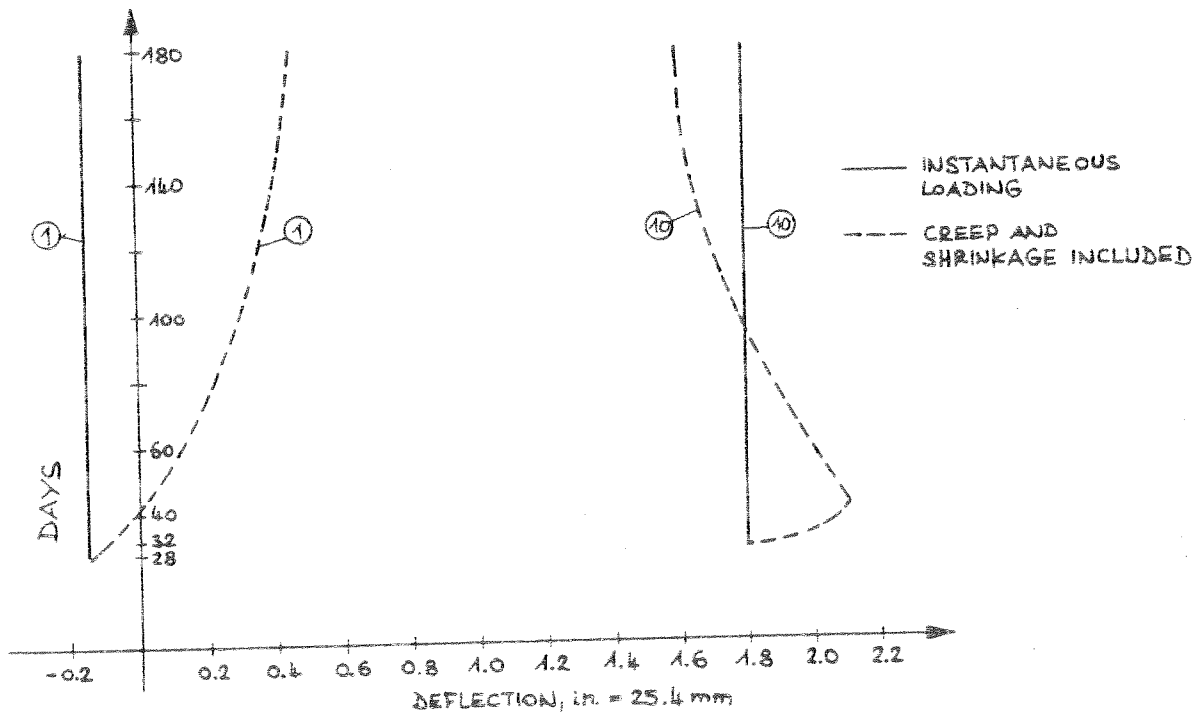
(b) TIME - DEPENDENT DEFLECTIONS

FIG. 6.15 SADDLE SHELL - INFLUENCE OF CREEP AND SHRINKAGE

Fig. 6.15b shows the deflections of the tip and crown point as they vary with time. It can be seen that at the beginning the deflection of the crown point is directed upwards. Then, with increasing creep and shrinkage deformations, this deflection changes its sign. As the crown deflects downwards the tip point moves upwards.

In Fig. 6.16 it is demonstrated that it is necessary to compare the deflections of several points of the shell. If only the tip point would have been selected one would draw the conclusion that there is only a minor influence.

The beginning and the location of the first cracks is different from the instantaneous case. First cracks form already under dead load (Fig. 6.17). Affected here is mainly the edge beam and not the shell. However with increasing load after 180 days the crack pattern of the instantaneous loading case is approached (Fig. 6.18 and 6.19). The redistribution of stresses is shown exemplarly in Fig. 6.20 to 6.23.

Due to creep and shrinkage compression stresses in concrete layers decrease (e.g. concrete layer 10 in Fig. 6.20) on the other hand steel stresses increase. Since creep is assumed to be the same in tension as in compression, creep and shrinkage are acting against each other in tension. Obviously the shrinkage effects in the top layer 1 for t = 40 days are greater than the creep effects (Fig. 6.20). Due to creep alone the tension forces would be decreasing. The effect on the stress resultants is shown in Fig. 6.21, and it can be seen that the redistribution of stresses is considerable. E.g. the normal force acting on concrete after 180 days is less than half the value of 28 days whereas the steel normal force at 28 days increases to almost 4 times its value.
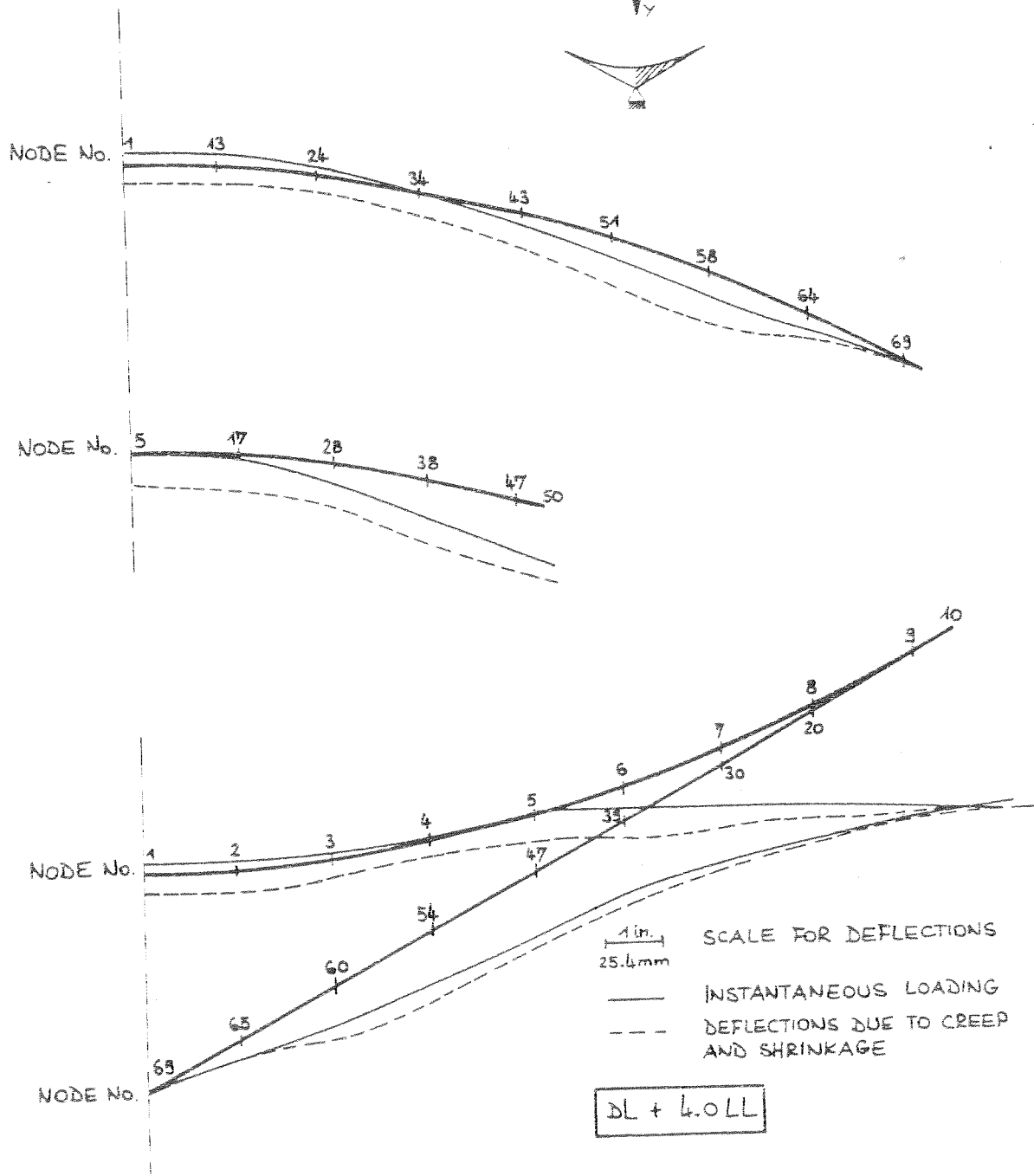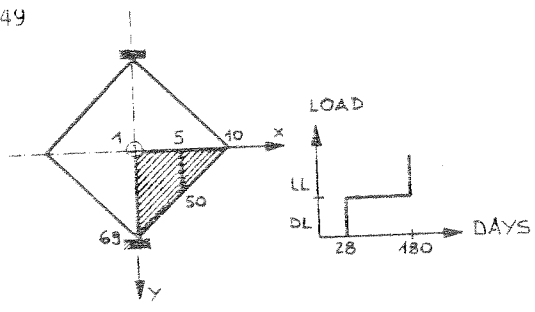
49

NODE No. 1

NODE No. 5

NODE No.

NODE No.

SCALE FOR DEFLECTIONS

INSTANTANEOUS LOADING

DEFLECTIONS DUE TO CREEP AND SHRINKAGE

DL + 4.0 LL

FIG. 6.16 SADDLE SHELL - DEFLECTIONS OF THE SHELL

LOAD

DAYS

28   180

DL , 180 DAYS

DAYS

LL

DL

TOP

BOTTOM

CRACKS START AT THE TOP LAYER

CRACKS START AT THE BOTTOM LAYER

COMPLETELY CRACKED, CONCRETE CONTRIBUTES STILL

NUMBERS SHOW CRACK DEPTH

FIG. 6.17   SADDLE SHELL – CRACK PROPAGATION , DEPTH AND AVERAGE DIRECTIONS

DL + 6.0 LL, 180 DAYS

CRACKS START AT THE TOP LAYER

CRACKS START AT THE BOTTOM LAYER

COMPLETELY CRACKED, CONCRETE CONTRIBUTES STILL

COMPLETELY CRACKED

NUMBERS SHOW CRACKDEPTH

FIG. 6.18 SADDLE SHELL - CRACK PROPAGATION, DEPTH AND AVERAGE DIRECTIONS

≃ DL + 7.5 LL , 180 DAYS

STEEL
YIELDED

TOP

BOTTOM

— CRACKS START AT THE TOP LAYER

— CRACKS START AT THE BOTTOM LAYER

≈ COMPLETELY CRACKED, CONCRETE CONTRIBUTES STILL

≡ COMPLETELY CRACKED

NUMBERS SHOW CRACK DEPTH

FIG. 6.19 SADDLE SHELL - CRACK PROPAGATION, DEPTH AND AVERAGE DIRECTIONS

TOP CONCRETE
LAYER 1

STEEL
LAYER 1

BOTTOM CONCRETE
LAYER 10

STEEL
LAYER 2

180

140

100

DAYS

60

40
32
28

STRESS IN
STEEL
$(ksi = 6.9 \text{N/mm}^2)$

5.0   0   -5.0   -10.0   -15.0   -20.0

STRESS IN
CONCRETE
$(ksi = 6.9 \text{N/mm}^2)$

0.2   0   -0.2   -0.4   -0.6   -0.8

TOP   STEEL LAYER 1

x,y

z

BOTTOM   STEEL LAYER 2

10 CONCRETE LAYERS

CROSS SECTION OF ELEMENT 2

z   x

LOAD

LL
DL

28   180   DAYS
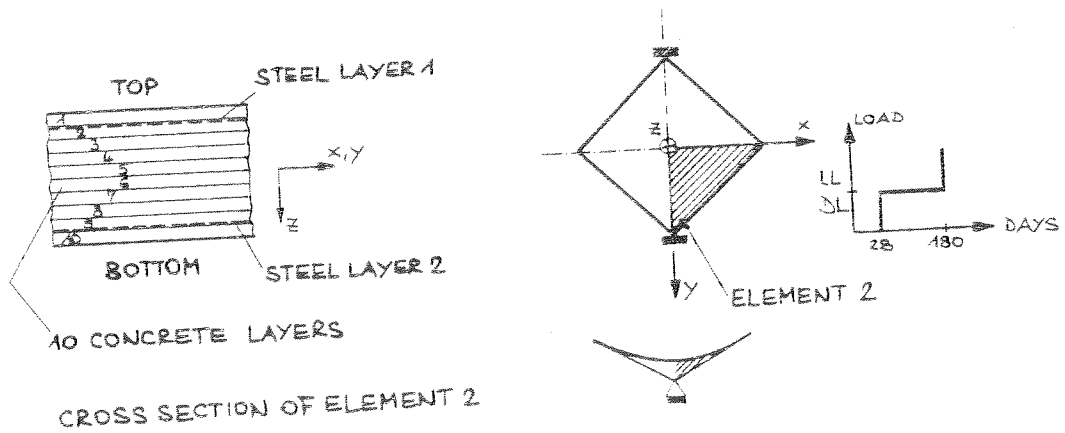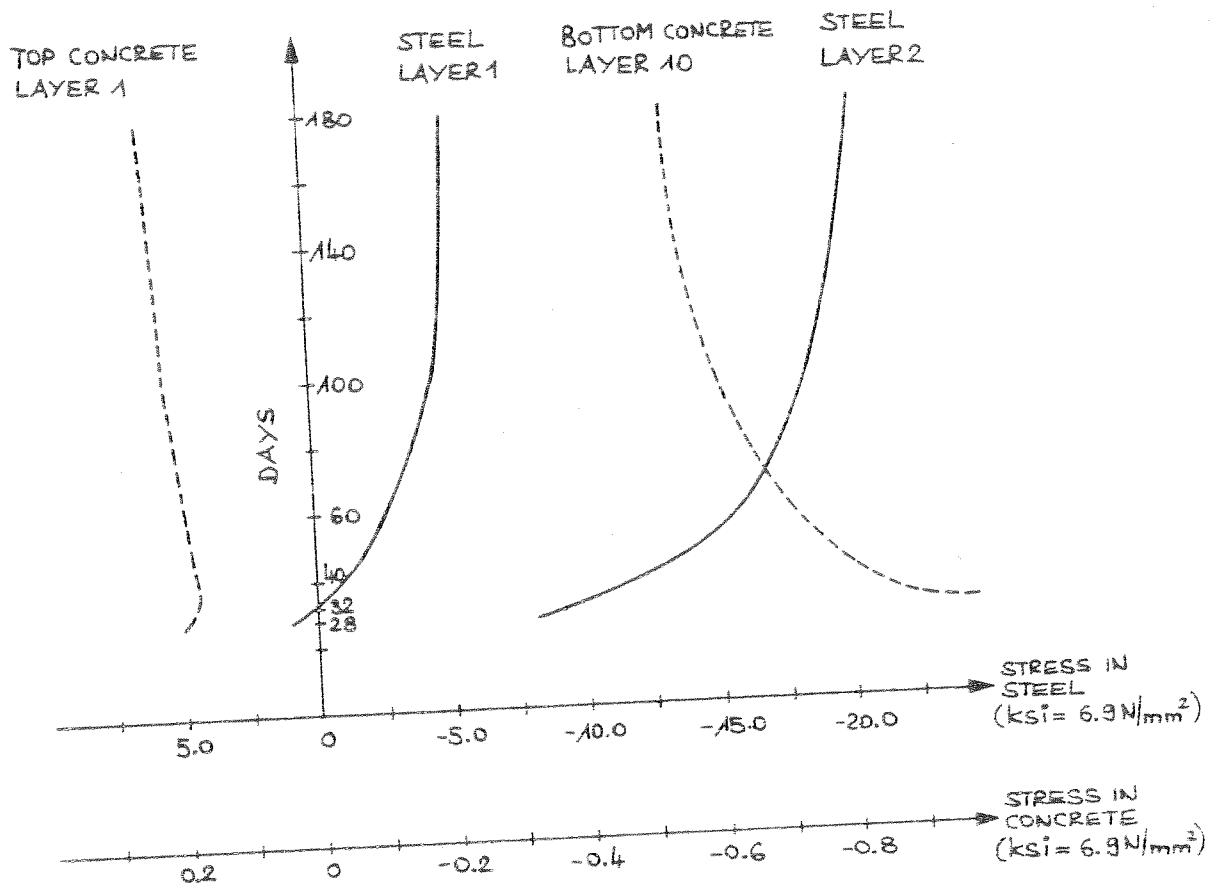
Y   ELEMENT 2

FIG. 6.20 SADDLE SHELL - STRESS REDISTRIBUTION IN BEAM (ELEMENT 2)

$M_c^{28} = 840$ k-in. $(= 95 kNm)$, $N_c^{28} = -158$ kips $(= -703 kN)$

$M_c^{180} = 540$ k-in. $(= 61 kNm)$, $N_c^{180} = -68$ kips $(= -303 kN)$
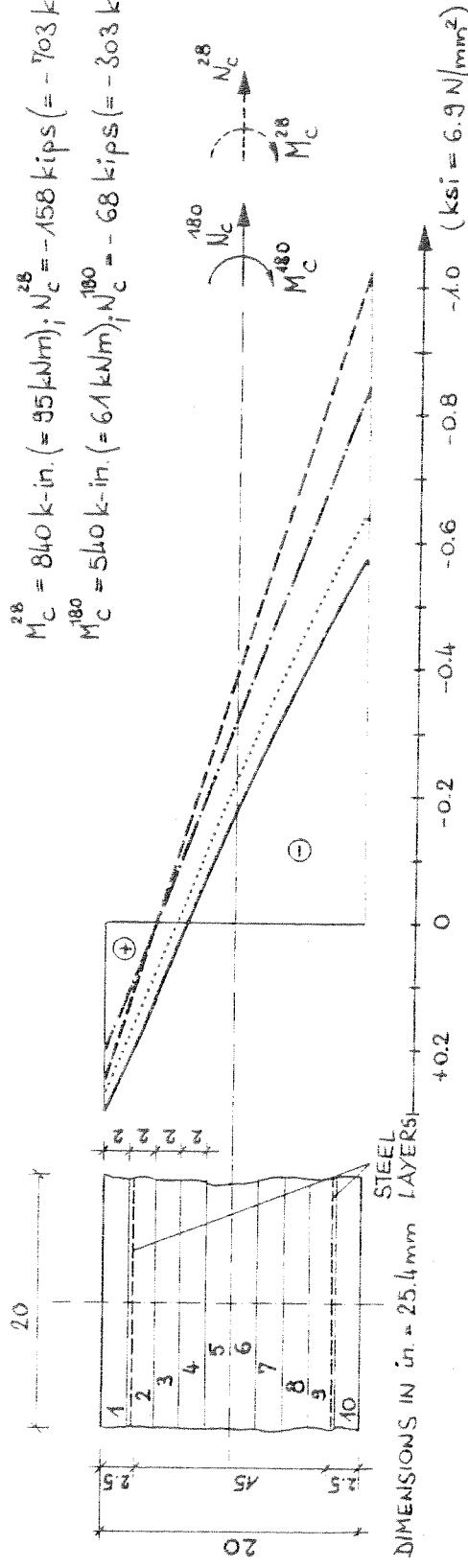
$M_s^{28} = 331$ k-in. $(= 38 kNm)$, $N_s^{28} = -37$ kips $(= -165 kN)$

$M_s^{180} = 580$ k-in. $(= 192 kNm)$, $N_s^{180} = -133$ kips $(= -592 kN)$

N_c^{28} M_c^{28} N_c^{180} M_c^{480}

N_s^{28} M_s^{28} N_s^{180} M_s^{180}

STRESSES IN CONCRETE LAYERS

-1.0 -0.8 -0.6 -0.4 -0.2 0 $+0.2$ (ksi = 6.9 N/mm²)

-20 -16 -12 -8 -4 0 $+4$ (ksi = 6.9 N/mm²)

STEEL LAYERS

DIMENSIONS IN in. = 25.4 mm

2 2 2 2

1 2 3 4 5 6 7 8 9 10

2.5 45 2.5

20

--- 28 DAYS
-·- 40
···· 100
— 180

ELEMENT 2

X Y Z M

LOAD LL DL 28 180 DAYS
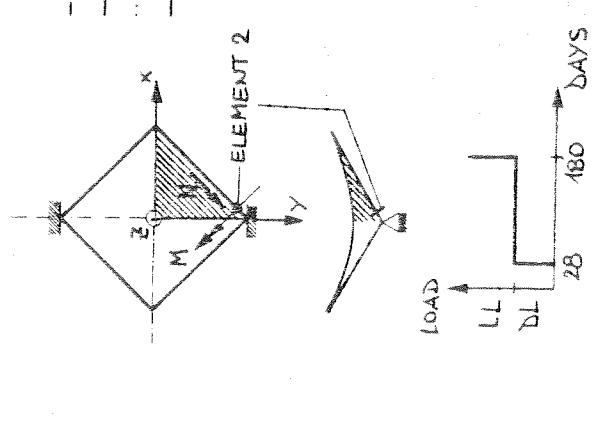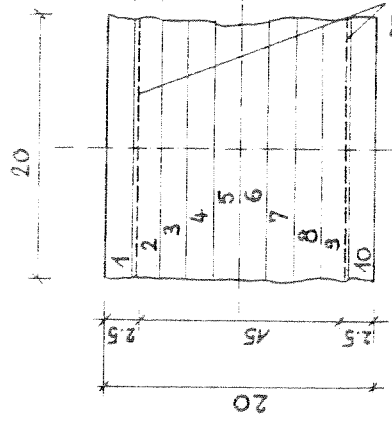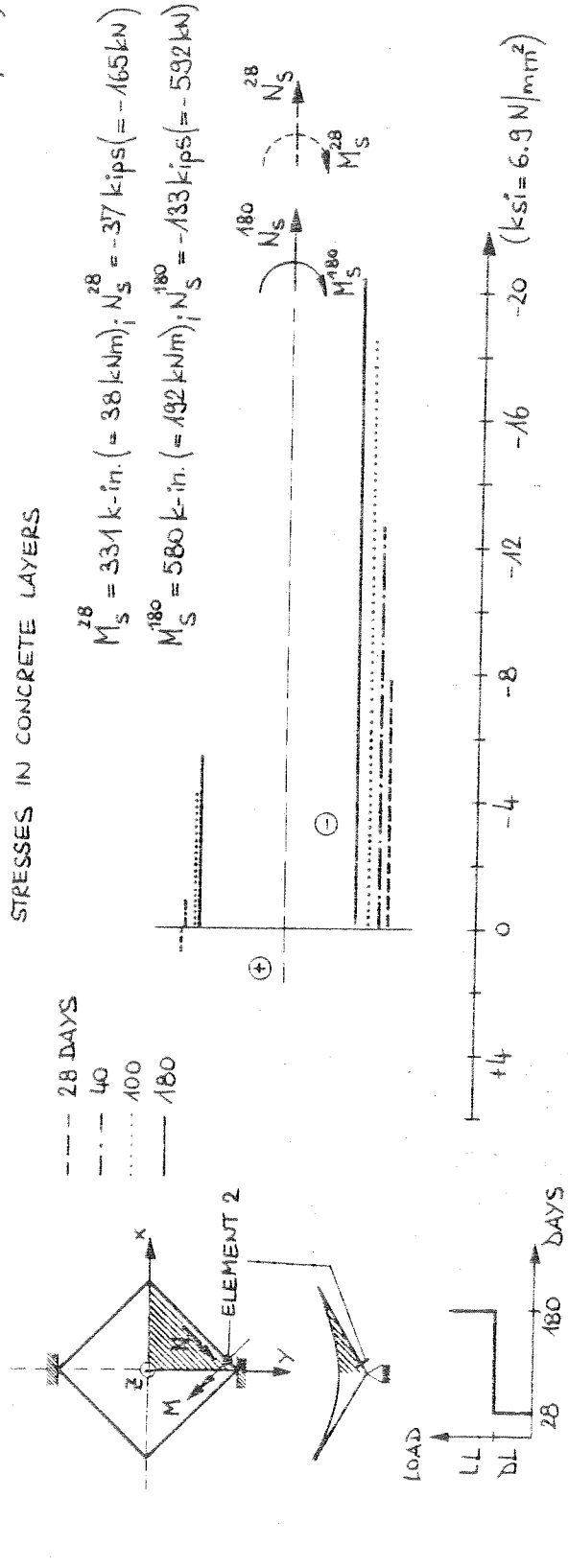
FIG. 6.21 SADDLE SHELL - STRESS REDISTRIBUTION IN BEAM (ELEMENT 2)

Another example for a shell element is given in Fig. 6.22. There, the top concrete layer 1 is subjected to larger tension stresses, therefore creep effects have more influence than shrinkage effects.

In Fig. 6.23 the stress redistribution in the shell cross section x = 0 between the abutments reveals that the tensile forces acting on concrete increase and simultaneously the normal force in steel changes sign and becomes negative. The concrete compression force near the edge decreases. A statical check as done in paragraph 6.1 proves that equilibrium conditions are satisfied at 28 days as well as at 180 days.

6.4 Numerical Experiences

In the subsequent section some experiences are compiled to demonstrate that the solution of a nonlinear analysis is very sensitive and must be checked critically.

First of all it is important that the unbalanced forces at the end of a load increment remain small compared to the total nodal forces otherwise the result may be completely wrong. Fig. 6.24 shows e.g. a solution where the number of permitted iterations was chosen too small, namely 6 for the relatively large load increments of 0.25 LL to 1.0 LL (see also [19]).

In Fig. 6.25 it can be seen what happens if a load increment is chosen too large, i.e. that within one increment too many elements crack. In this example (creep and shrinkage was included) the increment from DL + 6.5 LL to DL + 7.0 LL was too large. Within this increment cracks propagated through the shell thickness causing a significant change in the overall stiffness. For the same example oscillations of deflection increments and unbalanced forces are illustrated (Fig. 6.26). Compared with
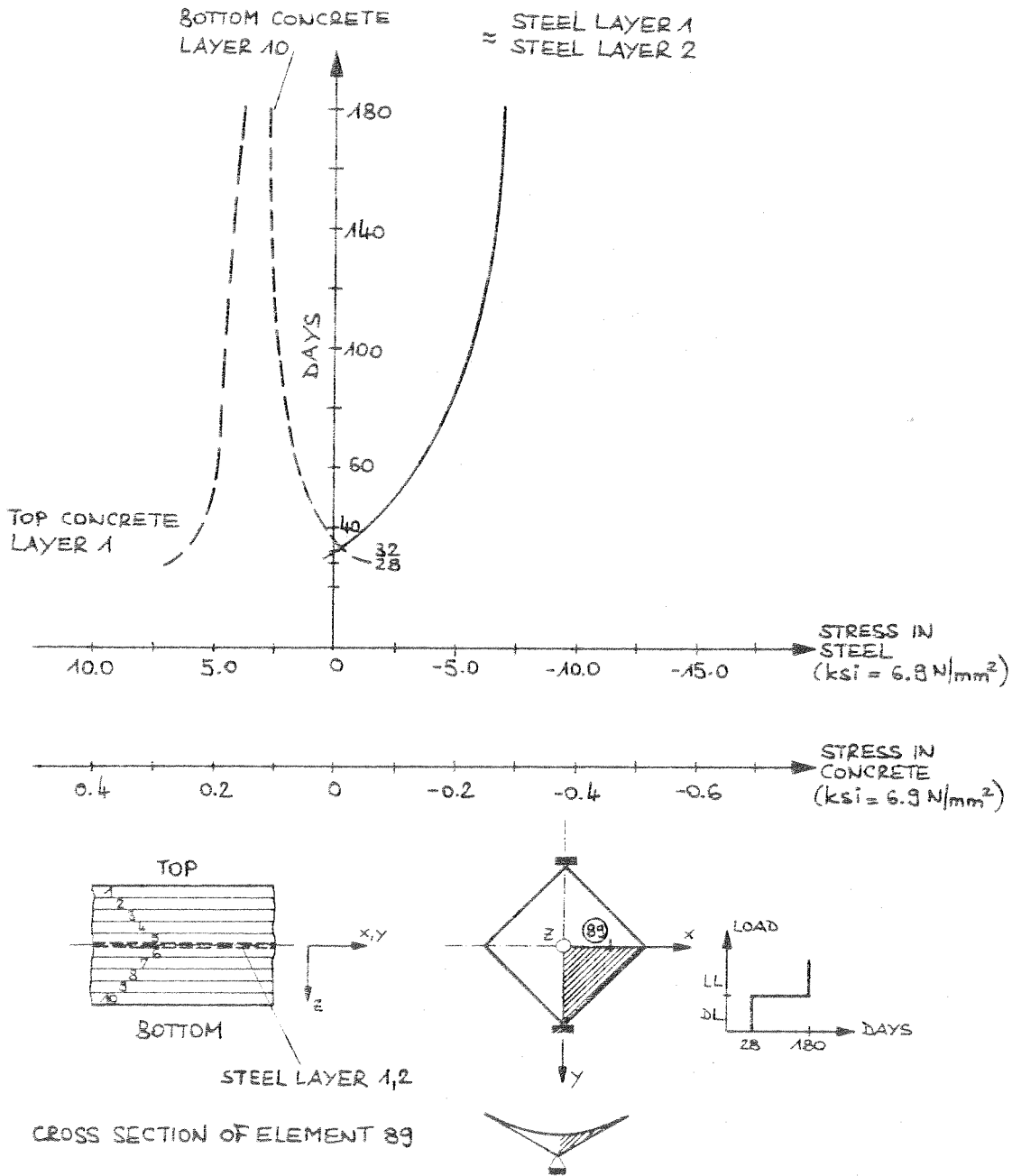
BOTTOM CONCRETE
LAYER 10

STEEL LAYER 1
≈ STEEL LAYER 2

TOP CONCRETE
LAYER 1

DAYS

180

140

100

60

40
32
28

STRESS IN
STEEL
(ksi = 6.8 N/mm²)

10.0   5.0   0   -5.0   -10.0   -15.0

STRESS IN
CONCRETE
(ksi = 6.9 N/mm²)

0.4   0.2   0   -0.2   -0.4   -0.6

TOP

BOTTOM

x,y

z

STEEL LAYER 1,2

CROSS SECTION OF ELEMENT 89

z   89   x

y

LOAD

LL

DL

DAYS

28   180

FIG. 6.22   SADDLE SHELL - STRESS REDISTRIBUTION IN SHELL (ELEMENT 89)
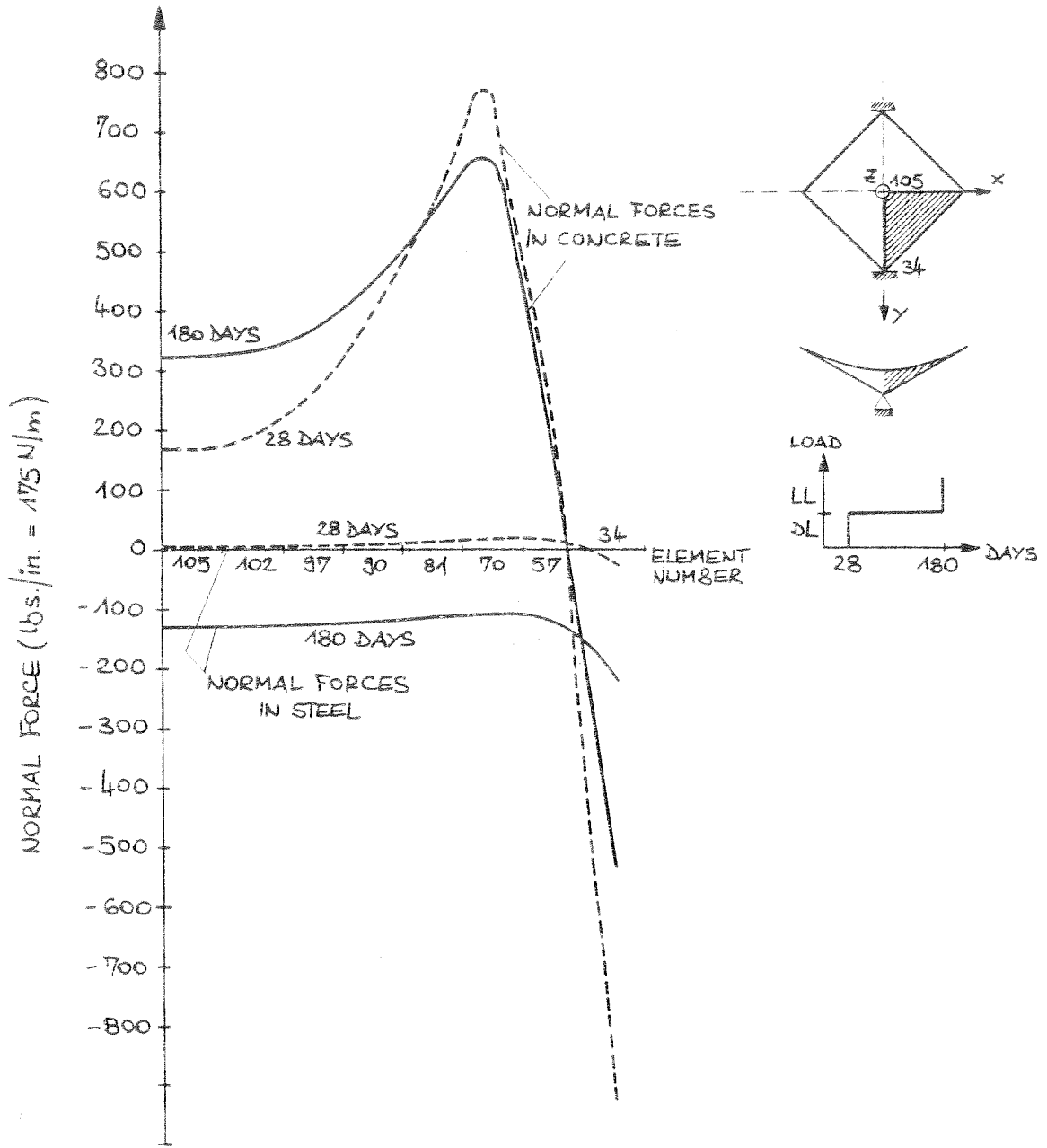
FIG. 6.23 SADDLE SHELL - STRESS REDISTRIBUTION IN SHELL
CROSS SECTION

58
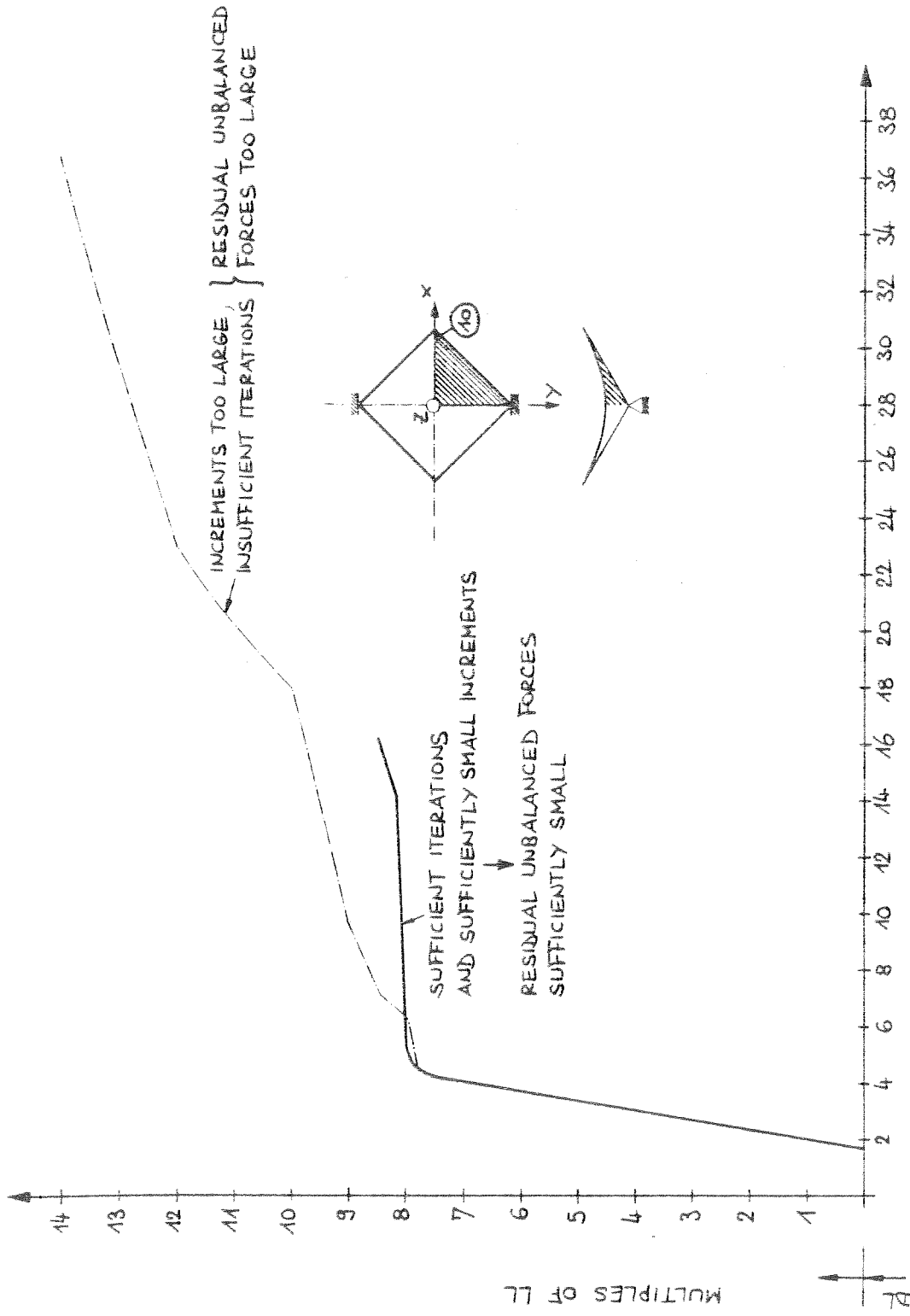
FIG. 6.24 SADDLE SHELL LOAD-DEFLECTION CURVES, NODE 10 (in. = 25.4 mm)

59
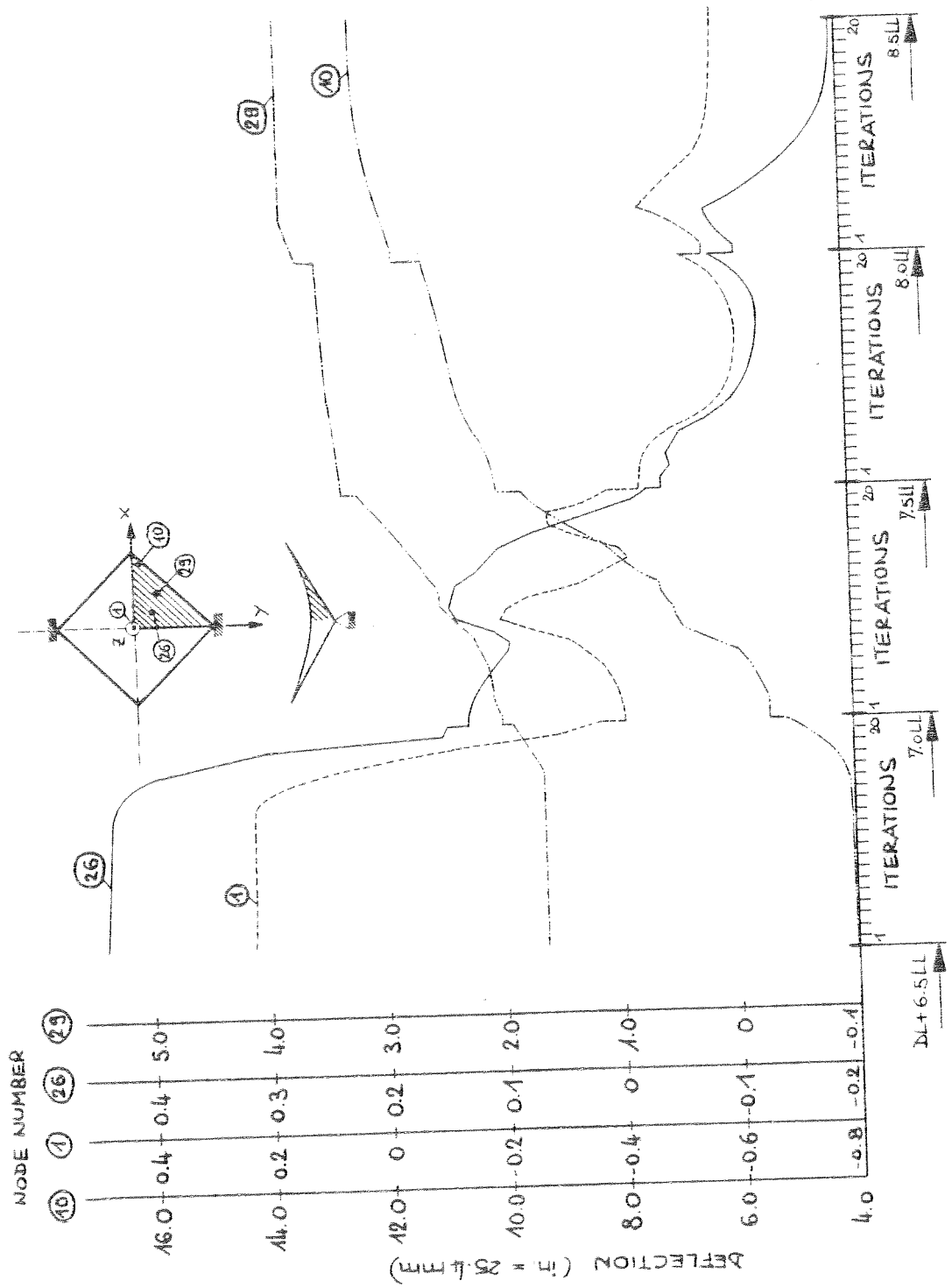
FIG. 6.25 SADDLE SHELL - OSCILLATIONS DUE TO LARGE INCREMENTS
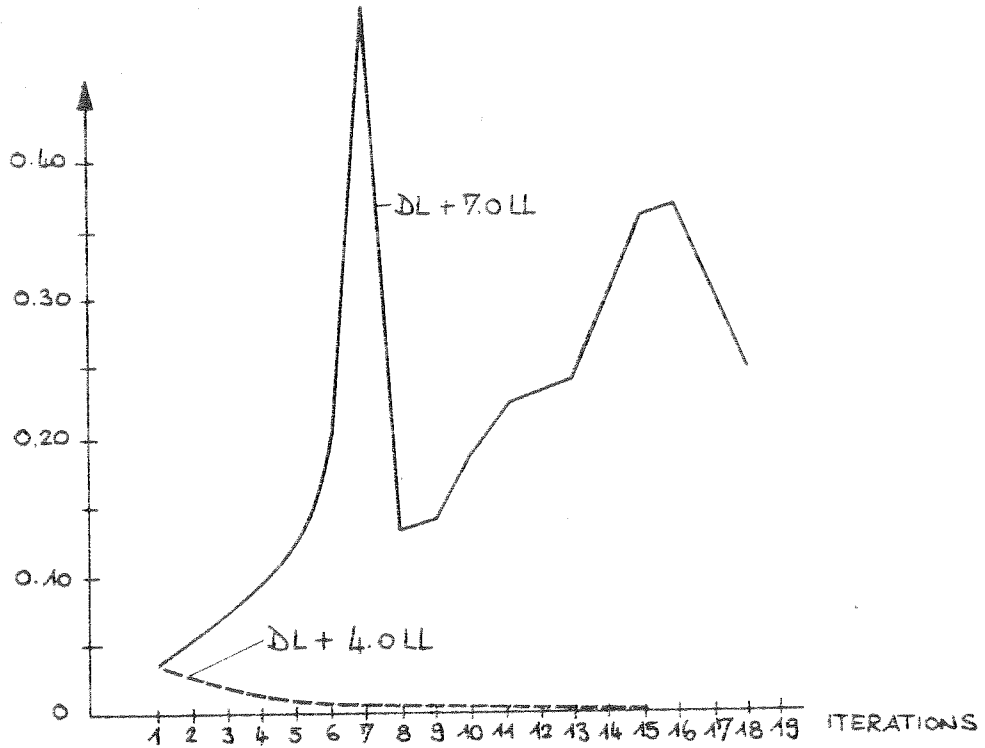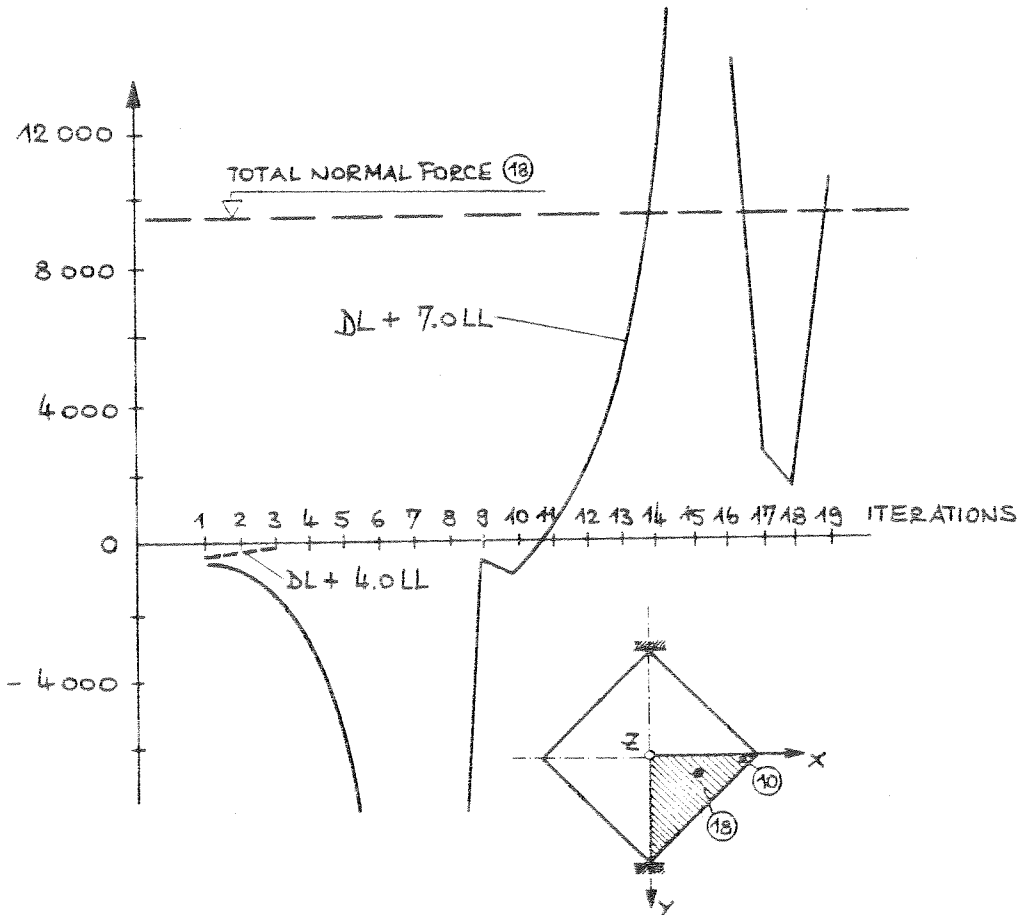
FIG. 6.26 SADDLE SHELL - OSCILLATIONS DUE TO LARGE INCREMENTS

MULTIPLES OF LL

DL

DEFLECTIONS NODE 10 , in. = 25.4 mm
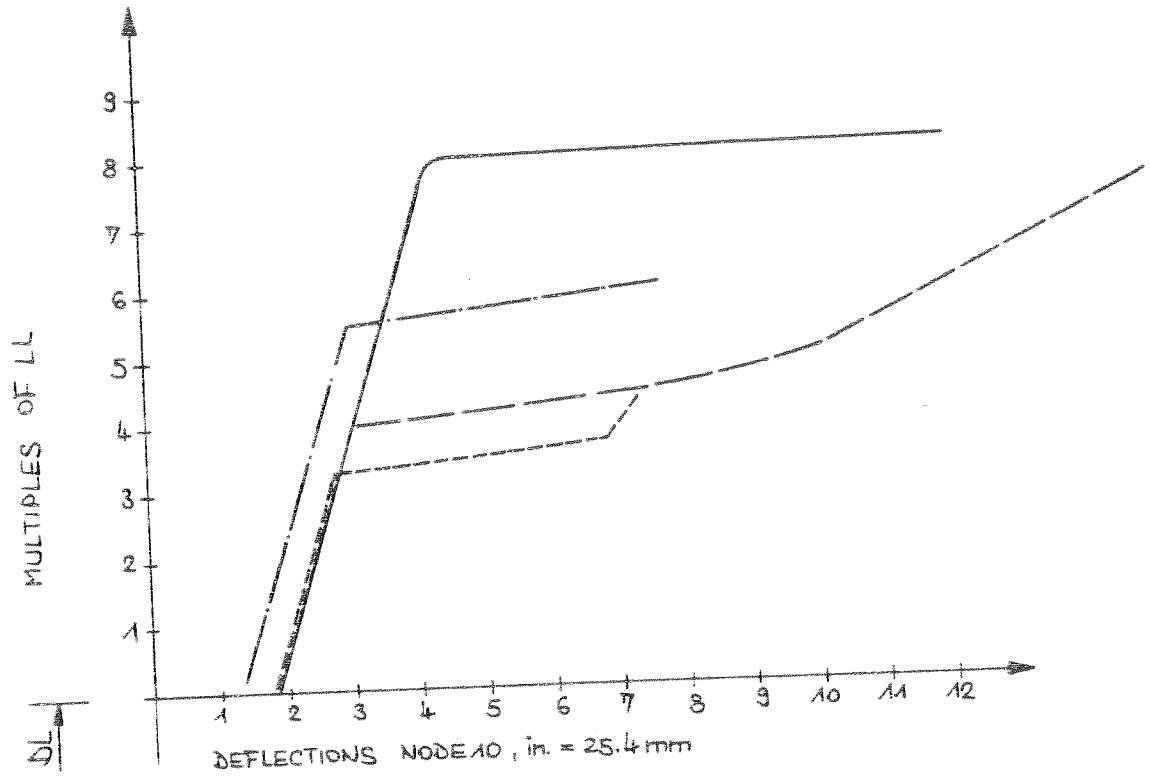
1)   —·—   LIN [14]

2)   ——   NOTACS

3)   – – –   NOTACS , NO TENSION STIFFENING

4)   -----   NOTACS, NO TENSION STIFFENING
           (SMALLER STEPS)
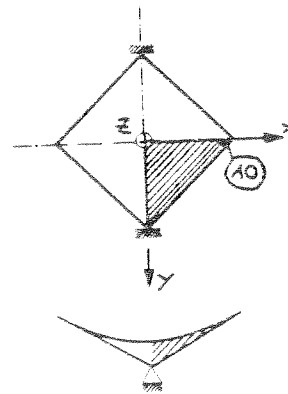
FIG. 6.27   SADDLE SHELL - LOAD-DEFLECTION CURVES
           FOR DIFFERENT MATERIALS

STEEL YIELDED

≈ DL + 8.0 LL

⟨△⟩ CRACK DOMAIN FOR DL + 4.0 LL (COMPARE WITH FIG. 6.10)

△   CRACK DOMAIN FOR DL + 8.0 LL (COMPARE WITH FIG. 6.13)
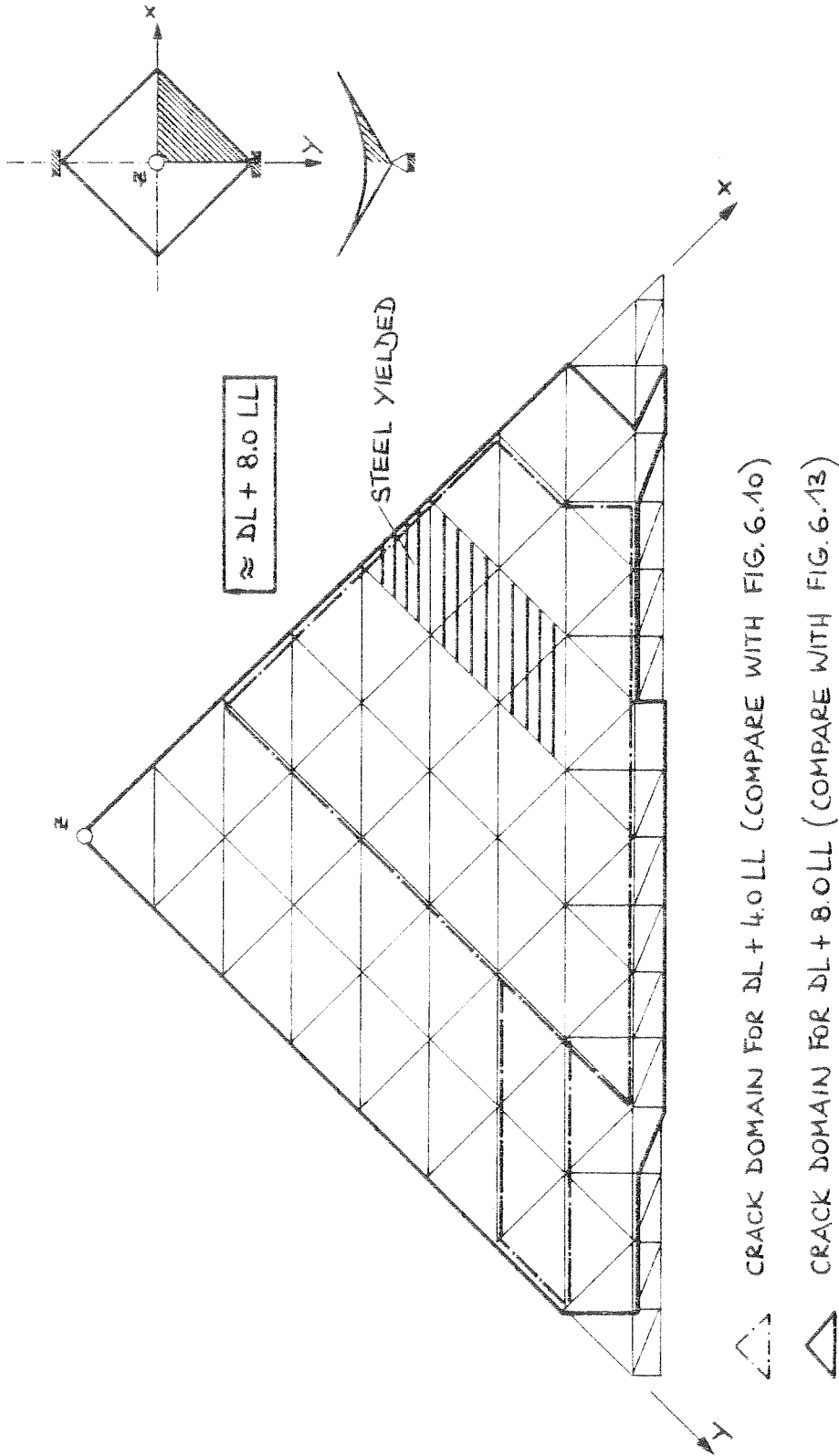
6.28 SADDLE SHELL - CRACK PROPAGATION, NO TENSION STIFFENING ASSUMED

62

the load level DL + 7.0 LL the iteration at the load level DL + 4.0 LL shows a fast convergence.

One big problem results from local failure of a structure. The numerical procedure will try to shift the load to areas still capable of carrying additional load, i.e. the iterations will not converge. In such a case engineering reasoning has to assist the numerical solution. (The failure of this shell is also initiated by local failure of the tip region.) Here a method - applying springs in the pathological areas - described in [20] might help to overcome the problem.

6.5 Influence of Material Properties on the Solution

As already discussed in [19] the assumptions of the tensile strength of concrete f_t', the yield strength f_y, the reinforcement ratio ρ and the tension stiffening effect have considerable influence on the load deflection relations and also on the convergence of the numerical procedure.

Particularly, numerical problems arise for underreinforced structures for which the following conditions holds:

$$f_t'/f_y > \rho \qquad (6.1)$$

First it might happen that the true ultimate capacity (depending on f_y) is overestimated. Second, the convergence can be expected to be much slower since the load which cannot be carried any more by the cracked element has to be shifted to the neighboring elements.

For conditions

$$f_t'/f_y \leq \rho \qquad (6.2)$$

additional load can be carried by the cracked element, however strains and deformations become much larger. A large reinforcement ratio is beneficial to the numerical procedure since the released unbalanced forces after

cracking are smaller than for small ratios.

As also emphasized in [19] residual unbalanced forces, ever so small, should be transmitted to the next load increment. The value of the tensile strength is mainly responsible for the beginning of cracking, i.e. the non-linear behavior.

In Fig. 6.27 load deflection curves for different assumptions of the material properties of concrete in tension are presented. The solution of Lin [14] was obtained for a 20% smaller tensile strength and for a tension stiffening curve decreasing cubically to zero at a ultimate strain of 0.0005. The sharp bend of the load deflection curve occurs already at DL + 5.5 LL. Two reasons are responsible for this. First the tensile strength is smaller and hence the abrupt change in stiffness is reduced to about DL + 6.0 LL. Second, because of the coarser mesh used, a larger area is affected, once cracking has started, i.e., the mesh size is already a parameter which affects the nonlinear curve. The difference in the deflection below this load level can be attributed to the same reasons.

The solution of Lin was stopped by arbitrarily chosen tolerances at DL + 6.0 LL. Since neither concrete yielding nor steel yielding was observed at this load level the load capacity was obviously not yet reached.

The other two solutions were obtained assuming no tension stiffening at all. The different beginning of the flat branch of the load deflection curve is due to the different sizes of load increments. Although both solutions are not really usable -the one because it is incomplete, the other because it is inaccurate- one can learn that the tension stiffening assumption is a major parameter which has to be investigated thoroughly. Again, numerically the same ultimate load can be expected as for the case

which includes a tension stiffening effect. This is underlined by the crack pattern (Fig. 6.28) obtained for solution 3 of Fig. 6.27 which is similar to the crack pattern determined before (Fig. 6.13) for DL + 8.0 LL. From a practical point of view, limitations of the deflections would probably reduce the permissible load.

The cracked shear constant β was taken as 0.5 as well as 1.0. No essentially different behavior could be observed due to this effect.

7. GABLE SHELL

7.1 Linear Analysis

In Fig. 7.1 results are compared with a solution obtained with the same program but using more elements. The agreement is excellent if the support is simulated by boundary elements fixed at the inner node (alternative b in Fig. 5.6). If the boundary element is placed at the corner point (alternative a) deflections are completely different. This was also found out by Kabir [15] who, for this reason, has given the corner element a fictious high stiffness. This example makes it clear that one has to be very careful in order to simulate properly a boundary condition.

A simple and rough statical check to prove that the loads are transmitted to the supports is presented in Fig. 7.2.
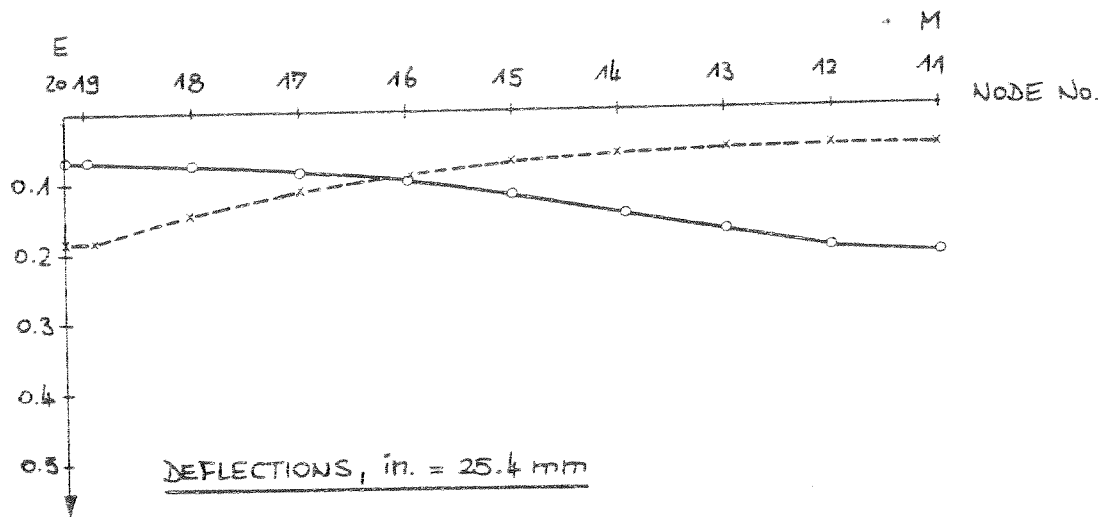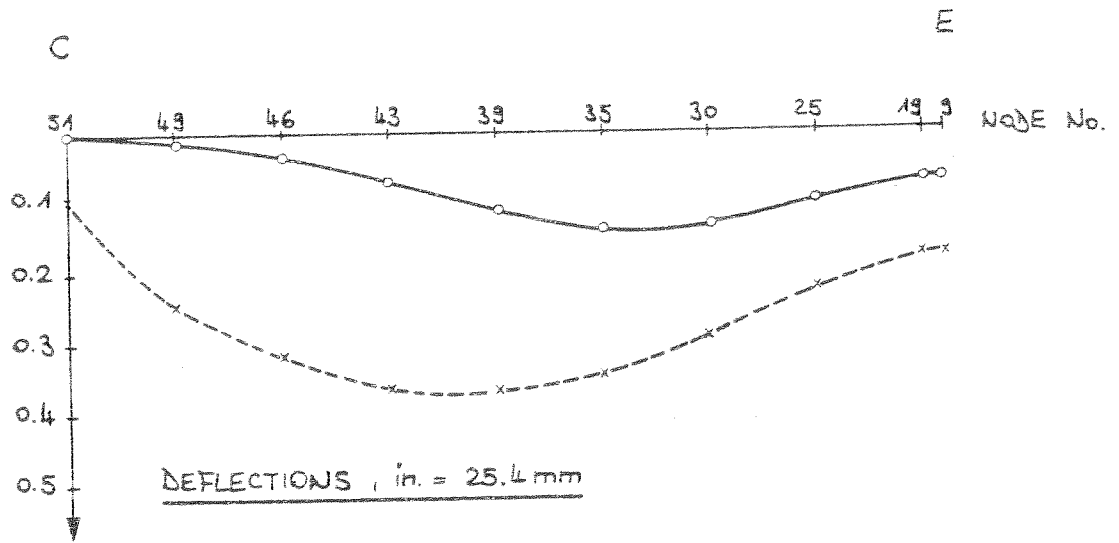
Studies on the behavior of gable shells based in linear analyses were made by Schnobrich [16]. The following conclusions may be drawn from his studies.

The size and location of the crown beam have a considerable influence on the deflections and the bending moments. The deflections increase with the size of the beam. A crown beam with its centroid above the shell

TABLE 7.1 GABLE SHELL, LOAD-DEFLECTION RELATION, NODE 11

LOAD INCREMENT * DL+	TOTAL LOAD * DL+	NUMBER OF ITERATIONS	DEFLECTION NODE 11 (in. = 25.4 mm)	DEFLECTION INCREMENT NODE 11 (in. = 25.4 mm)
12.0 LL	12.0 LL	1	0.385	0.385
		2	0.515	0.130
		3	0.564	0.049
1.0 LL	13.0 LL	1	0.609	0.045
		2	0.627	0.018
		3	0.648	0.021
		4	0.672	0.024
		5	0.702	0.030
1.0 LL	14.0 LL	1	0.778	0.076
		2	0.798	0.020
		3	0.807	0.009
		4	0.817	0.010
		5	0.826	0.009
1.0 LL	15.0 LL	1	0.930	0.114
		2	0.985	0.055
		3	0.988	0.003
0.5 LL	15.5 LL	1	1.090	0.102
		2	1.366	0.276
		3	1.544	0.178
		4	1.712	0.168
		5	2.350	0.638
0.5 LL	16.0 LL	1	4.650	2.300
		2	1397.0	1392.35

* MULTIPLES OF LINE LOAD LL

FIG. 7.1 GABLE SHELL - EDGE BEAM , LINEAR ANALYSIS

NORMAL FORCES N_y AT BB' IN kips

DUE TO DL	DUE TO LL
6.8	2.3
29.8	10.7
29.3	10.6
12.1	3.6
11.0	3.4
10.4	1.7
9.7	1.5
13.1	2.3
13.0	2.1
19.8	7.9
$\frac{1}{2}C^{DL}=155.0$	$\frac{1}{2}C^{LL}=46.1$
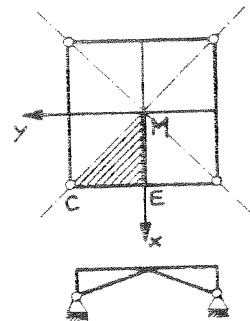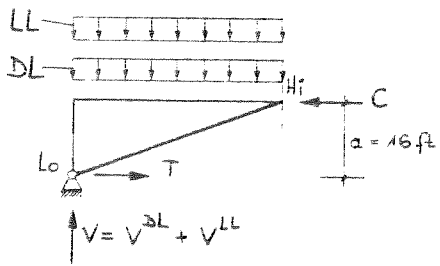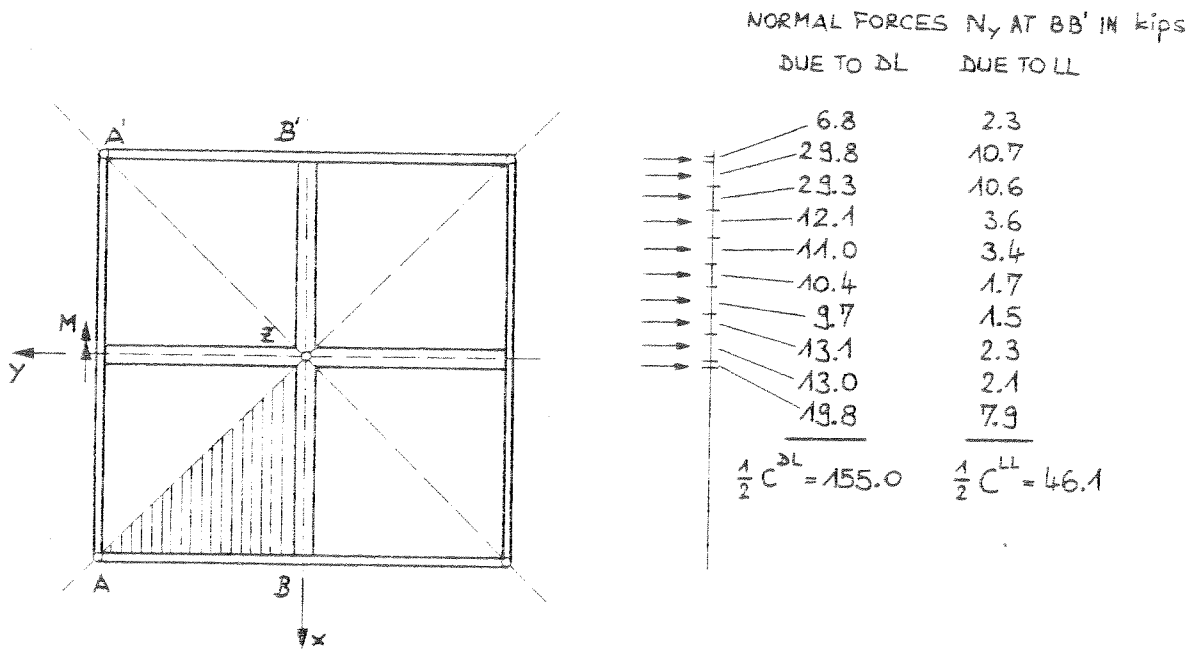
(a) VERTICAL LOADS ($\frac{1}{8}$ TH OF SHELL)

DL $\triangleq$ 57 kips
LL $\triangleq$ 18 kips

REACTION

$V^{DL} = 59$ kips
$V^{LL} = 19$ kips

(b) MOMENTS ALONG A'A

DUE TO DL : 4480 k-ft
DUE TO LL : 1470 k-ft

$C^{DL} * 16ft = 4960$ k-ft
$C^{LL} * 16ft = 1475$ k-ft

(c) HORIZONTAL FORCES

$C^{DL} = 310$ kips
$C^{LL} = 92.2$ kips

$T^{DL} = 295$ kips
$T^{LL} = 97$ kips

FIG. 7.2 GABLE SHELL - ROUGH STATICAL CHECK

reduces the deflections. A variation in the size of the edge beam has little influence. Bending moments in the crown beam are much less than in the edge beam. Membrane theory overestimates the normal forces considerably, especially for the crown beam. That means, that a design on the basis of the membrane theory ends up with the beam cross sections being too large which has an unfavorable influence on the deflections. The need for crown beams is questionable; possibly a thickening or strengthening of the shell would be sufficient.

The above conclusions agree with the few results obtained by Kabir [15] and the author (Fig. 7.3 to 7.6).

7.2 Nonlinear Analysis

The linear analysis indicates that the ultimate load must be very high. The maximum tensile stress in the shell due to DL + LL is only 180 psi (= 12 N/mm^2) of which about 1/6 th is due to LL. For that reason cracks are to be expected for a load level of about DL + 11 LL. Hence, the first load step is chosen as DL + 12 LL followed by three increments of 1.0 LL and 4 increments of 0.5 LL.

From Table 7.1 and Fig. 7.7 it can be seen that up to DL + 15.0 LL the behavior is only slightly nonlinear. First cracks occur along the diagonal near the support at DL + 12 LL. The spreading is limited up to DL + 15 LL. In the next load increment the cracks propagate through the depth but failure is caused by exceeding the concrete compression strength in the edge beams at the supports (Fig. 7.8), hence the ultimate capacity is DL + 15.5 LL.

Yield line theory (Fig. 7.9) predicts an ultimate load of DL + 16.8 LL. However in this case yield line theory is based on the wrong idea that

DEFLECTIONS, in. = 25.4 mm

NORMAL FORCES, kips = 4.5 kN (COMPRESSION $\ominus$)

BENDING MOMENTS, k-in. = 113.6 Nm $\ominus$
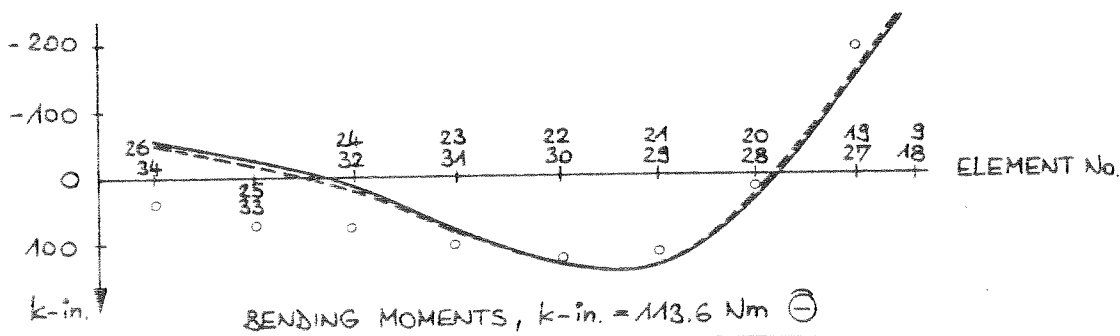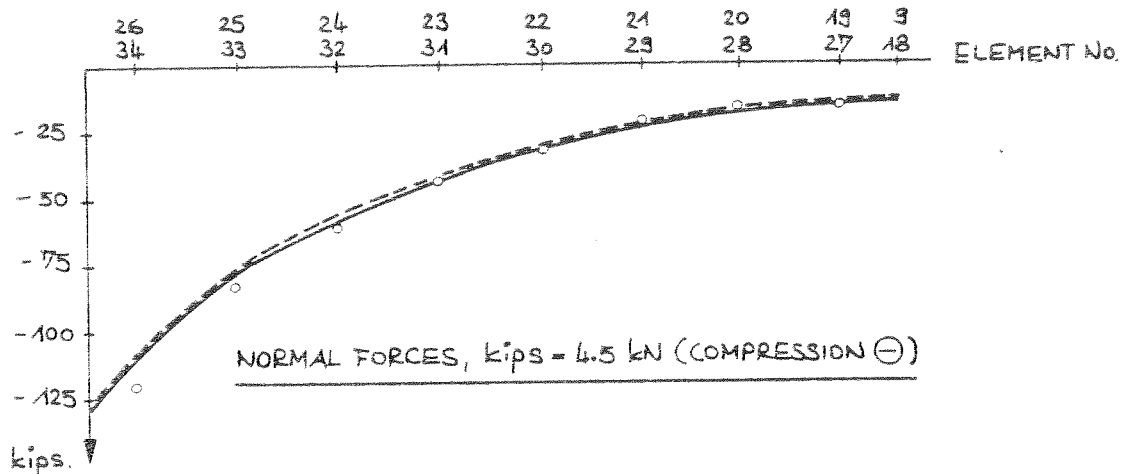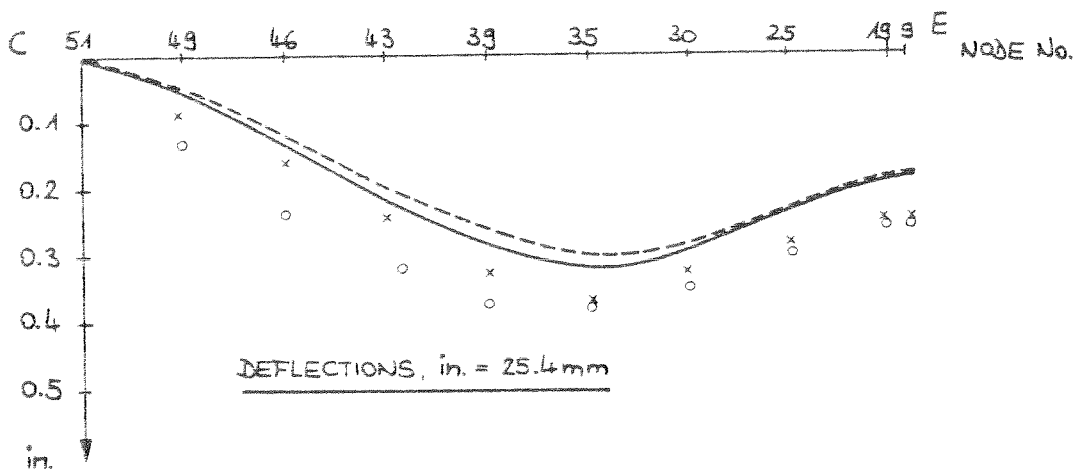
	b	d	B	D
———	14	7	14	14
- - - -	14	10	14	14
o o o o	12	8	12	16 [15]
x x x x	24	12	12	16 [15]

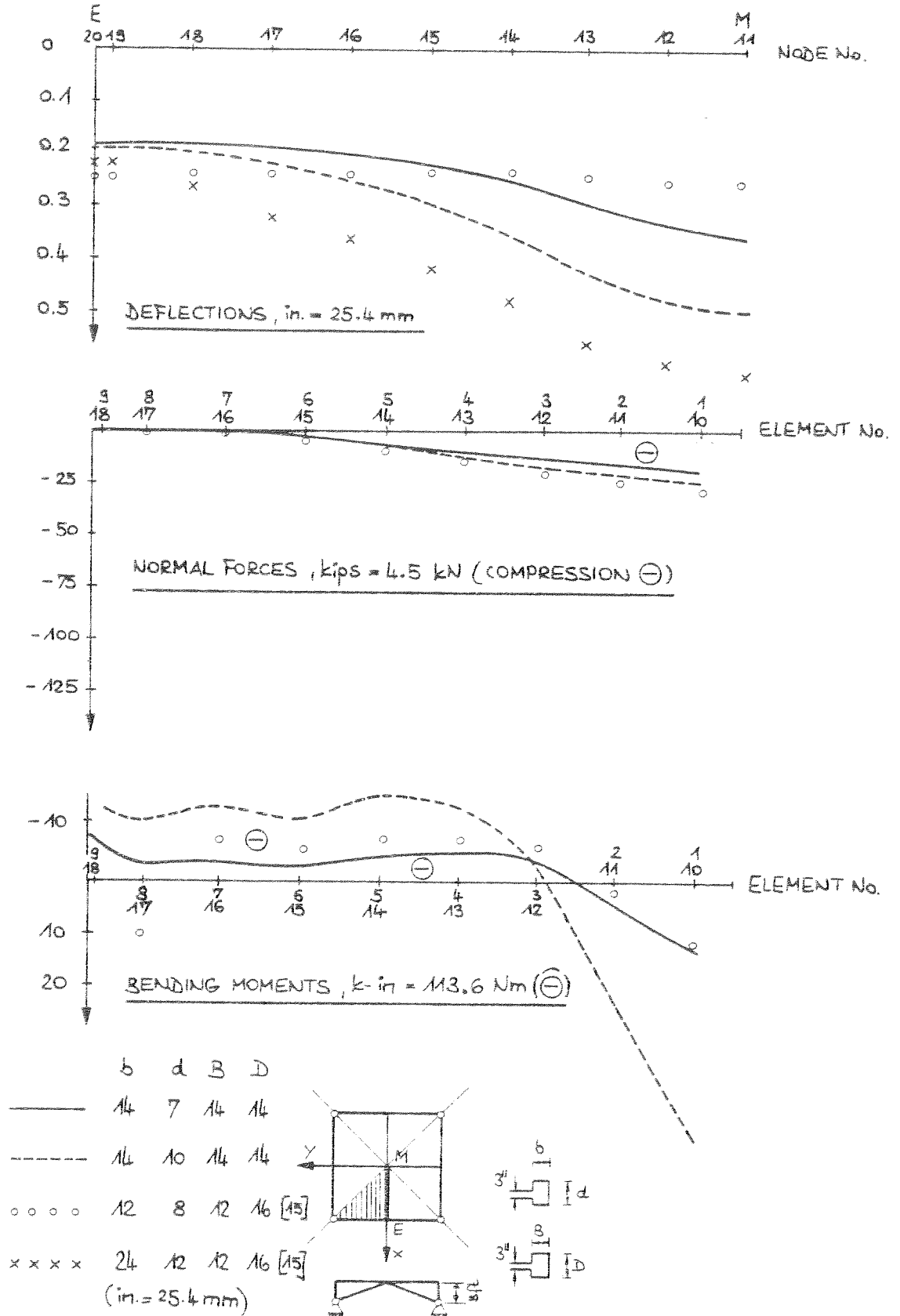(in. = 25.4 mm)
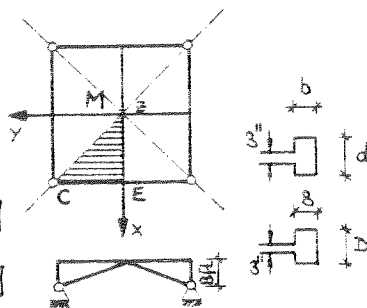
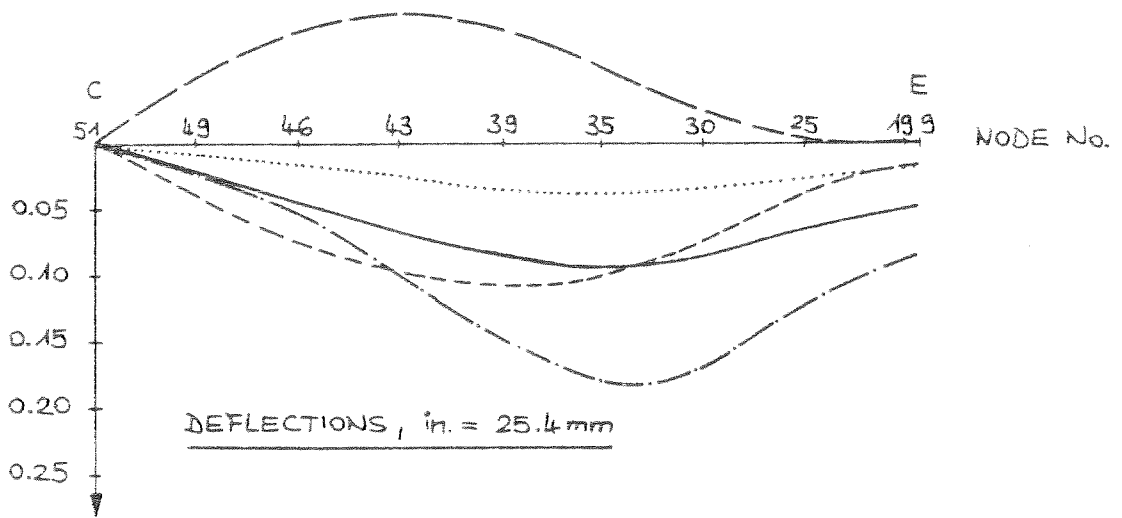7.3 GABLE SHELL – EDGE BEAM, VARIATION OF BEAM SIZES

FIG. 7.4 GABLE SHELL - CROWN BEAM, VARIATIONS OF BEAM SIZES

C · · · · · · · · · · E
NODE No.

51   49   46   43   39   35   30   25   19 9

0.05
0.10
0.15
0.20
0.25

DEFLECTIONS, in. = 25.4 mm

26   25   24   23   22   21   20   19
34   33   32   31   30   29   28   27

ELEMENT No.

-25
-50
-75
-100
-125

⊖

MEMBRANE THEORY
DL SHELL

MEMBRANE THEORY
DL + LL

NORMAL FORCES, kips = 4.5 kN (COMPRESSION ⊖)

-100
-50
0
50
100

⊖

23   22   21   20   19
31   30   29   28   27

26   25   24   26
34   33   32

ELEMENT No.

BENDING MOMENTS, k-in. = 113.6 Nm
(⊖)
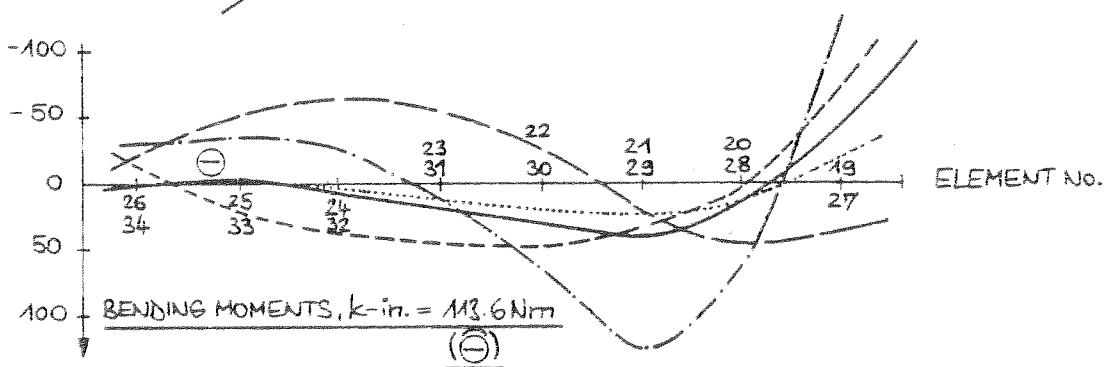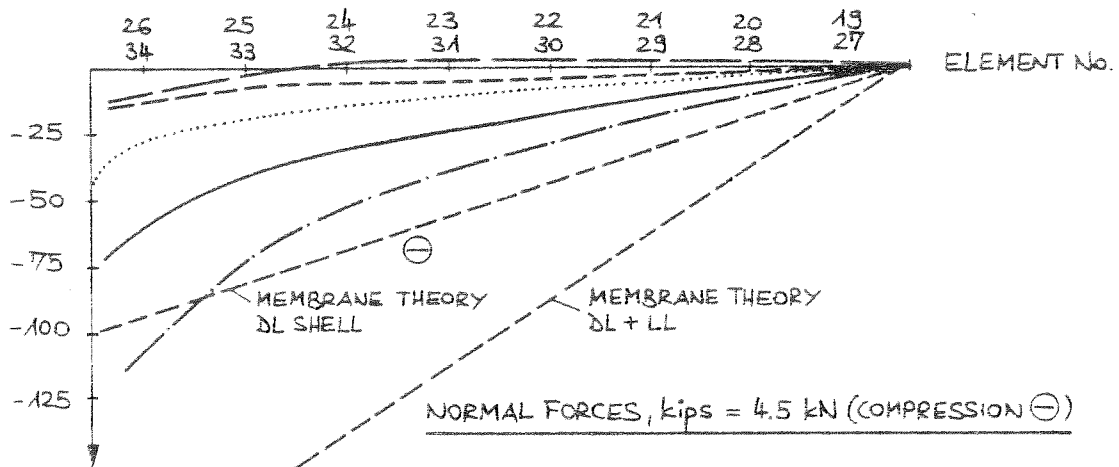
1) ———   DL SHELL

2) - - - -   DL EDGE BEAM

3) — — —   DL CROWN BEAM

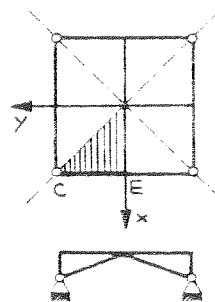4) · · · · · · LL

5) — · —   1) + 2) + 3) + 4)

FIG. 7.5 GABLE SHELL - CROWN BEAM, LINEAR ANALYSIS
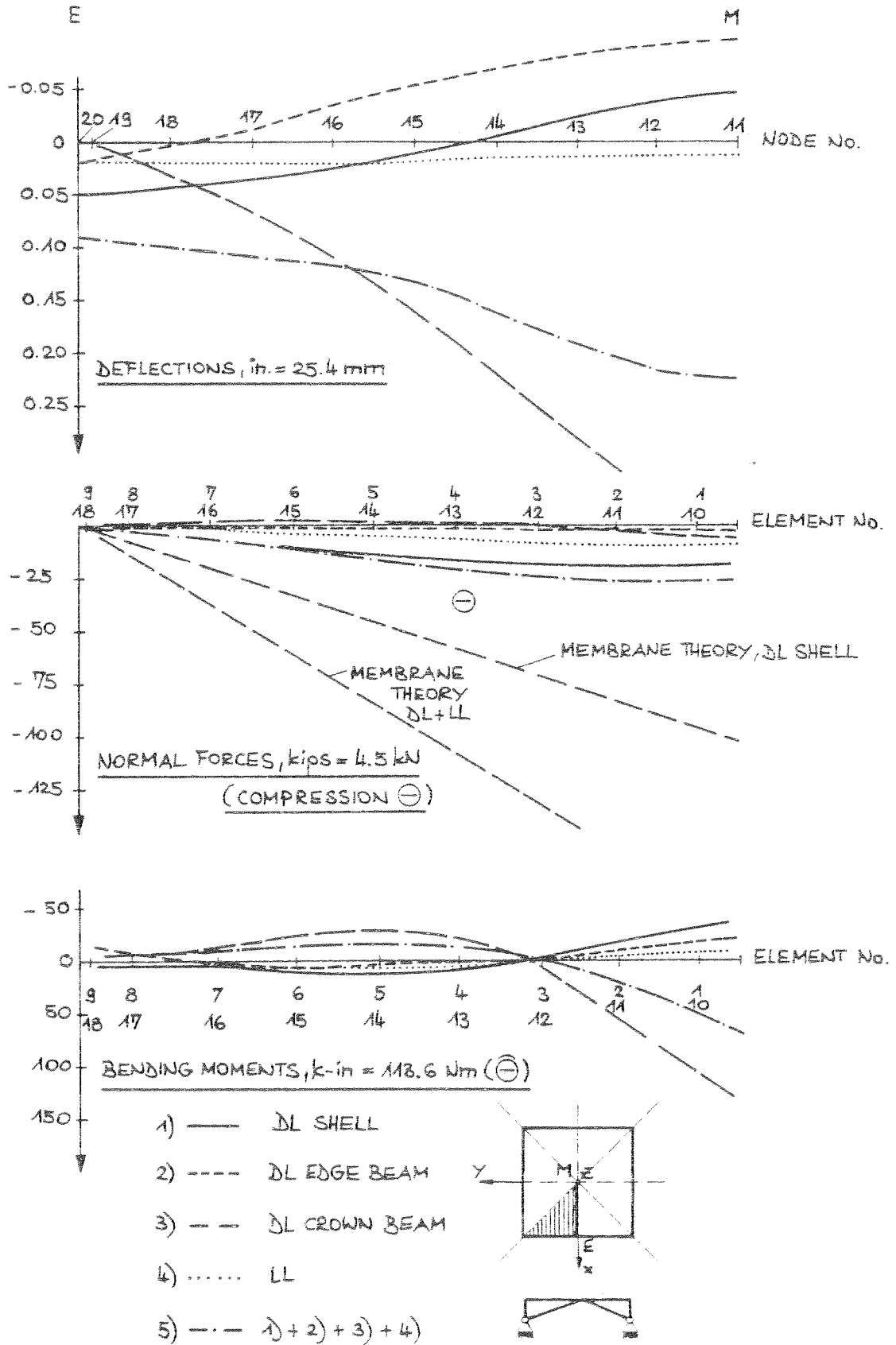
FIG. 7.6 GABLE SHELL - CROWN BEAM , LINEAR ANALYSIS
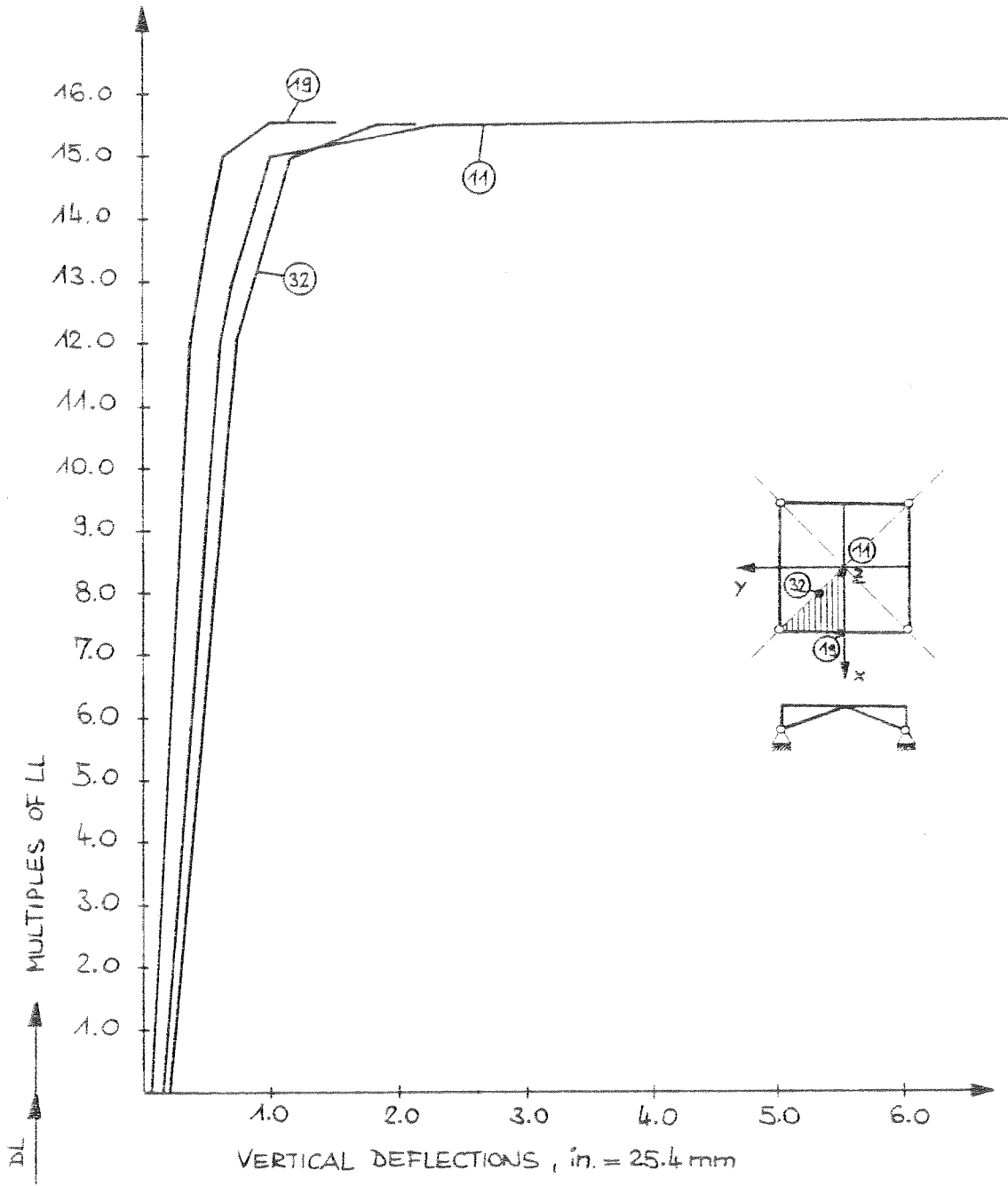
FIG. 7.7 GABLE SHELL, LOAD - DEFLECTION CURVES

FIG. 7.8 GABLE SHELL, CRACK PROPAGATION, DEPTH AND AVERAGE DIRECTIONS
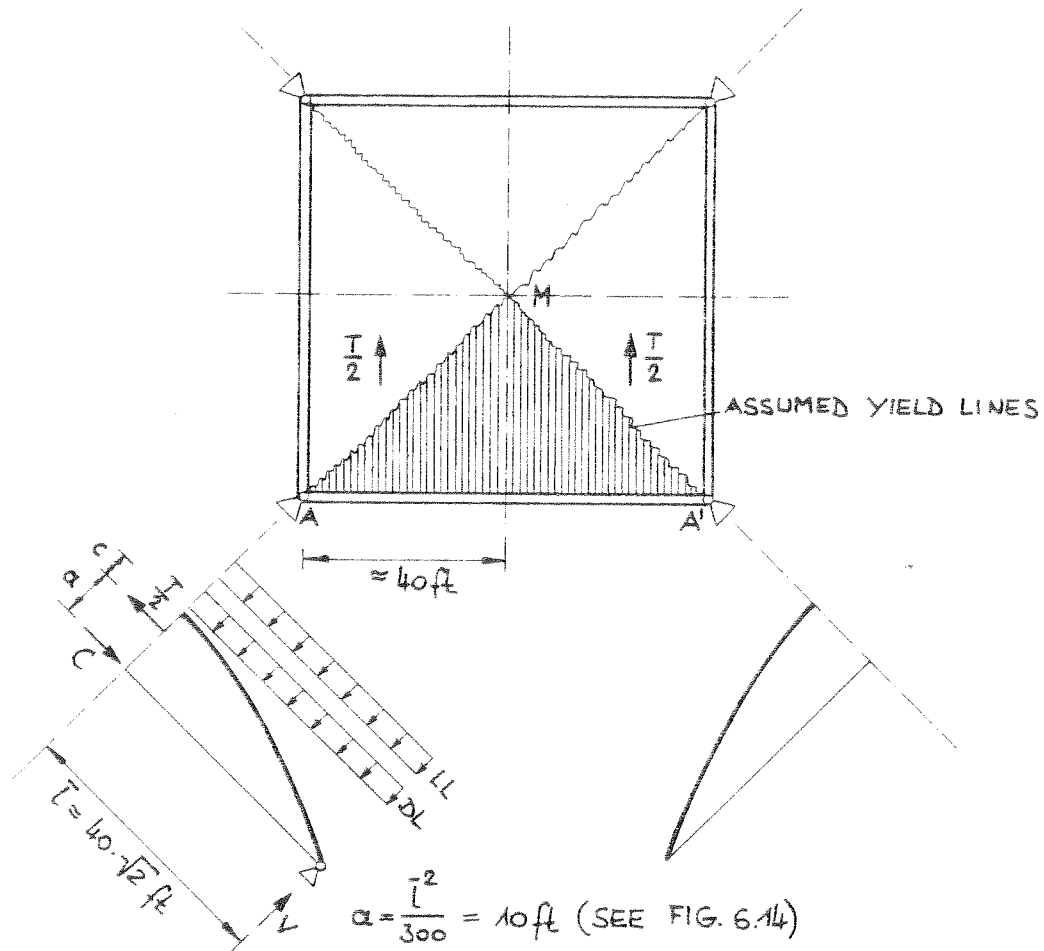
TOTAL NORMAL FORCE T ALONG DIAGONALS AM AND A'M :

$T = 12$ kips/ft $\cdot$ 80 ft $= 960$ kips (SEE FIG. 6.14)

(a) INTERNAL MOMENT M_i^{ULT} ALONG A'A

$\qquad M_i^{ULT} = T \cdot a = 960 \cdot 10 = 9600$ k-ft

(b) EXTERNAL MOMENT M_a (1/4TH OF THE SHELL)

$\qquad \begin{matrix} DL \approx 114 \text{ kips} \\ LL \approx 36 \text{ kips} \end{matrix} \Big\rangle$ (SEE FIG. 7.2) ; CROWN BEAM NEGLECTED)

$\qquad M_a \approx (114 + f \cdot 36) \cdot 1/3 \cdot 40 = 1520 + f \cdot 480 \; [\text{k-ft}]$

(c) EQUILIBRIUM OF LOWER 1/4TH SHELL

$\qquad M_a = M_i^{ULT} \implies f = 16.8$

ULTIMATE LOAD : DL + 16.8 LL

FIG. 7.9 GABLE SHELL , YIELD LINE THEORY

the failure is caused by yielding of the steel whereas the nonlinear analysis predicted failure of concrete. This example emphasizes that yield line theory has to be applied carefully, i.e., that additional considerations are sometimes necessary. In this case a rough estimate of the ultimate capacity of the edge beam proves that it will fail prior to the shell reinforcement. The maximum normal force for DL is $N^{DL} = 135$ kips and for LL the normal force is $N^{LL} = 40$ kips (Fig. 7.5). Assuming an ultimate normal force of $N = 750$ kips (Fig. 4.3) the ultimate load capacity would be DL + 15 LL which is less than predicted by yield line theory and comes close to the value obtained by nonlinear analysis.

7.3 Nonlinear Analysis Including Creep and Shrinkage

Fig. 7.10 and Fig. 7.11 compare load deflection curves for instantaneous loading with those obtained for sustained loads. One can observe a great time-dependent influence. Within 180 days deflections have increased to about 4 times their values at 28 days. However, one must admit that the deflections are still small.

In this structure the stresses originating from dead load are relatively small and hence creep effects are of minor importance compared to shrinkage effects. The additional deformations are therefore mainly affected by shrinkage. Shrinkage causes tensile stresses in the shell and hence additional compressive forces are evoked in the stiffer edge members which resist the shrinkage deformations of the shell. This redistribution can be seen in Fig. 7.12. These additional forces are responsible for the reduction of the ultimate load capacity to about DL + 14 LL.

The crack propagation starts earlier and is more intense (e.g.

cracks through the thickness along the diagonal) than for instantaneous
loading (Fig. 7.13).

7.4 Comparison with other Solutions

The example analyzed by Kabir [15] has the following properties:

length   :   L = 80 ft (24 m)
rise   :   h = 8 ft (2.4 m) $(L/2)/h = 5.0$
thickness   :   t = 3 in. (7.5 cm) $(L/2)/t = 160$

cross section edge beam :   16 in. x 12 in. = 192 sq in.

(40 cm x 30 cm = 1200 cm^2)

cross section crown beam: A: 8 in. x 24 in. = 192 sq in.
(20 cm x 60 cm = 1200 cm^2)

B: 12 in. x 48 in. = 576 sq in.

(30 cm x 120 cm = 3600 cm^2)

The shell reinforcement is the same but the reinforcement ratio is higher,
namely ρ = 0.53%.

The reinforcement ratio for the beams are:

edge beam   : ρ = 5.3%

crown beam A : ρ = 5.3%

crown beam B : ρ = 3.5%

The material properties are the same except for the tensile strength which
was assumed by Kabir to be f_t' = 270 psi (1.9 N/mm^2).

The ultimate load for the examples calculated by Kabir are about half
the value of the example of this study. An explanation is given by the
yield line theory. The yield line theory is better applicable for the
example of Kabir since the shell is flatter and the thickness and the ten-
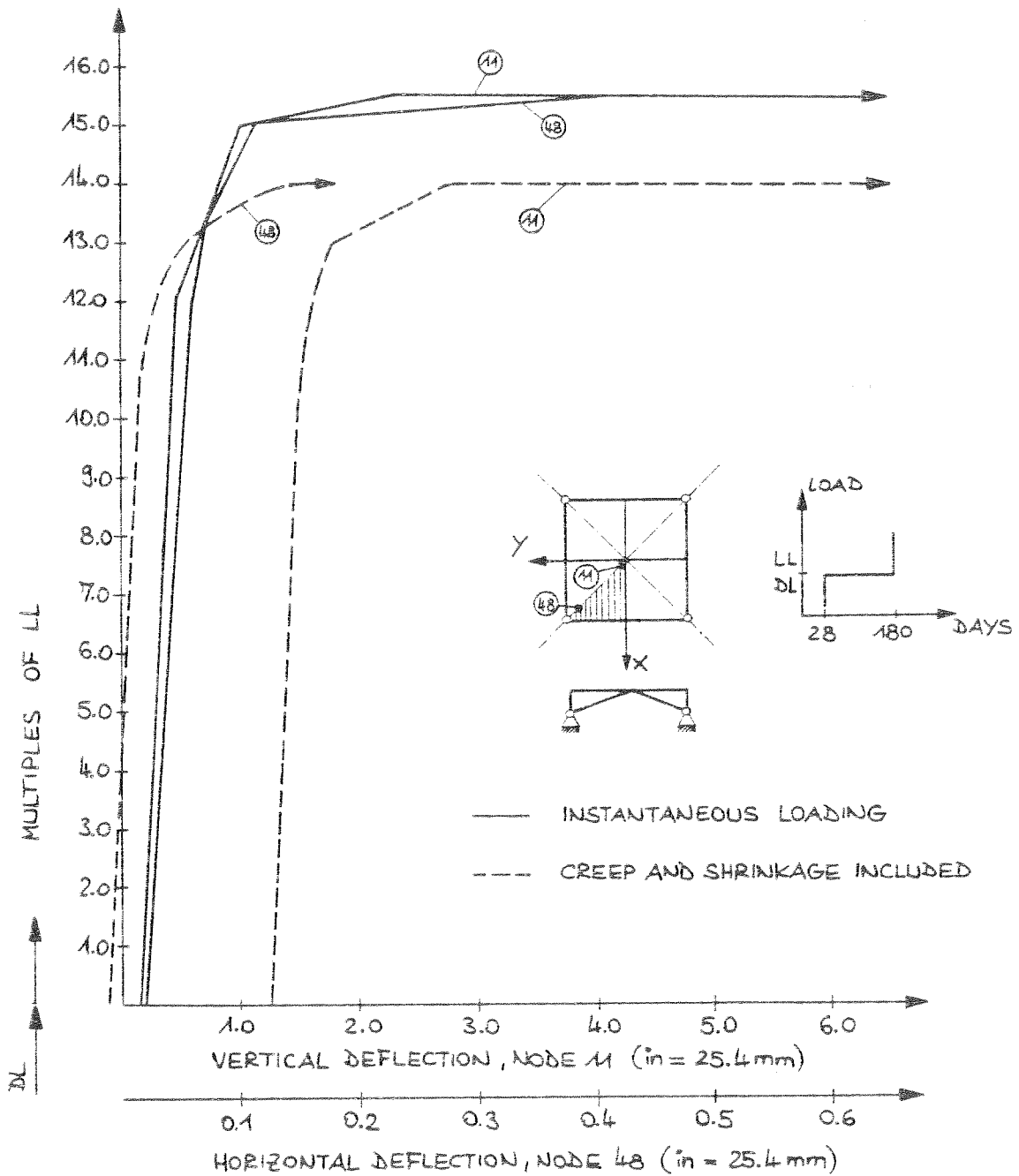sile strength are smaller too, i.e. failure will occur by yielding as

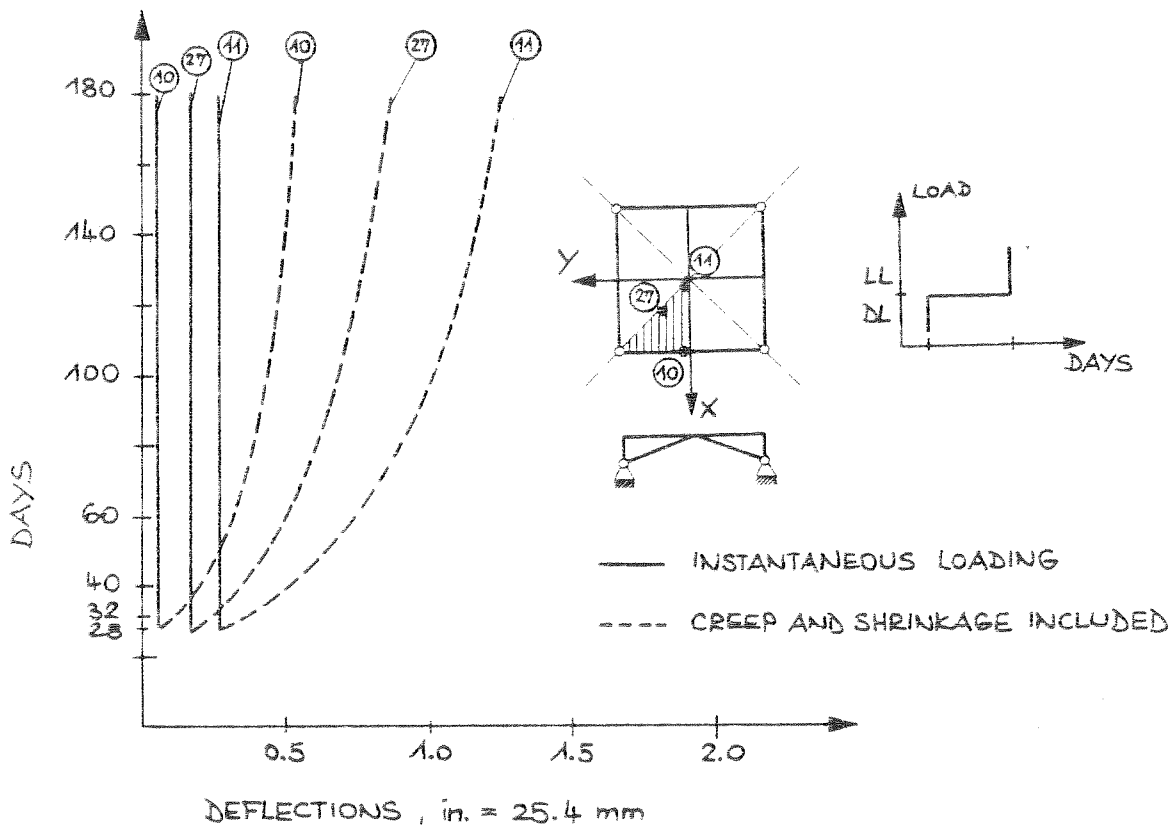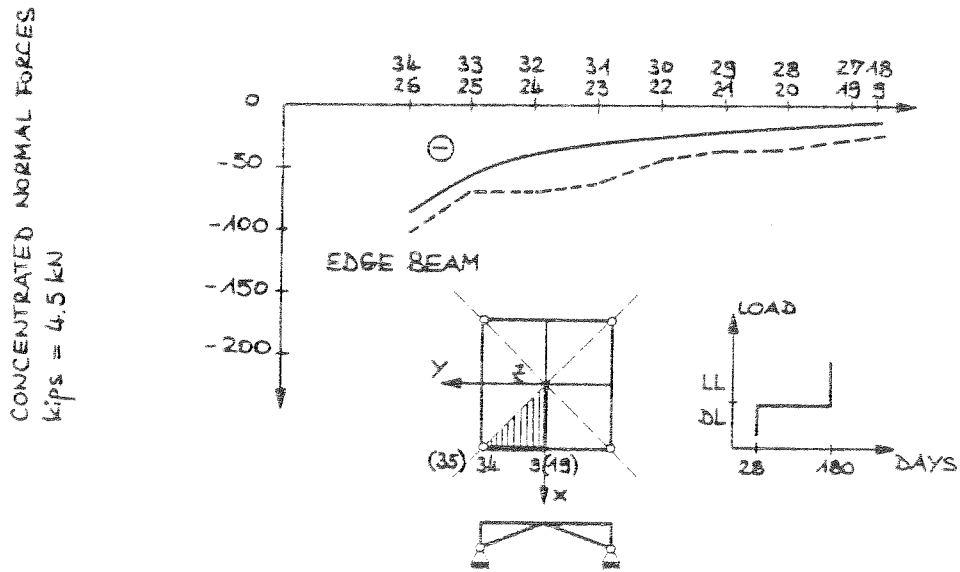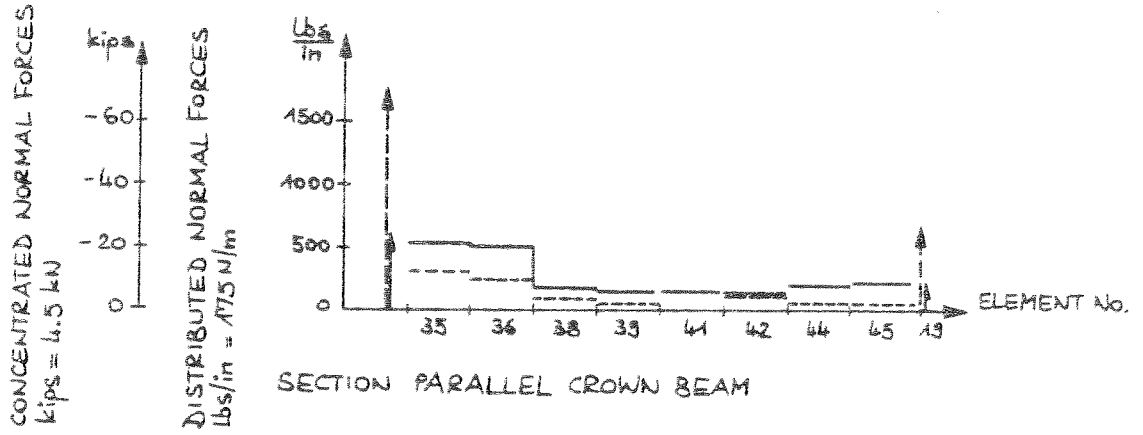FIG. 7.10 GABLE SHELL, INFLUENCE OF CREEP AND SHRINKAGE

FIG. 7.11 GABLE SHELL, INFLUENCE OF CREEP AND SHRINKAGE

81

CONCENTRATED NORMAL FORCES
kips = 4.5 kN

DISTRIBUTED NORMAL FORCES
Lbs/in = 175 N/m

$\frac{Lbs}{in}$

kips
- 60
- 40
- 20
0

1500
1000
500
0

35 36 38 39 41 42 44 45 19   ELEMENT No.

SECTION PARALLEL CROWN BEAM

CONCENTRATED NORMAL FORCES
kips = 4.5 kN

34 33 32 31 30 29 28 27 18
26 25 24 23 22 21 20 19 9

0
-50
-100
-150
-200

⊖

EDGE BEAM

Y

(35) 34 3 (19)
x

LOAD

LL
DL

28   180   DAYS

——— INSTANTANEOUS LOADING, 28 DAYS

- - - CREEP AND SHRINKAGE INCLUDED, 180 DAYS

7.12 GABLE SHELL, NORMAL FORCE REDISTRIBUTION

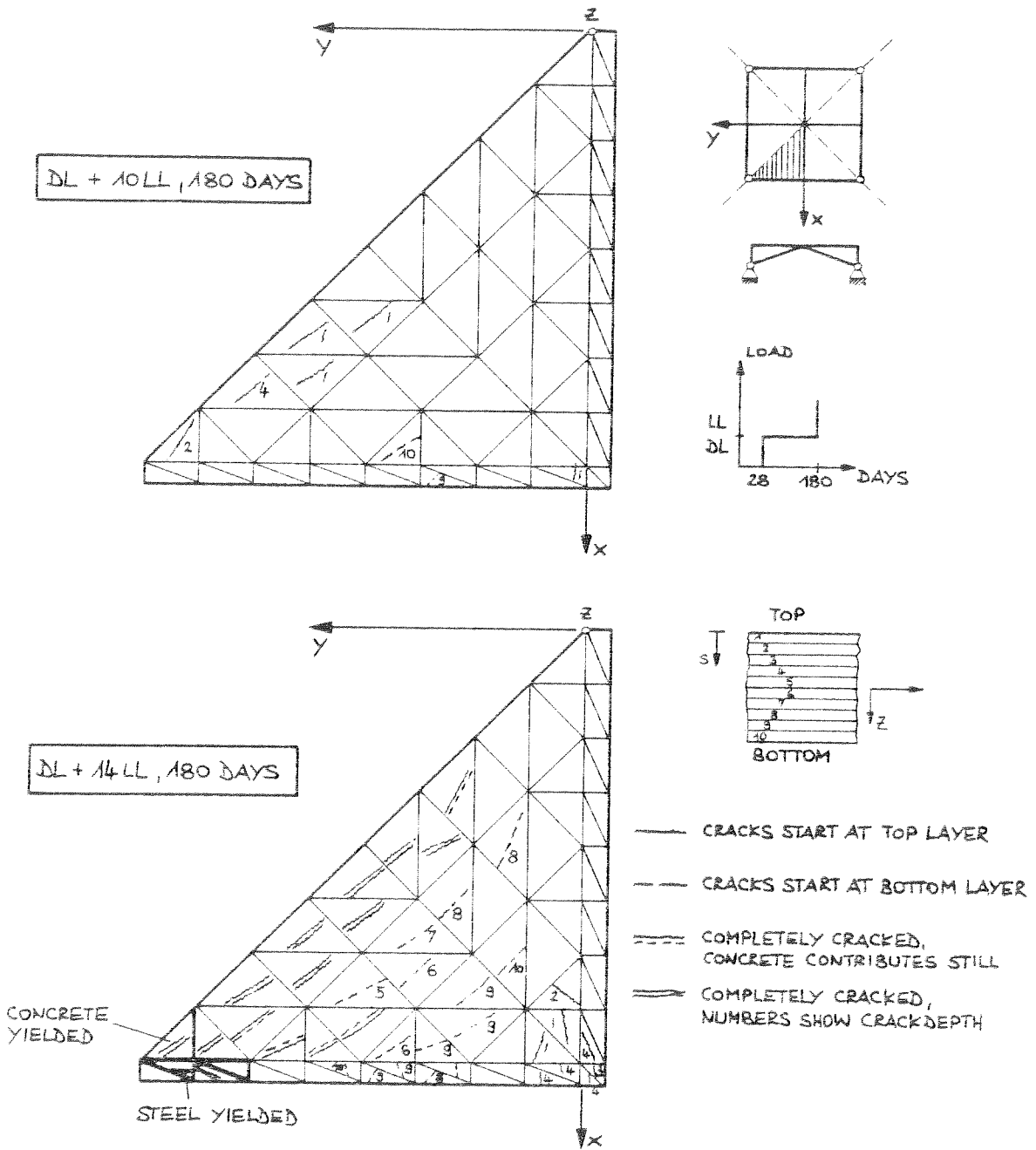FIG. 7.13 GABLE SHELL, CRACK PROPAGATION, DEPTH AND AVERAGE DIRECTIONS

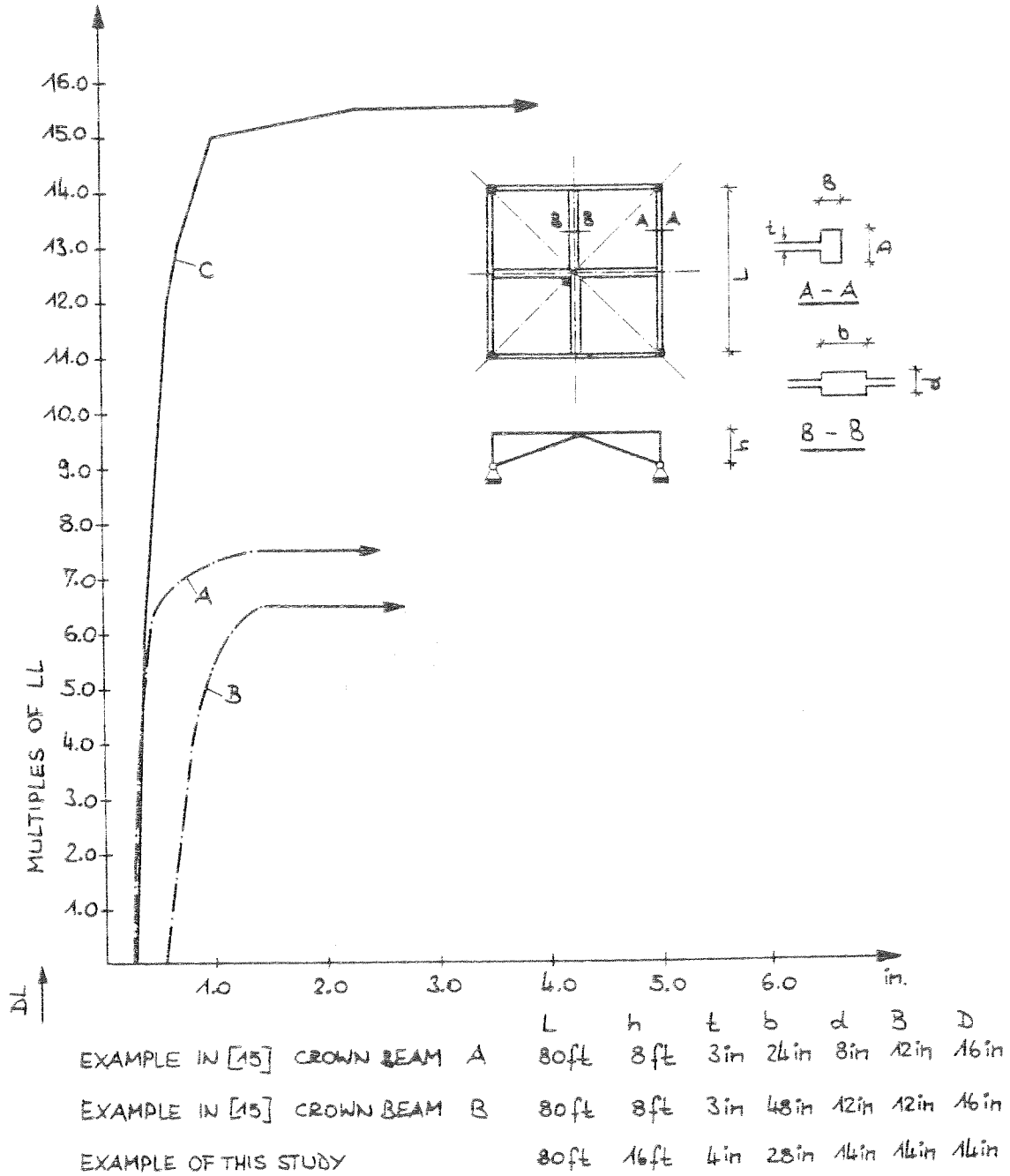|		L	h	t	b	d	B	D
EXAMPLE IN [15]	CROWN BEAM A	80ft	8ft	3in	24in	8in	12in	16in
EXAMPLE IN [15]	CROWN BEAM B	80ft	8ft	3in	48in	12in	12in	16in
EXAMPLE OF THIS STUDY		80ft	16ft	4in	28in	14in	14in	14in

FIG. 7.14   GABLE SHELL   COMPARISON WITH OTHER RESULTS

presumed. Due to yield line theory the ultimate load is proportional to the rise of the shell, i.e. that for half the rise the ultimate load is reduced to half the value. For this example the ultimate load would be approximately DL + 8 LL which is close to the solution obtained by Kabir for the gable shell with the smaller crown beam A. For the gable with the larger crown beam B he determines a lower ultimate load. In the opinion of the author both systems should have the same ultimate load since for flat shells the ultimate load depends essentially on the amount of shell reinforcement which is the same for both structures. However cracking will start earlier in the case of the larger crown beam (larger deflections) which causes a more distinct nonlinear load deflection curve with a faster decreasing slope. It is believed that the prediction of the ultimate load in [15] is based on arbitrarily chosen tolerances which stopped the solution prior to its failure. A further investigation of the results for this load step would prove that the structure would be able to pick up additional load even though the deflections were quite large.

8.   INVERTED UMBRELLA SHELL

8.1   Linear Analysis

For this shell the finite element mesh of the gable shell can be used. The only thing required to change is the boundary conditions. Again a rough statical check of the linear analysis is made and presented in Fig. 8.1.

In Fig. 8.2 the behavior of the individual members, beams and the shell itself is demonstrated. From this it can be seen that the edge beam has the greatest influence on the deflections. Membrane theory predicts

normal forces which are too large but gives a closer solution than was the case for the gable shell.

8.2 Nonlinear Analysis

This structure shows a marked nonlinear behavior from the very beginning (Fig. 8.4). Responsible for this is the early cracking of the edge beam. First cracks are observed under DL + LL. Later on at the load level DL + 3.0 LL cracks propagate into the shell (Fig. 8.5). At about DL + 6.5 LL the cracking is essentially terminated but the load capacity is not yet exhausted. The further behavior is approximately linear up to DL + 7.75 LL. At this load level the steel in the edge beam yields and the concrete in the valley beam reaches its compressive strength (Fig. 8.6).

Fig. 8.7 shows deflections at several load levels. The shape of the curves compares well with the deflection profiles observed in tests [9]. These deflection profiles give also an idea for the assumption of the yield lines. The yield line theory is applied in Fig. 8.8. The yield line theory for this type of shell turned out to be a very uncertain means to determine the ultimate load which is proportional to the lever arm a of the total compression force C. This lever arm may take values between 1 ft and 2 ft and thus the ultimate load capacity may differ by 100%. Here, with the lever arm assumed to be 1.7 ft an ultimate load of DL + 5.5 LL is calculated.

8.3 Nonlinear Analysis Including Creep and Shrinkage

Until now only one run could be made. Unfortunately the program was stopped too early at a load level of DL + 3.0 LL (Fig. 8.9). It is assumed that approximately the same ultimate load is reached as for instantaneous loading since the failure is essentially caused by yielding of the steel

LEVER ARM IN ft. RELATIVE TO Lo POINT   NORMAL FORCES ALONG AA' IN kips

Lever arm	DUE TO DL	DUE TO LL
16	+34	+24.7
15	+50	+17.4
13	+3	+5.4
11	−3	+0.7
9	−4.8	−1.0
7	−2	−0.3
5	~0	−1.1
3	−24.5	−8.6
1	−24.4	−9.6
0	−87	−27

SYMMETRY

$$V = V^{DL} + V^{LL}$$
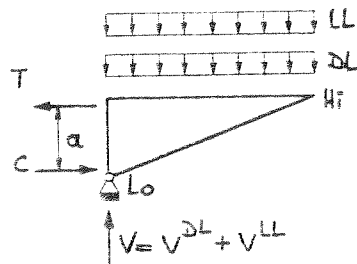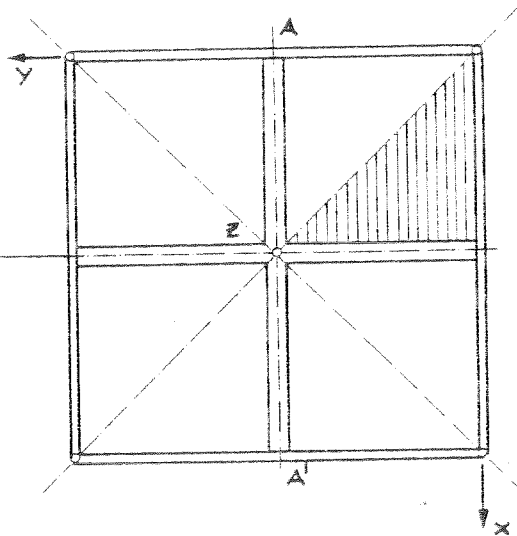
(a) VERTICAL LOADS $\left(\frac{1}{8}\text{TH OF THE SHELL}\right)$

$$DL \hat{=} 57 \text{ kips}$$
$$LL \hat{=} 18 \text{ kips} \Big\rangle (\text{SEE FIG. 7.2})$$

REACTION

$$V^{DL} = 59 \text{ kips}$$
$$V^{LL} = 19 \text{ kips}$$

(b) MOMENTS ALONG $\overline{A'A}$

DUE TO DL : 4480 k-ft $\Big\rangle (\text{SEE FIG. 7.2})$
DUE TO LL : 1470 k-ft

$$\sum_{i=1}^{10} a_i T_i^{DL} = 4300 \text{ k-ft.}$$
$$\sum_{i=1}^{10} a_i T_i^{LL} = 1400 \text{ k-ft.}$$

(c) HORIZONTAL FORCES

TENSION $T^{DL} = 147 \text{ kips}$
TENSION $T^{LL} = 48 \text{ kips}$

COMPRESSION $C^{DL} = 143 \text{ kips}$
COMPRESSION $C^{LL} = 48 \text{ kips}$

FIG. 8.1 INVERTED UMBRELLA SHELL, ROUGH STATICAL CHECK

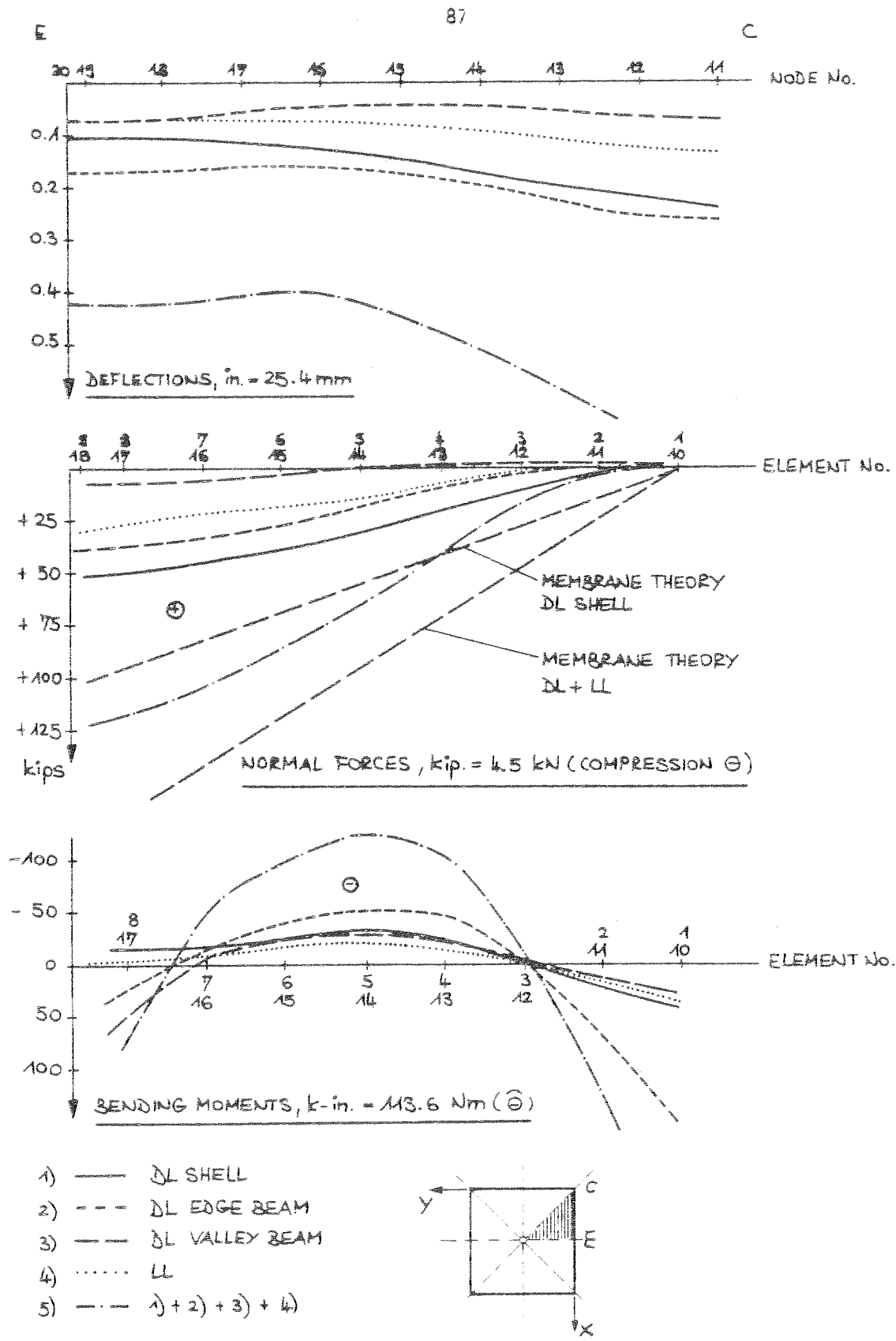E   C

| 20 19 | 18 | 17 | 16 | 15 | 14 | 13 | 12 | 11 | NODE No. |

0.1
0.2
0.3
0.4
0.5

DEFLECTIONS, in. = 25.4 mm

| 8 | 8 | 7 | 6 | 5 | 4 | 3 | 2 | 1 | ELEMENT No. |
| 18 | 17 | 16 | 15 | 14 | 13 | 12 | 11 | 10 | |

+ 25
+ 50
+ 75
+ 100
+ 125

⊕

MEMBRANE THEORY
DL SHELL

MEMBRANE THEORY
DL + LL

kips

NORMAL FORCES, kip. = 4.5 kN (COMPRESSION ⊖)

− 100
− 50

⊖

| 8 | | | | | | 2 | 1 | |
| 17 | | | | | | 11 | 10 | ELEMENT No. |

0

| 7 | 6 | 5 | 4 | 3 | |
| 16 | 15 | 14 | 13 | 12 | |

50
100

BENDING MOMENTS, k-in. = 113.6 Nm (⊖)

1) ——— DL SHELL
2) - - - DL EDGE BEAM
3) —— — DL VALLEY BEAM
4) ····· LL
5) —·— 1) + 2) + 3) + 4)

Y

C
E

X

FIG. 8.2 INVERTED UMBRELLA SHELL, EDGE BEAM, LINEAR ANALYSIS
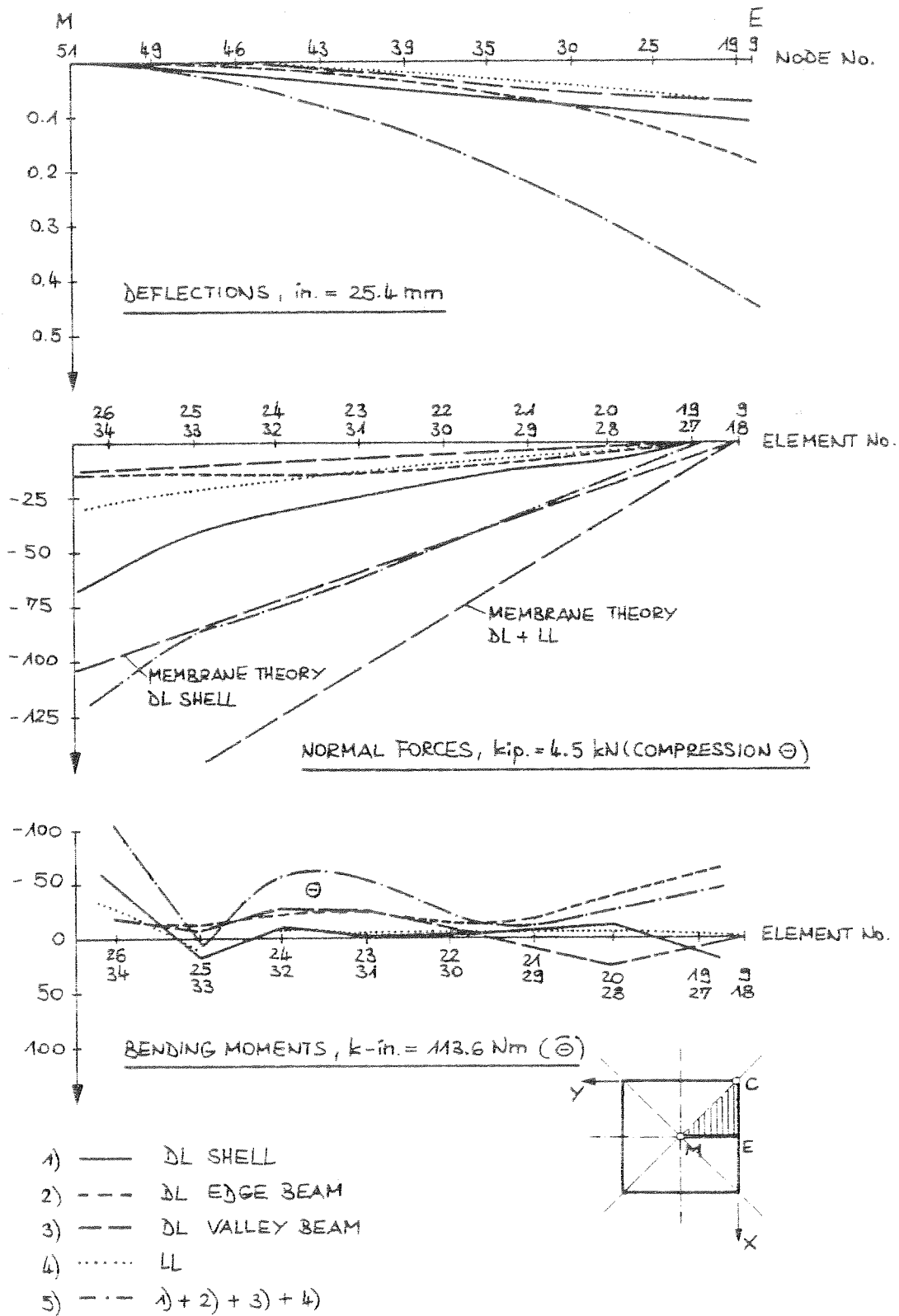
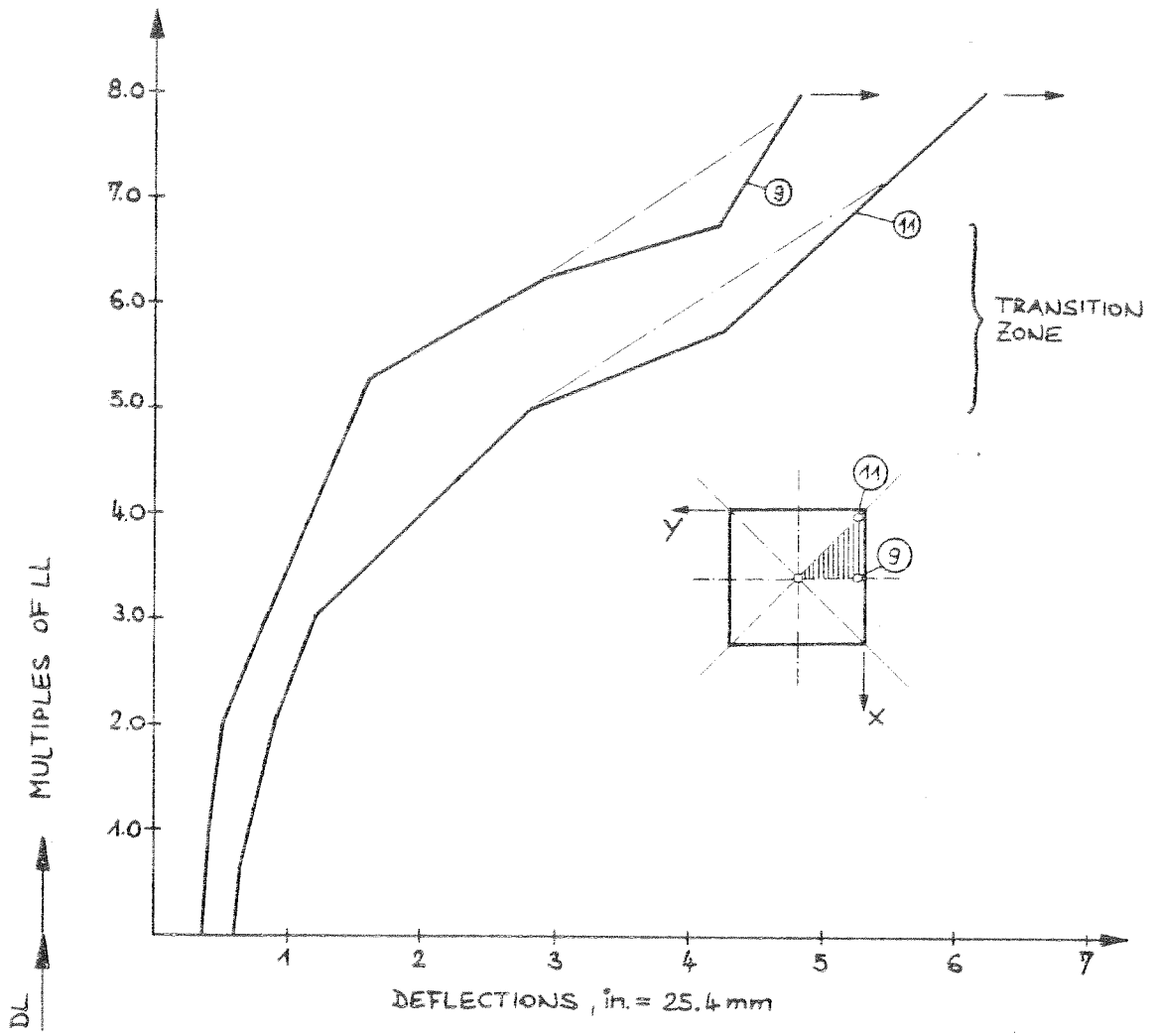FIG. 8.3 INVERTED UMBRELLA SHELL, VALLEY BEAM, LINEAR ANALYSIS
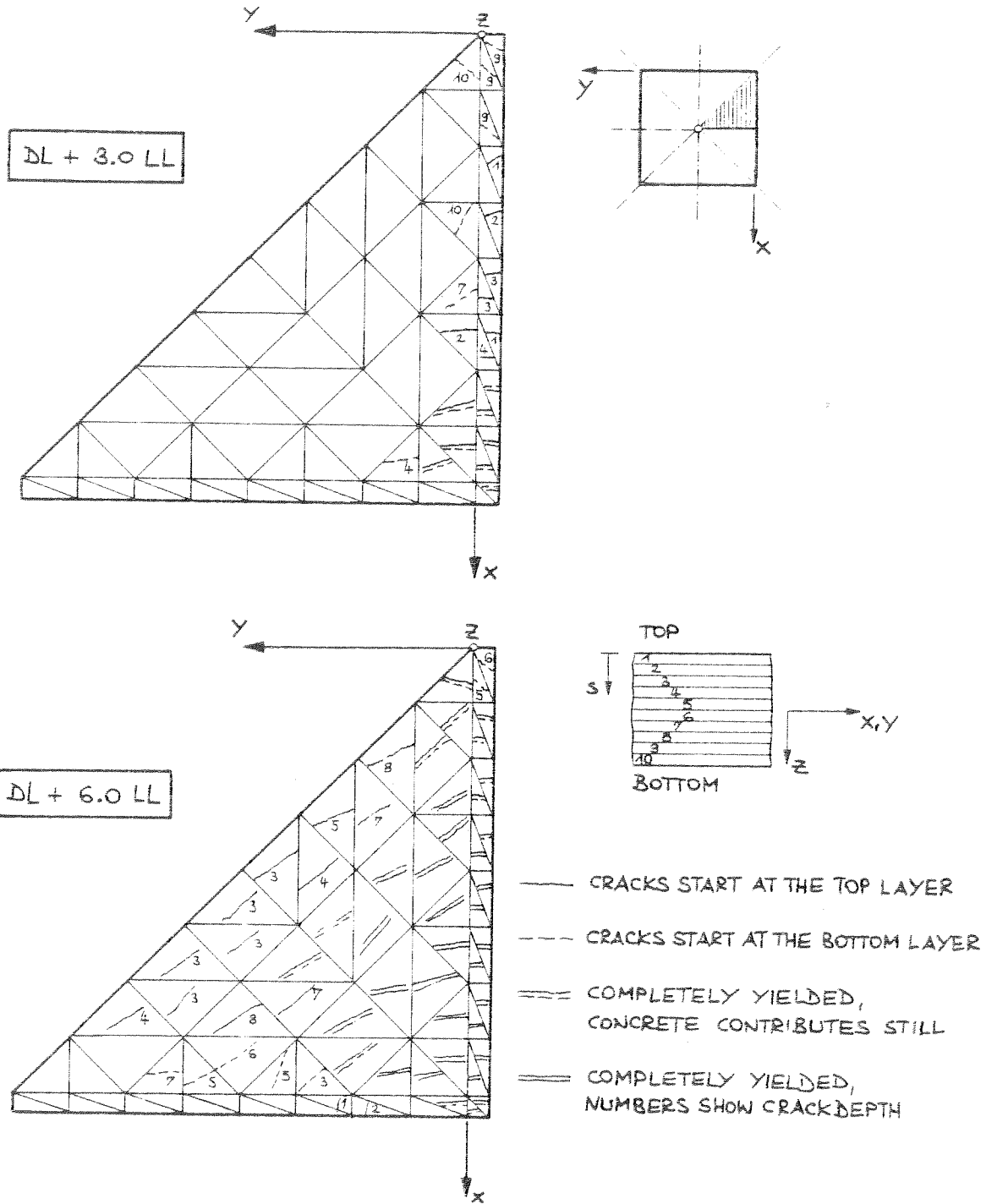
FIG. 8.4 INVERTED UMBRELLA SHELL, LOAD-DEFLECTION CURVES

DL + 3.0 LL

DL + 6.0 LL

TOP

BOTTOM

———— CRACKS START AT THE TOP LAYER

— — — CRACKS START AT THE BOTTOM LAYER

≡≡ COMPLETELY YIELDED, CONCRETE CONTRIBUTES STILL

═══ COMPLETELY YIELDED, NUMBERS SHOW CRACK DEPTH

FIG. 8.5 INVERTED UMBRELLA SHELL, CRACK PROPAGATION, DEPTH AND AVERAGE DIRECTIONS

CRACKS ON THE TOP SIDE

DL + 7.75 LL

TOP

BOTTOM

CRACKS ON THE BOTTOM SIDE

STEEL YIELDED

CONCRETE YIELDED
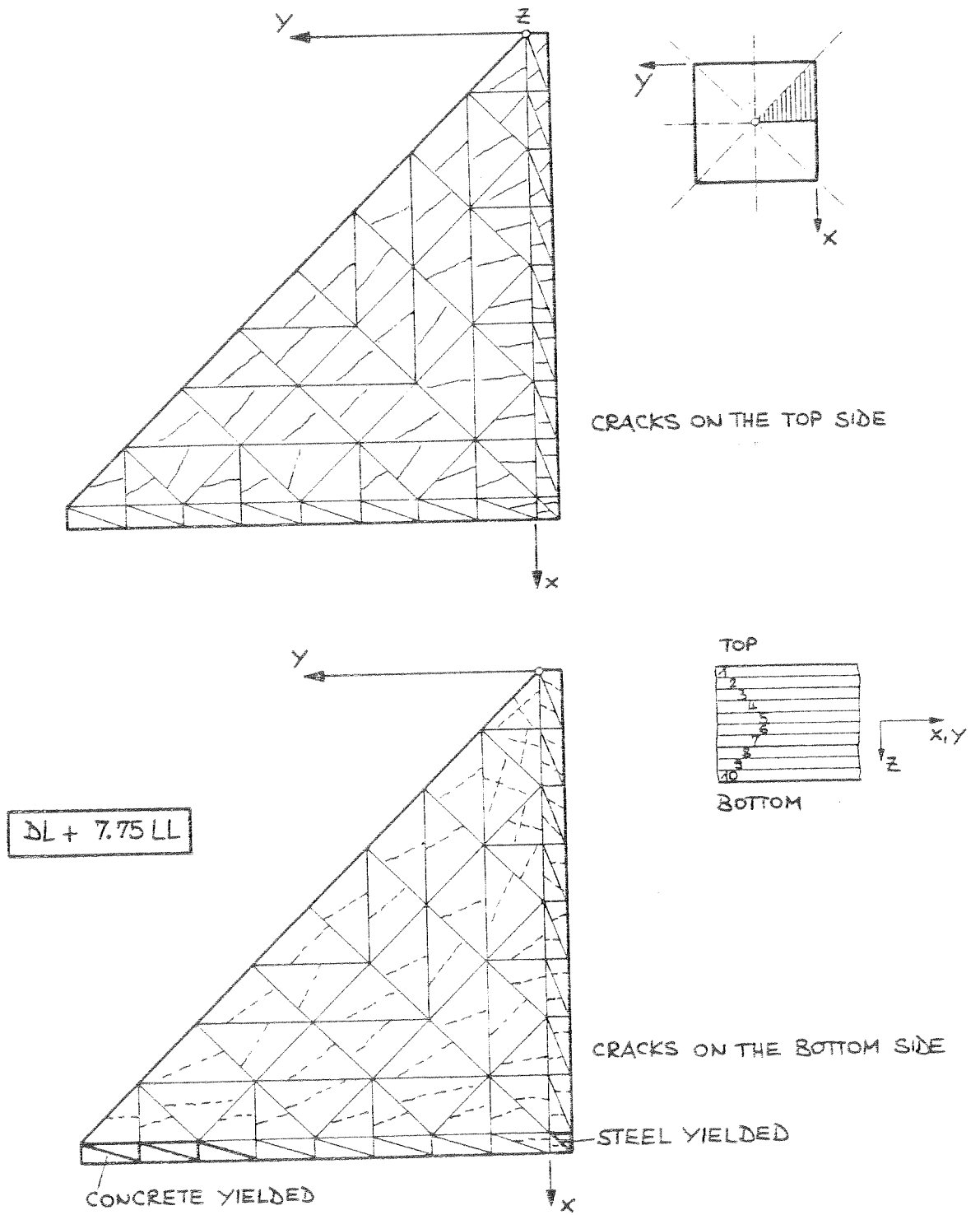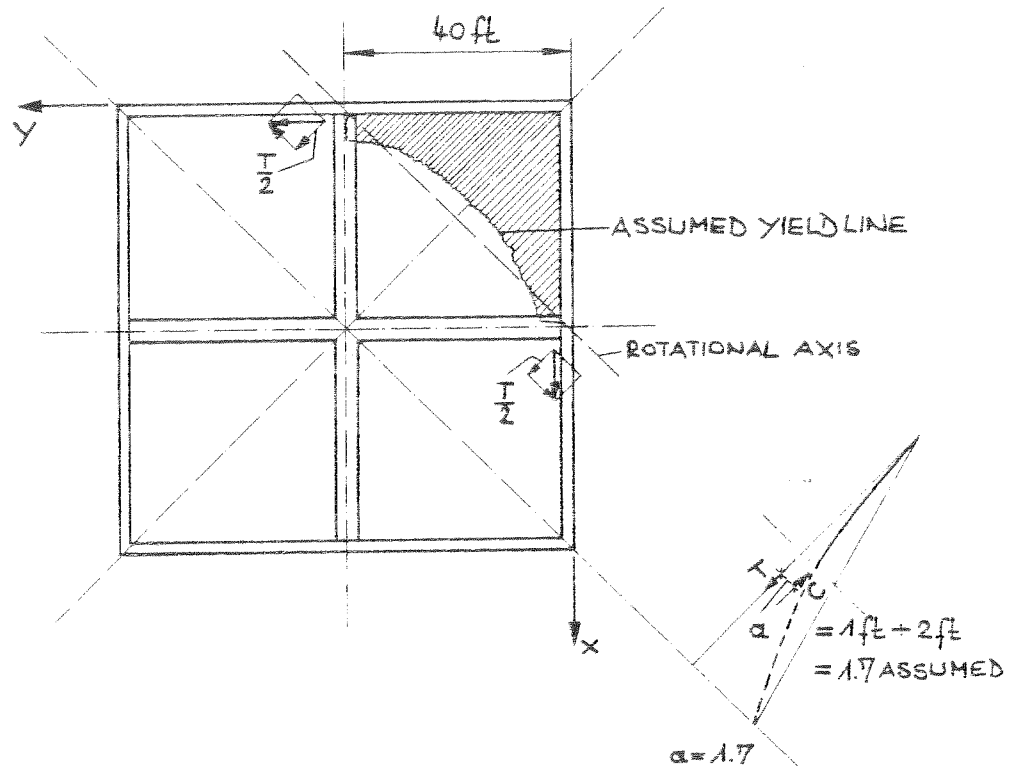
FIG. 8.6 INVERTED UMBRELLA SHELL, CRACK PATTERNS
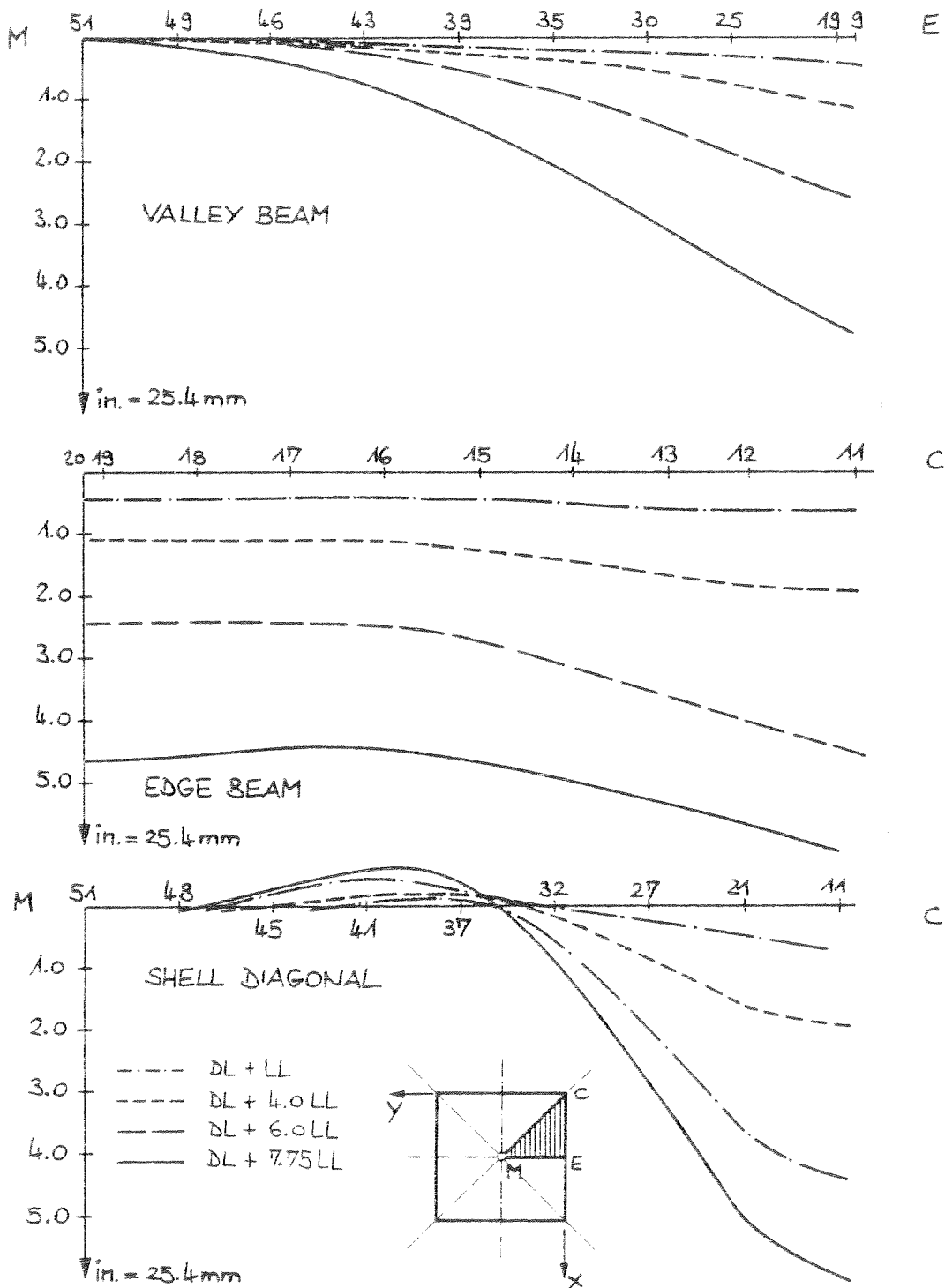
FIG. 8.7 INVERTED UMBRELLA SHELL — DEFLECTIONS

EQUILIBRIUM OF THE EDGE SECTION :

TENSION FORCE (EDGEBEAMS) $T = \frac{\sqrt{2}}{2} \cdot 2 \cdot 60\,000 \cdot 10.12 = 860$ kips

  INTERNAL MOMENT : (1/8 OF THE SHELL)

   $\begin{array}{l} DL \approx 57 \text{ kips} \\ LL \approx 18 \text{ kips} \end{array} \Big\rangle$ (SEE FIG. 8.1)

   $M_{ext} = (57 + f \cdot 18) \cdot 1/3 \cdot \sqrt{2}/2 \cdot 40$

   $M_{int}^{ULT} = M_{ext} \rightsquigarrow f = 5.5$

  $\rightsquigarrow$ ULTIMATE LOAD : DL + 5.5 LL

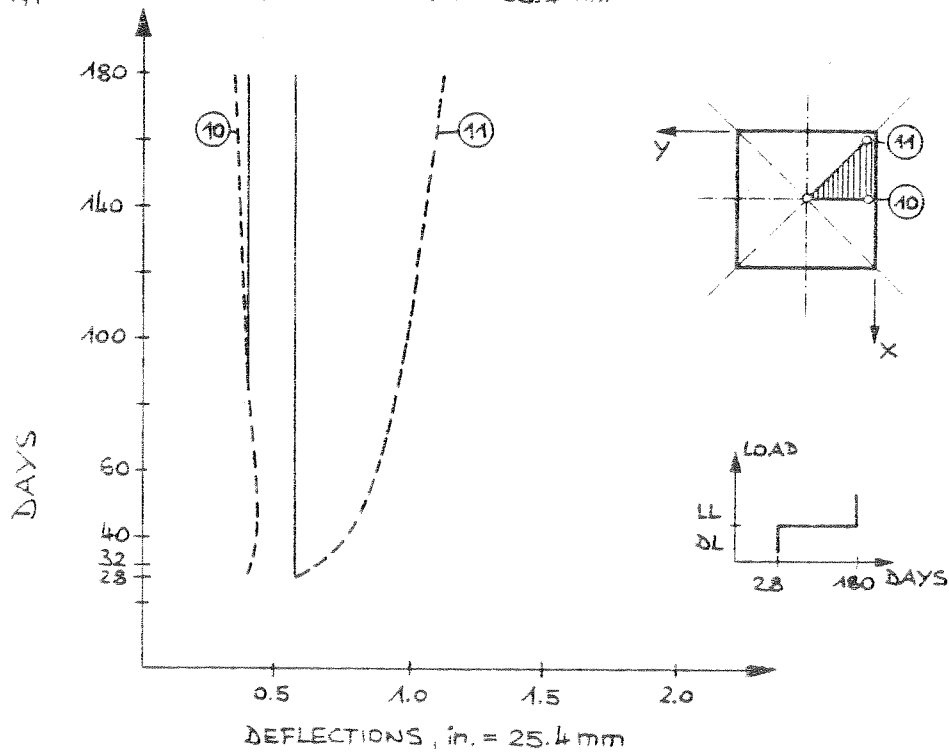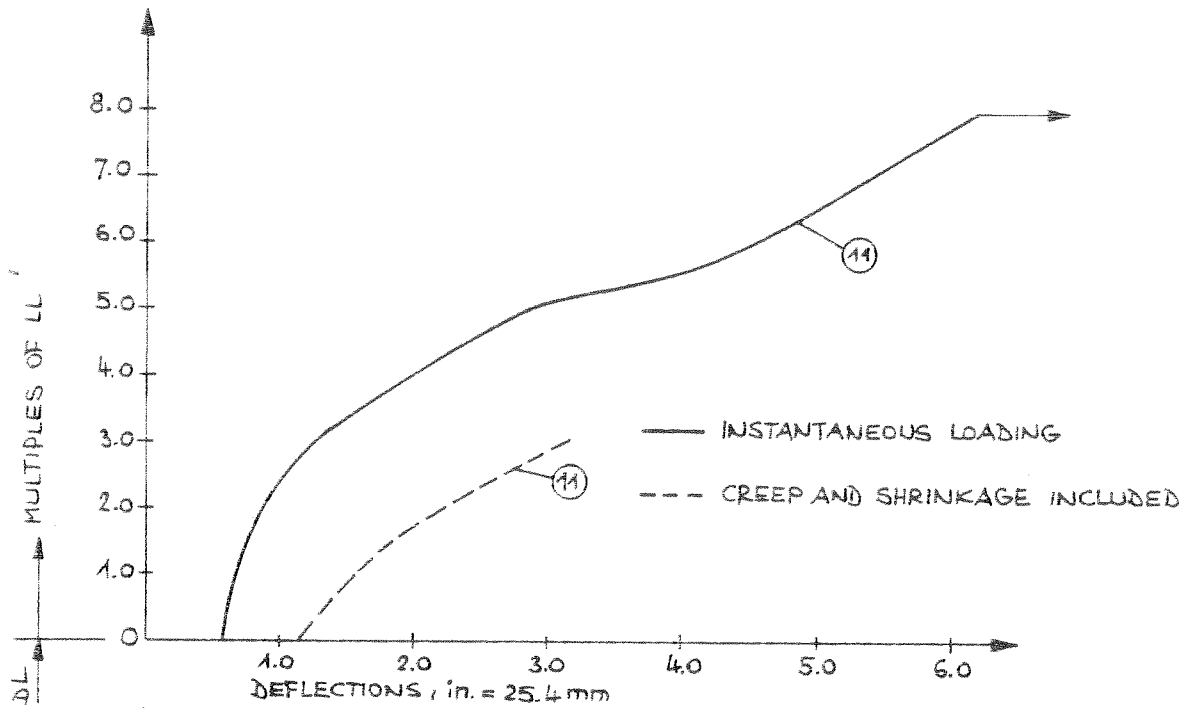FIG. 8.8   INVERTED UMBRELLA SHELL, YIELD LINE THEORY

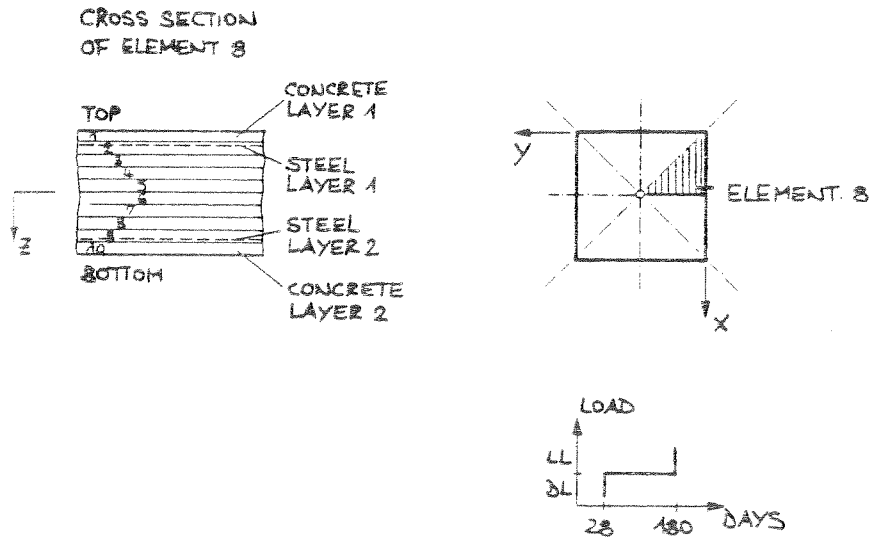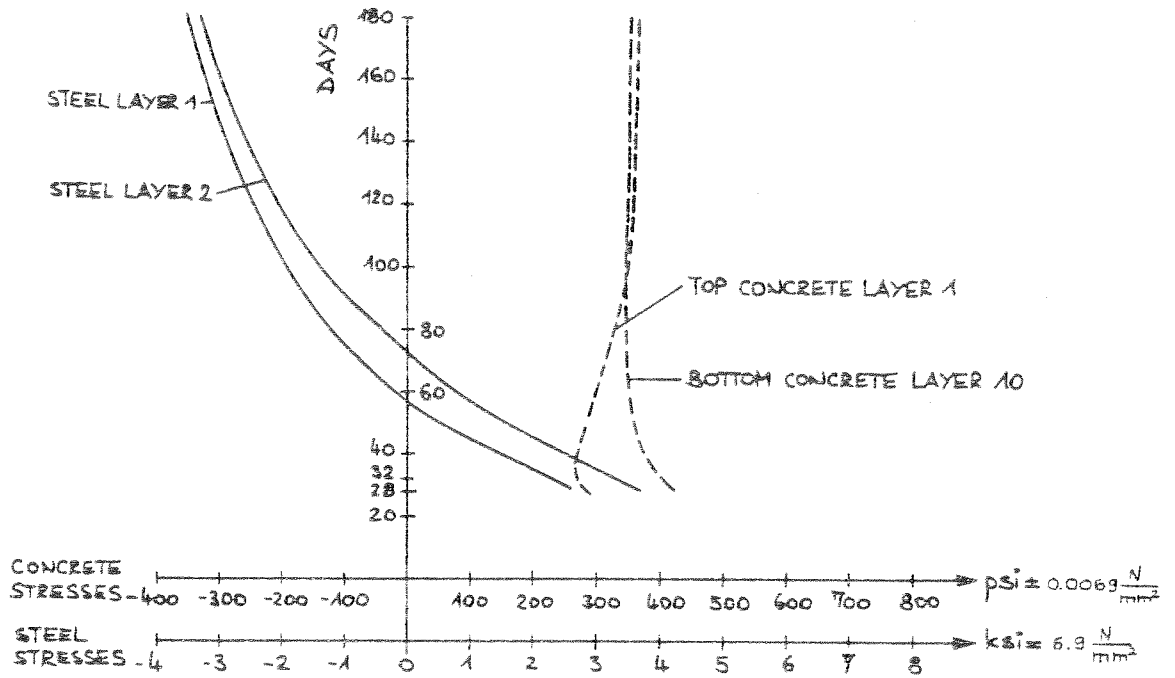FIG. 8.9 INVERTED UMBRELLA SHELL, INFLUENCE OF CREEP AND SHRINKAGE

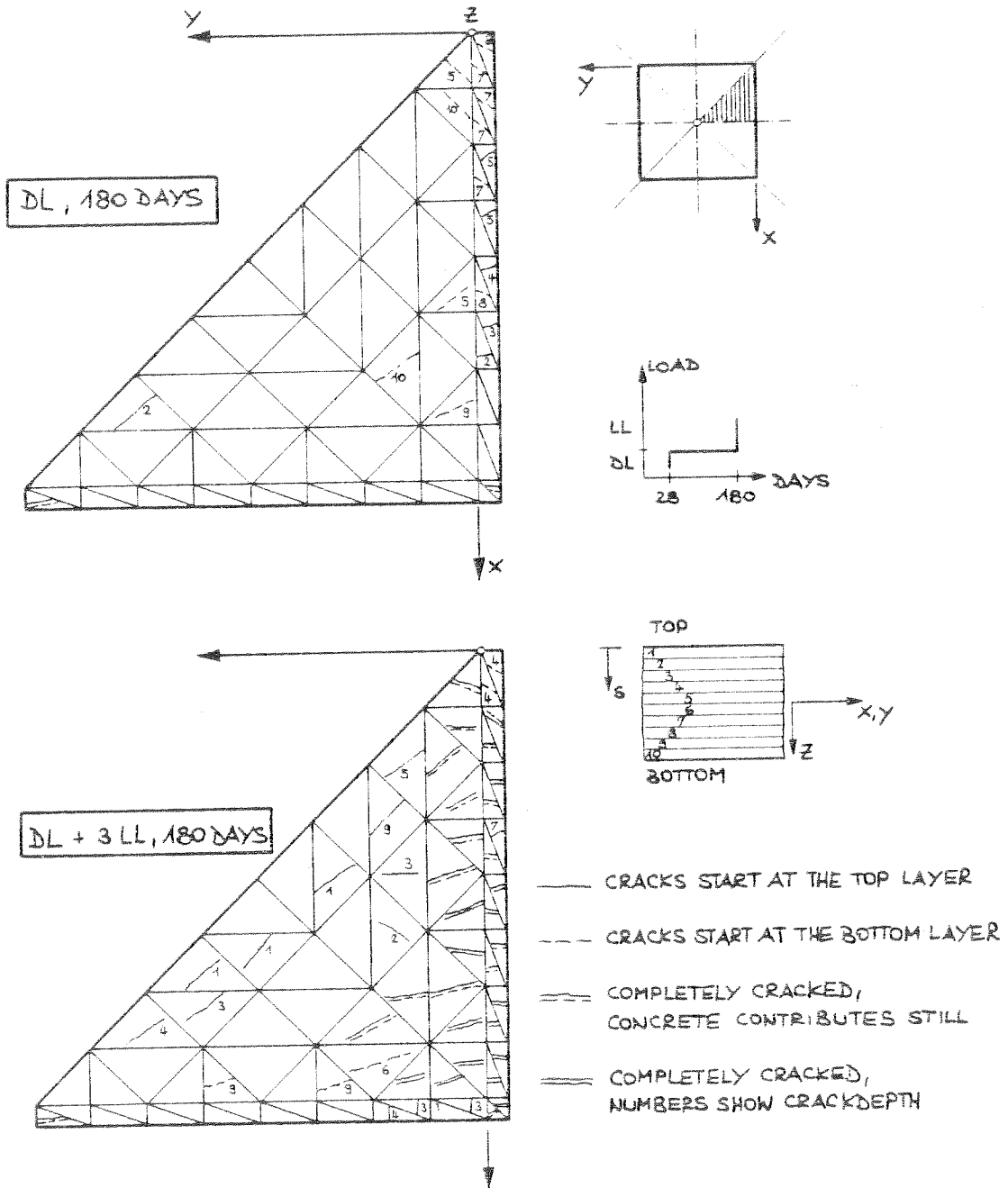FIG. 8.10 INVERTED UMBRELLA SHELL, STRESS REDISTRIBUTION

FIG. 8.11 INVERTED UMBRELLA SHELL, CRACK PROPAGATION
AND AVERAGE DIRECTIONS

reinforcement. Creep and shrinkage effects are of about the same order. In areas where tension dominates these effects are opposite. This can be seen in Fig. 8.10. At times less than 40 days creep strains are larger, therfore concrete tension stresses decrease. After 40 days shrinkage strains become predominant and cause concrete stresses to grow. Since the steel stresses become negative the average concrete stresses of all layers must be increasing, i.e. that shrinkage is more effective than creep. A comparison of the crack patterns with (Fig. 8.11) and without creep and shrinkage (Fig. 8.5) show that the time-dependent effects cause a much more intensive cracking.

8.4 Comparison with other Solutions

White reports in [9] on a test series performed on PVC- and microconcrete models. Investigated was a shell of square plan with

$$L = 24 \text{ ft } (7.2 \text{ m})$$
$$h = 3 \text{ ft } (0.9 \text{ m})$$
$$t = 1.5 \text{ in. } (3.8 \text{ cm})$$

$$(L/2)/h = 4$$
$$(L/2)/t = 96$$

The cross section of the edge beam is 6 in. x 4 in. (15 cm x 10 cm) = 24 sq in. (150 cm^2). The valley beam is specified as a thickened rib with increasing width.

The reinforcement ratio of the shell is $\rho = 0.6\%$ and that of the edge beam is $\rho = 3.2\%$. The yield strength of steel was 48 ksi (331 N/mm^2).

The ultimate load was reached at 145 psf (7 KN/m^2) which corresponds to approximately DL + 6 LL. The failure was initiated by yielding of the edge beam reinforcement followed by intense cracking along the diagonal. The rupture took place along a circle with a diameter $r = L/4\sqrt{2}$ (see Fig. 8.8). For a yield strength of 60 ksi (414 N/mm^2) the ultimate load would be

approximately DL = 8.0 LL which corresponds with the value obtained in this study. However, it should be kept in mind that the structure studied here is quite different and cannot really be compared with the structure investigated experimentally.

9. COMPARISON AND RECOMMENDATIONS FOR FURTHER STUDIES

Even though the few results of this investigation cannot be considered comprehensive, a useful summary of the information obtained is given in Fig. 9.1 and Fig. 9.2.

Recommendations for further studies are listed below:

1. Improvement and extension of the program NOTACS.

   Some ideas are given in [19].

2. Variation of the shell geometry.

   This means, variation of the shell thickness t, the rise h, and the length L.

3. Variation of the beam cross sections and eventually their location (above or below the shell mid-depth).

4. Variation of the reinforcement ratios of the shell and the beam cross sections.

5. Variation of the material properties,

   e.g. ratio f_t'/f_y, tension stiffening, cracked shear modulus.

6. Variation of creep and shrinkage input data,

   i.e. different load histories, load intensities, environmental conditions etc.

7. Variation of loadings

   Concentrated loads, unsymmetrical loads, support deflections

The aim should be:

1. To get information on the variability of the nonlinear behavior and the ultimate load for different shell and beam geometries as well as different reinforcement ratios.

2. To get information on the influence of tensile strength and tension stiffening.

3. To get information on the influence of creep and shrinkage effects.

	GABLE SHELL	SADDLE SHELL	INVERTED UMBRELLA SHELL
GEOMETRY			
SUPPORTS			
$2 \cdot h/L$	$1/2.5$	$1/2.5$	$1/2.5$
$2 \cdot t/L$	$1/120$	$1/120$	$1/120$
BEAMS	EDGE-, CROWN-	EDGE-	EDGE-, VALLEY-
REINFORCEMENT RATIO β	SHELL: 0.4% BEAM:2.5%	SHELL:0.4% BEAMS:2.5%	SHELL:0.4% VALLEY&.:2.6% EDGEB.:5.2%
CONCRETE (ft^3)	3000 ≙ 100%	3000 ≙ 100%	3000 ≙ 100%
STEEL (sq.in.ft) (WITHOUT ABUTEMENTS)	2600 ≙ 100% 3320	2600 ≙ 100% 3320	2600 ≙ 120% 4480

FIG. 3.1 COMPARISON – INPUT DATA

	GABLE SHELL		SADDLE SHELL	INVERTED UMBRELLA SHELL	
LOCATION AND VALUE OF MAXIMAL STRESSES FOR DL + LL (IN psi = 0.007 N/mm²)	+180, −620		+390, −1500	−690, >471	
RATIOS	EDGE BEAM	INNER BEAM (CROWN)	EDGE BEAM	EDGE BEAM	INNER BEAM (VALLEY)
MAX. BENDING MOMENT / MAX. NORMAL FORCE	$\frac{1}{1}$	$\frac{2}{1}$	$\frac{4}{1}$	$\frac{1}{1}$	$\frac{1}{1}$
MAX. DEFLECTION DUE TO BEAM / MAX. DEFLECTION DUE TO SHELL	$\frac{2}{1}$	$\frac{7}{1}$	$\frac{3.3}{1}$	$\frac{1.1}{1}$	$\frac{1}{3}$
MAX. DEFLECTION DUE TO EDGE B. / MAX. DEFLECTION DUE TO INNER B.	$-\frac{1}{4}$		—	$\frac{3.3}{1}$	
DEFLECTIONS ARE ESSENTIALLY INFLUENCED BY	CROWN BEAM		EDGE BEAM	EDGE BEAM	
MEMBRANE THEORY APPROXIMATION	POOR		GOOD	FAIR- POOR	

FIG. 3.1 CONTINUATION — BEHAVIOR IN LINEAR REGIME

LOCATION OF FIRST CRACKS	GABLE SHELL	SADDLE SHELL	INVERTED UMBRELLA SHELL
LOAD LEVEL	DL + 12·LL	DL + 4·LL	DL + 4·LL
LOAD DEFLECTION CURVE	SLIGHTLY NONLINEAR	ALMOST LINEAR	STRONGLY NONLINEAR
FAILURE	BRITTLE - DUCTILE	BRITTLE	DUCTILE
LOCATION OF FAILURE	IN CORNER AREA (BEAM)	IN THE AREA OF FIRST CRACKS (SHELL)	IN CENTER OF EDGES (BEAM)
ULTIMATE LOAD	DL + 15.5·LL	DL + 8·LL	DL + 7.75·LL
MAX. DEFLECTION = 4 in. REACHED AT	DL + 15.5 LL	DL + 7·LL	DL + 5.5·LL
YIELD LINE THEORY APPROXIMATION	FAIR (POOR)	GOOD	POOR (QUESTIONABLE)

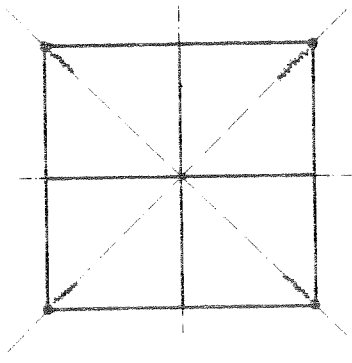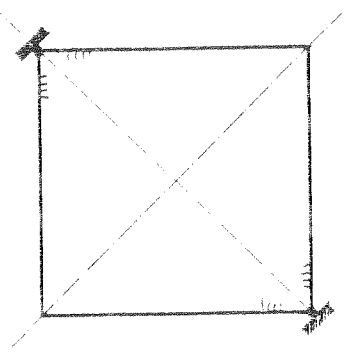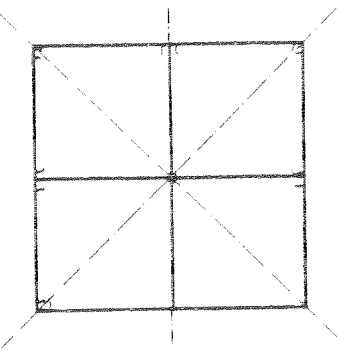FIG. 3.1 CONTINUATION - BEHAVIOR IN NONLINEAR REGIME

	GABLE SHELL	SADDLE SHELL	INVERTED UMBRELLA SHELL
LOCATION OF FIRST CRACKS			
LOAD LEVEL	DL, 180 DAYS	DL, 60 DAYS	DL, 40 DAYS
LOAD DEFLECTION CURVE	SLIGHTLY NONLINEAR	SLIGHTLY NONLINEAR	STRONGLY NONLINEAR
$\dfrac{\text{DEFLECTION INST. LOADING}}{\text{DEFLECTION, INCL. CREEP + SHRINK.}}$	$\sim \dfrac{1}{3.5}$	$\dfrac{1}{2}$	$\dfrac{1}{2.5}$
ULTIMATE LOAD	DL + 14·LL	DL + 8·LL	DL + 8·LL
MAX. DEFLECTION = 4 in. REACHED AT	DL + 14·LL	DL + 6.5 LL	DL + 3.5 LL

FIG. 9.1 CONTINUATION BEHAVIOR IN NONLINEAR AND TIME-DEPENDENT REGIME

16.0
15.0
14.0
13.0
12.0
11.0
10.0
9.0
8.0
7.0
6.0
5.0
4.0
3.0
2.0
1.0

MULTIPLES OF LL

DL

GABLE

— INSTANTANEOUS LOADING

--- CREEP AND SHRINKAGE INCL.

SADDLE

INVERTED UMBRELLA

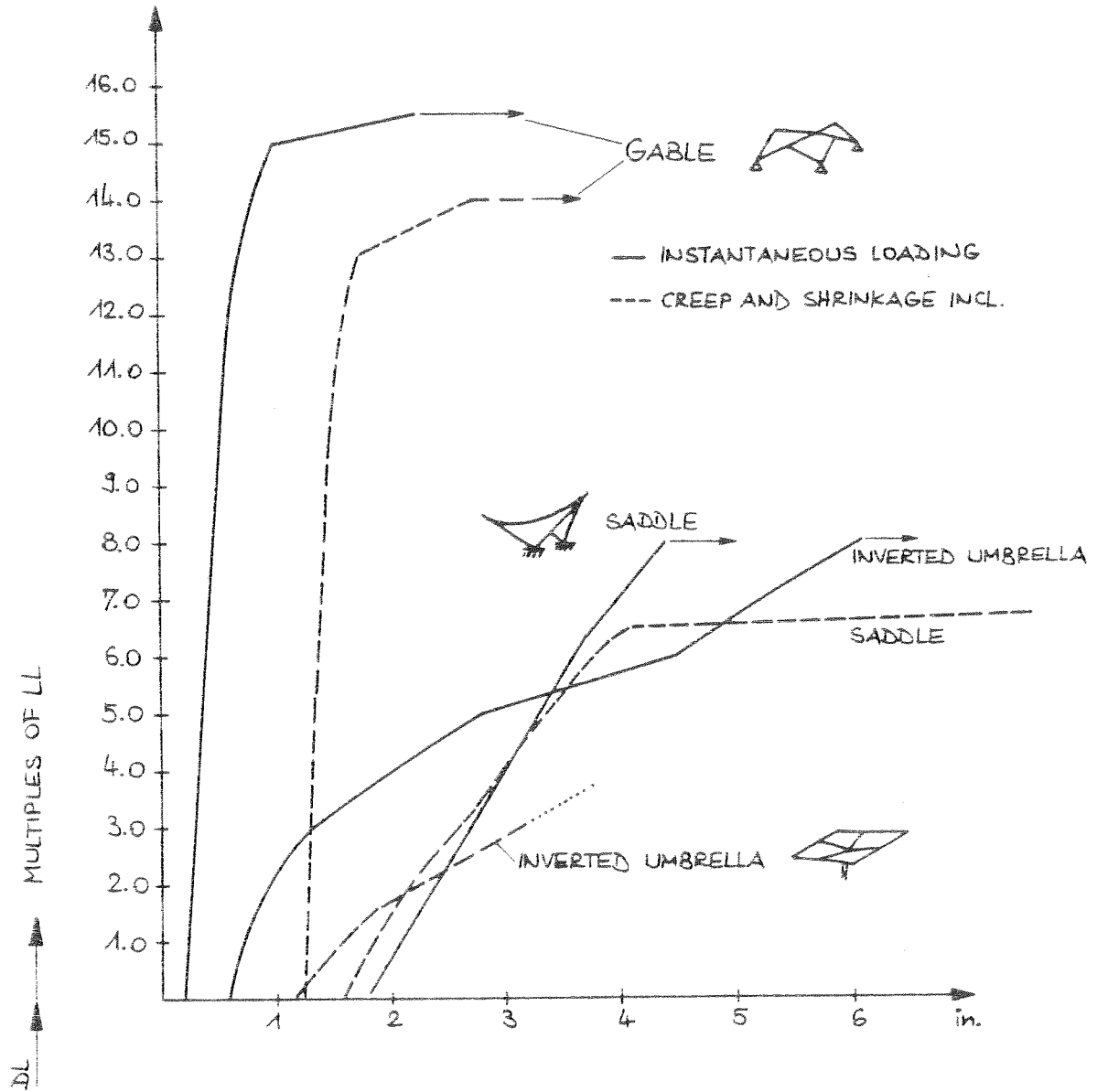SADDLE

INVERTED UMBRELLA

1   2   3   4   5   6   in.

FIG. 3.2 COMPARISON , LOAD-DEFLECTION CURVES

10. REFERENCES

[1] "Glass Fiber Reinforced Self-Supporting Concrete Roof", _Engineering News Record_ 17, April 28, 1977

[2] "Elementary Analysis of Hyperbolic Paraboloid Shells", _Portland Cement Association Bulletin_ ST 85, Skokie, Illinois 1960

[3] G. K. Tester, "Beitrag zur Berechnung der Hyperbolischen Paraboloidschale", _Ingenieur Archiv_ 16, 1974, S. 39-44

[4] F. Candela, "General Formulas for Membrane Stresses in Hyperbolic Paraboloid Shells", _Journal of the American Concrete Institute_ V, 32 No. 4, Oct. 1960, pp. 353-371.

[5] H. D. Ramirez, A. C. Scordelis, D. Ngo, "Membrane Stresses in Hyperbolic Paraboloid Shells Having a Parallelogram Shape in Plan", _Journal of the American Concrete Institute_, Dec. 1969, Vol. 66, pp. 994-1000

[6] A. C. Scordelis, H. D. Ramirez, D. Ngo, "Membrane Stresses in Hyperbolic Paraboloid Shells Having an Arbitrary Quadrilateral Shape in Plan", _Journal of the American Concrete Institute_, Jan. 1970, Vol. 67, pp. 36-44

[7] A. C. Scordelis, "Analysis and Design of HP Groined Vaults", Paper presented at _IASS World Congress on Space Enclosures_, July 4-9, 1976, Montreal, Canada

[8] "Students Clear Gym Moments Before Roof Fails", _Engineering News Record_, Sept. 24, 1970.

[9] R. N. White, "Reinforced Concrete Hyperbolic Paraboloid Shells", _Journal of the Structural Division, ASCE_, Vol. 101, No. ST 9, Sept. 1975, pp. 1961-1979

[10] A. C. Scordelis, "Finite Element Analysis of Reinforced Concrete Structures", Proceedings of the Speciality Conference on Finite Element Methods in Civil Engineering, Montreal 1972.

[11] W. C. Schnobrich, "Behavior of Reinforced Concrete Predicted by Finite Element Method", Proceedings of the Second National Symposium on Computerized Structural Analysis and Design, George Washington University, Washington D.C., March 1976

[12] R. Wegner, "Finite Element Models for Reinforced Concrete", Proceedings of the U.S.-Germany Symposium on Formulations and Computational Methods in Finite Element Analysis, Massachusetts Institute of Technology, Cambridge, August 1976

[13] J. Eibl, G. Ivanyi, "Studie zum Trag- und Verformungsverhalten von Stahlbeton", Deutscher Ausschuß für Stahlbeton, Heft 260, W. Ernst & Sohn, Berlin, 1976

[14] C. S. Lin, "Nonlinear Analysis of Reinforced Concrete Slabs and Shells", UC-SESM Report No. 73-7, University of California, Berkeley 1973

[15] A. F. Kabir, "Nonlinear Analysis of Reinforced Concrete Panels, Slabs and Shells for Time Dependent Effects", UC-SESM Report No. 76-6, University of California, Berkeley 1976

[16] W. C. Schnobrich, "Analysis of Hipped Roof Hyperbolic Paraboloid Structures", Journal of the Structural Division, ASCE, Vol. 98, ST 7, July 1972

[17] A. Pucher, "Ueber den Spannungszustand in doppelt gekruemmten Flaechen", Beton und Eisen 33, October 1934, S. 198 ff.

[18] ACI Committee 209, "Prediction of Creep, Shrinkage and Temperature
Effects in Concrete Structures", ACI Special Publications SP-27, April
1970

[19] G. Mueller, "Numerical Problems in Nonlinear Analysis of Reinforced
Concrete", UC-SESM Report No. 77-5, University of California, Berkeley,
September 1977

[20] E. Whitman and E. H. Gaylord, "Analysis of Unbraced Multi-Story Steel
Rigid Frames", Journal of Structural Division, ASCE, 94, 1968,
pp. 1143-1163
see also
E. Ramm, "Geometrische nichtlineare Elastostatik und finite Elemente",
Bericht Nr. 76-2, Institute für Baustatik, Universitaet Stuttgart,
1976, pp. 72-76 and 99-104

[21] Branson, D. E., "Deformation of Concrete Structures", McGraw-Hill,
New York, 1977